

University of New Hampshire

## University of New Hampshire Scholars' Repository

---

Master's Theses and Capstones

Student Scholarship

---

Spring 2023

# AUTOMATIC BANKFULL WIDTH EXTRACTION OF NEW HAMPSHIRE AND VERMONT RIVERS

Desmond Kager

*University of New Hampshire, Durham*

Follow this and additional works at: <https://scholars.unh.edu/thesis>

---

### Recommended Citation

Kager, Desmond, "AUTOMATIC BANKFULL WIDTH EXTRACTION OF NEW HAMPSHIRE AND VERMONT RIVERS" (2023). *Master's Theses and Capstones*. 1706.

<https://scholars.unh.edu/thesis/1706>

This Thesis is brought to you for free and open access by the Student Scholarship at University of New Hampshire Scholars' Repository. It has been accepted for inclusion in Master's Theses and Capstones by an authorized administrator of University of New Hampshire Scholars' Repository. For more information, please contact [Scholarly.Communication@unh.edu](mailto:Scholarly.Communication@unh.edu).

AUTOMATIC BANKFULL WIDTH EXTRACTION OF NEW HAMPSHIRE AND  
VERMONT RIVERS

By

DESMOND KAGER

B.S. Environmental Science, University of Vermont, 2021

THESIS

Submitted to the University of New Hampshire  
in Partial Fulfillment of  
the Requirements for the Degree of

Master of Science

in

Hydrology

May, 2023

This thesis has been examined and approved in partial fulfillment of the requirements for the degree of Master of Science in Hydrology by:

Thesis Director, Anne Lightbody, Associate Professor of Hydrology

Michael Palace, Associate Professor of Earth Sciences

Shane Csiki, MPA, CFM, State Geologist and Director of New Hampshire Geological Survey

On May 2, 2023

Original approval signatures are on file with the University of New Hampshire Graduate School.

## ACKNOWLEDGEMENTS

I thank Dr. Anne Lightbody, University of New Hampshire Earth Sciences Graduate Coordinator, Associate Professor of Hydrology, and my thesis director. For the past two years, without her constant enthusiasm, dedicated professionalism, unending wisdom, devotion and steadfast support, this endeavor would not have been possible. I remain so deeply grateful.

In addition to my advisor, Dr. Anne Lightbody, I thank the rest of my thesis committee including: Dr. Michael Palace, University of New Hampshire Associate Professor of Earth Sciences and Dr. Shane Csiki, Geography, Director of New Hampshire Geological Survey, who generously provided invaluable expertise, advice, and guidance. I am especially thankful.

I thank the whole of the University of New Hampshire Hydrology and Earth Sciences Graduate Schools for imparting their incredible knowledge and technical support during my stay here at the University of New Hampshire. I would like to thank the State Water Resources Research Institute Program grant and the Dingman Scholarship for the generous funding and support which made my research possible. I am truly appreciative.

I thank Trevor Fenoff and Lauren Kaehler for their tremendous partnership in the classroom and field along the waterways of New Hampshire and Vermont. I thank Jon-Erik Tryggestad for his enthusiastic and insightful support of this project. Special thanks also go to Maya Harris and Gavin Drake for their valuable time with the input of raw sample data.

Lastly, I thank my father Donald Kager and mother Mary Bridget Cooke-Kager, my older brother Ciaran and my younger sister Bridget who were with me every step of the journey.

## Table of Contents

ACKNOWLEDGEMENTS .....	iii
List of Tables .....	viii
List of Figures .....	ix
ABSTRACT .....	xii
Chapter 1: Introduction .....	1
1.1 Importance of Studying Bankfull Width.....	1
1.2 Natural Variations in Bankfull Width.....	2
1.3 Anthropogenic Influences on Bankfull Width.....	3
1.4 Remote Sensing Techniques for Bankfull Width .....	4
1.5 Research Goals.....	7
Chapter 2: Methods.....	8
2.1 Study Area .....	8
2.1.1 Ammonoosuc River .....	8
2.1.2 Cocheco River.....	9
2.1.3 Dog River.....	10
2.1.4 Lamprey River .....	10
2.1.5 Stevens Branch.....	11
2.1.6 Sugar River .....	11
2.2 Field Measurements of Bankfull Width.....	12
2.2.1 Assessing Quality of Field Bankfull Measurements.....	13
2.2.2 Evaluating Uncertainty in Field Bankfull Width Measurements.....	14
2.3 Bankfull Regression Equation .....	14
2.4 Remote Sensing of Bankfull Width .....	15
2.4.1 Remote Data Sources .....	15
2.4.2 Manually Preprocessing DEMs .....	16
2.4.3 Bank Detection and Floodplain Analysis Calibration .....	17
2.4.4 Calibration Model and Data.....	19
2.4.5 Validation.....	21
2.5 Statistical Analysis.....	21
2.5.1 Comparing Field, Remote and Regression Widths.....	21
2.5.2 Evaluating the Influence of Bed and Bank Material on River Width.....	22
2.5.3 Assessing Longitudinal Variation in Bankfull Width.....	22
Chapter 3 Results and Discussion.....	24
3.1 Remote Sensing of Bankfull Width .....	24
3.1.1 Calibration Results.....	24
3.1.2 Validation Results .....	24
3.1.3 Bankfull Widths from Remote Sensing, Field Measurements and Regression .....	25
3.2 Bankfull Width for Study Rivers .....	26
3.2.1 Ammonoosuc River .....	26
3.2.2 Cocheco River.....	26
3.2.3 Dog River.....	27

3.2.4 Lamprey River .....	27
3.2.5 Stevens Branch.....	28
3.2.6 Sugar River .....	28
3.3 Effect of Bed and Bank Substrate on Bankfull Width .....	29
3.4 Spatial Variability in Bankfull Width.....	29
Chapter 4: Conclusion.....	31
4.1 Automatic Bankfull Width Detection in New England .....	31
4.2 Method Limitations and Suggestions for Future Research.....	31
4.3 Contributions to River Science .....	35
Figures.....	36
Tables .....	61
Appendix A .....	65
Appendix B .....	76
Appendix C .....	89
Appendix D.....	92
LIST OF REFERENCES .....	98

## List of Tables

Table 1. Assessed clusters representing riparian corridor, watershed area, bank material, and bed substrate.

Table 2. Best Parameter values used as model inputs for automatic bankfull width detection for each river cluster. Optimal values for slope break ratio and slope percentage were selected based on calibration. based on lowest RMSE values for all study sites with highlighted clusters calibration and validation model runs combined.

Table 3. Root mean square error (RMSE) and Normalized RMSE between field and remotely derived estimates of bankfull width for each cluster in the six study rivers and their corresponding clusters.

Table 4. Average Field, Remote and Regression point data and total Average Remote reach data for all Rivers.

Table 5. Upstream and downstream average remotely derived bankfull widths for the river reaches immediately upstream and downstream study sites with of all active dams within study rivers.

## List of Figures

Figure 1. Typical cross section showing various hydrological measurements. Bankfull width depicted in light blue, active channel width depicted in dark blue (Federal Interagency Stream Restoration Working Group).

Figure 2 In the field, bankfull location is determined by the presence of permanent vegetation. Arrow A is pointing to the elevation of the abandoned floodplain above the current bankfull stage and arrow B shows the active floodplain indicating current bankfull stage (Stream Geomorphic Assessment Handbooks).

Figure 3. Study rivers and corresponding watersheds.

Figure 4. Examples of different bed and bank materials encountered on study rivers. (a) Sandy bank and cobble bed on the Dog River. (b) Bedrock bank and bed on the Dog River. Undercut sandy banks and bed Lamprey River (Bottom Left), Boulder bed and bank material Sugar River (Bottom right).

Figure 5. Example of field bankfull width measurement taken closer than 5 meters to a tributary that causes a noticeable widening in the hydro-flattened water surface, which influences cross section placement.

Figure 6. Example where field bankfull width measurement was taken is in a region where banks are poorly defined due to bedrock outcrop (a) or wetlands (b).

Figure 7. Example of measurement taken in location where there is a major error with hydro-flattening of the digital elevation model (DEM) for the Stevens Branch (a). Typical DEM near a bankfull measurement on the Stevens Branch (b).

Figure 8. Example from the Lamprey River of a field width measurement obtained in a location where the bankfull width change among 3 adjacent cross sections is greater than 5 meters. Blue shading shows riverbanks.

Figure 9. Example from the Dog River of a region with rapid channel change. (a) Satellite imagery from 2015, which is close to the time of LiDAR flights for most study rivers. (b) Satellite imagery of the same reach in 2021, which is close to the 2022 field measurements, showing a change of more than 5 meters, which would lead to the exclusion of any field measurements in this reach.

Figure 10. Example from the Cochecho River of a location in which the GPS point corresponding to a bankfull width measurement is farther than 5 meters from the riverbank, likely as a result of the continuous tree cover interfering with the GPS signal.

Figure 11. Example from the Ammonoosuc River of a bankfull width measurement at a location within a multithreaded channel.

Figure 12. Outputs of GIS preprocessing methods for automatic bankfull width analysis.

Figure 13. Example cross section used to determine the bankfull point locations within a stream channel. Bank points in red are derived from the slope break ratio and slope break percentage by dividing the width of the channel by the width of the next highest increment and searching for a slope percentage value greater than user specified value (USGS toolbox).

Figure 14. Field measurements of bankfull width compared to the average of the three closest remotely sensed widths for all calibration locations in all of the study rivers. The equation and squared correlation coefficient for the best-fit straight line are shown on the plot. Horizontal bars indicate field uncertainty. Vertical bars indicate resolution uncertainty.

Figure 15. Field measurements of bankfull width compared to the average of the three closest remotely sensed widths for all validation locations in all of the study rivers. The equation and squared correlation coefficient for the best-fit straight line are shown on the plot. Horizontal bars indicate field uncertainty. Vertical bars indicate resolution uncertainty.

Figure 16. Field measurements of bankfull width compared to the average of the three closest remotely sensed widths for both calibration and validation locations in all of the study rivers. The equation and squared correlation coefficient for the best-fit straight line are shown on the plot. Horizontal bars indicate field uncertainty. Vertical bars indicate resolution uncertainty.

Figure 17. Field measurements of bankfull width compared to regression widths for both calibration and validation locations in all of the study rivers. The equation and squared correlation coefficient for the best-fit straight line are shown on the plot. Horizontal bars indicate field uncertainty. Vertical bars indicate resolution uncertainty.

Figure 18. Bankfull width compared to watershed area for all of the field measurement locations.

Figure 19. Ammonoosuc River longitudinal profile with raw and smoothed remotely sensed bankfull widths as a function of distance downstream of the Beacon Street Bridge, Littleton, NH. Colors indicate bed substrate.

Figure 20. Mean remotely sensed bankfull width for reaches M21–M2 on the Ammonoosuc River.

Figure 21. Cocheco River longitudinal profile with raw and smoothed remotely sensed bankfull widths as a function of distance downstream of the Bay Road Bridge, Farmington, NH. Colors indicate bed substrate.

Figure 22. Mean bankfull width along reaches M21–M2 on Cocheco River. The Cocheco flows from north to south.

Figure 23. Dog River longitudinal profile with raw and smoothed remotely sensed bankfull widths as a function of distance downstream of the Stony Brook Road Bridge, Northfield, VT. Colors indicate bed substrate.

Figure 24. Mean bankfull width along reaches M21–M2 on Dog River. Flow was from south to north.

Figure 25. Lamprey River longitudinal profile with raw and smoothed remotely sensed bankfull widths as a function of distance downstream of the Route 125 Bridge, Epping, NH. Colors indicate bed substrate.

Figure 26. Mean bankfull width along reaches M21–M2 on Lamprey River. The Lamprey flows from west to east.

Figure 27. Stevens Branch longitudinal profile with raw and smoothed remotely sensed bankfull widths as a function of distance downstream of the Old Town Road Bridge, Williamstown, VT. Colors indicate bed substrate.

Figure 28. Mean bankfull width along reaches M21–M2 on Stevens Branch. The Stevens Branch flows south to north.

Figure 29. Sugar River longitudinal profile with raw and smoothed remotely sensed bankfull widths as a function of distance downstream of the Treatment Plant Road Bridge, Newport, NH. Colors indicate bed substrate.

Figure 30. Mean bankfull width along reaches M21–M2 on Sugar River. The Sugar flows east to west.

Figure 31. Satellite photograph of the Sugar River reach M33–M32 with two hydroelectric dams, including remotely derived bankfull channel positions.

Figure 32. Satellite photograph of the Dog River reach M19B, which passes through a bedrock gorge, including remotely derived bankfull channel positions.

**ABSTRACT****AUTOMATIC BANKFULL WIDTH EXTRACTION OF NEW HAMPSHIRE AND  
VERMONT RIVERS**

By

Desmond Kager

University of New Hampshire May 2023

Understanding a river's morphology can help scientists measure erosion, improve understanding of flood hazards and better estimate riparian habitat. While there have been many developments in the field of fluvial geomorphology, there are still many challenges that exist in efficiently and accurately quantifying various important river metrics, such as the location of channel banks. Conducting field surveys of riverbanks is expensive and time consuming, leading many scientists to shift towards remote sensing techniques to measure river morphological features. This project aims to extract bankfull width measurements automatically from high-resolution Digital Elevation Models (DEMs) of rivers located in New Hampshire and Vermont. Six rivers located throughout Vermont and New Hampshire were identified, based on the availability of previous channel field surveys and high-resolution DEM data. The USGS stream channel and floodplain toolbox was used as well as a combination of other tools such as Terrain Analysis Using Digital Elevation Models (Tau DEM) and Whitebox Geospatial Analysis Tool (Whitebox GAT), to automatically generate bank points and bankfull width estimates of these six rivers. Specific input parameters for each river were evaluated to produce accurate widths. The best parameters were used to create a model to rapidly estimate bankfull widths of New Hampshire and Vermont rivers with similar topographic signatures. This study found that 49% of bankfull widths derived from remote sensing were within the 2.95 meters of estimated uncertainty among all study rivers.

However, no statistically significant difference between bankfull width and bed substrate or bank substrate was found among all the rivers.

## Chapter 1: Introduction

### 1.1 Importance of Studying Bankfull Width

Knowing the location of a river's banks can help scientists build better flood models for fluvial erosion and river restoration, gain a better understanding of flood hazards, and better assess a river's ecological health. Having continuous river width measurements can directly help identify areas of riparian habitat diversity (Faux et al., 2010). Continuous river width measurements can help provide more accurate input data for hydrologic and hydraulic models over large spatial scales (Golly and Turowski, 2017).

Bankfull width is also used in stream restoration to determine the appropriate dimensions of bridges, culverts and roads in order to accommodate infrequent high-flow events. In the United States, engineers are required to build infrastructure for the 100-year flood, meaning bridges, culverts and roads are designed to convey these flows (Ludy and Kondolf, 2012). However, this 100-year flood requirement has led to stream channels being designed to be much larger than their natural design, leading to large accumulation of sediment under bridges, requiring dredging after every large flood event. Rather than designing infrastructure to withstand these 100-year floods, infrastructure can be built over the floodplain so they can be designed for the two-year bankfull flow to incorporate a more natural stream channel (Jarrett et al., 2010). Since 13% of Americans currently reside within a 100-year flood zone, it is now more important than ever to be able to have accurate continuous width measurements of rivers (Wing, 2018).

Bankfull width is defined as the width of the surface water at the location where water begins to overflow into the active floodplain (Figure 1). The active floodplain is defined as the

flat portion of the valley adjacent to the channel that is constructed by the present river in the present climate (Leopold, 1994). Bankfull width is often used to measure hydrological and morphological characteristics because, unlike the wetted area of a river that changes daily, bankfull width fluctuates infrequently. In addition, in alluvial rivers, bankfull width represents the channel-forming discharge, which over time performs the most work in transporting sediment and shaping the river channel (Wolman and Miller, 1960). While the frequency of bankfull floods varies by both stream type as well as human influences, a natural channel experiences a bankfull flood every 1.2 to 1.5 years (Rosgen, 1994). Since bankfull conditions occur when water spills from the stream channel to the active floodplain, heavily incised channels may not experience bankfull conditions as often as rivers with shallow banks within close proximity to floodplains (Montgomery and Buffington, 1997).

Bankfull width is traditionally determined in the field by the identification of bankfull indicators including these highest depositional feature, the break in slope between the floodplain and channel margin, and the lower extent of permanent woody vegetation (Figure 2). Specific bankfull indicators vary based on stream type, level of impairment and vegetation coverage. Locating bankfull indicators is difficult in areas where there is erosion, channelization or lack of vegetation (Rosgen, 1994).

## 1.2 Natural Variations in Bankfull Width

Moving downstream within a watershed, rivers tend to increase in width as upstream drainage area increases due to decreasing longitudinal slope and increasing deposition downstream (Schumm, 1977). Various morphological characteristics of rivers including sinuosity, channel width, slope and depth have been previously found to be influenced by both

natural and anthropogenic factors (Anderson, 2004). Highly sinuous rivers are likely to have wider bankfull widths, particularly around meander bends. One study revealed that in the majority of cases, rivers tend to be the widest near the apex of their meander bends (Eke et al., 2014). Variables influencing channel width range from dams impeding flow and sediment to the specific species of riparian vegetation. Vegetation with deep roots can help stabilize banks and reduce erosion, thus narrowing channel width (Abernethy and Rutherford, 1998). Tree canopy coverage can also influence river width especially for smaller rivers, where trees reduce light available to the understory limiting the establishment of stabilizing vegetation, thus increasing channel width (Davies-Colley, 1997). Large woody debris (LWD) can also influence channel width by either armoring banks or by directing flow into the banks. The ability of LWD to control river width varies on the reach scale, making it difficult to measure its influence over the span of an entire river (Zimmerman and Maniaktr, 1967; Trimble, 1997). Bank material also has a substantial effect on channel width. In a previous study, narrower widths were observed in reaches lacking vegetation and those consisting mainly of clay and silty substances (Ferguson, 1973). Bed material also influences bankfull width on a regional scale. One study found that rivers with coarse bed materials were wider compared to rivers of similar drainage size composed of fine bed materials (Faustini et al., 2009).

### 1.3 Anthropogenic Influences on Bankfull Width

Anthropogenic factors such as dams also influence channel width. A study looking at long-term river geomorphic and vegetation changes in Argentina found that the construction of a dam increased channel width upstream and that the downstream channel morphology was an artifact of pre-dam construction (Casado et al., 2016). Dam removal also drastically influences

channel width. When most dams are removed, previously hindered water and sediment trigger the downstream channel to rapidly widen. However, the removal of the Homestead Dam on the Ashuelot River in 2011 led to channel widening mostly in areas upstream of the dam due to the strong resistance to erosion in the boulder reach where the dam was located (Gartner et al., 2015).

#### 1.4 Remote Sensing Techniques for Bankfull Width

Remote sensing techniques have been increasingly used by scientists to estimate and evaluate hydraulic geometry of rivers. Many types of river channel detection rely on visual image segmentation based on differences in color values, image texture analysis and/or manual training. For example, one method for extracting riverbank locations uses changes in roughness to detect bank locations from grayscale imagery by looking at differences between the low entropy water and high entropy land pixels (McKay and Blain, 2014). Another automatic method for measuring channel width involves using both the normalized difference water and vegetation indexes to classify bank locations (Yang et al., 2020). The geospatial tool River Width Cloud removes islands from the river channel, automatically flags data issues and efficiently calculates river width orthogonal to the centerline (Yang et al., 2020). Methods that rely on visual detection of the water surface can be accurate and efficient in most natural free-flowing rivers, but they are not as effective in heavily built-up environments which obstruct the view of the river (Weng, 2012). In addition, these methods are limited by the resolution of the aerial imagery; for example, techniques that rely on Landsat satellite imagery have a spatial resolution of 30 meters. Visual techniques are generally used to locate the water surface of the active channel, which fluctuates on a daily basis and is not a true representation of a rivers bankfull.

Alternatively, digital elevation models (DEMs) can be used to estimate bankfull river width. Bare-earth DEMs are a representation of the bare ground topography of Earth excluding trees, buildings and other surface objects (USGS). DEMs can be derived from various techniques including photogrammetry, land surveying, Synthetic Aperture Radar (SAR), Unmanned Aircraft System (UAS), Light Detection and Ranging (LiDAR) and aerial LiDAR. LiDAR uses light in the form of a pulsed laser to measure ranges to the earth. Combined with other instruments such as global navigation satellite system (GNSS), LiDAR generates precise three-dimensional information about surface characteristics (Earth Science Data Systems, NASA.(n.d.).Lidar.NASA.Retrieved, 2023).

High-resolution DEMs derived from remote sensing can be used to identify bankfull width by detecting a break in bank slope, often accomplished through a slope break threshold method. This threshold is used to identify the point where there is significant change in slope, identifying the location of bankfull in a stream channel as the location where the steep river bank transitions to the flatter floodplain. On reaches of rivers that are not prone to active floodplain building, the break in bank slope often corresponds to the bankfull stage (Vermont Agency of Natural Resources, 2004). Being able to properly identify breaks in stream slope to estimate bankfull width requires high-resolution DEMs, such as those produced from LiDAR. Having higher LiDAR resolution correlates with more accurate flood modeling. One study found that, at a minimum, the resolution of a DEM should be finer than the width of the river channel (Muthusamy et al., 2021). One automatic method that derives river width data from DEMs is GeoRW. GeoRW uses the first-order moment of slope or terrain factor and upstream drainage areas to estimate river width measurements from coarse resolution DEMs in mountainous watersheds (Tong et al., 2020). This method, however, is limited to mountainous watersheds and

is not accurate in watersheds with large flood control structures such as dams, which artificially increase river width (Tong et al., 2020). Another automatic method that derives river width data from DEMs is a QGIS plugin called the Bankfull Detection Tool, which is designed to extract the bankfull width of a cross section from a DEM by detecting the break in slope along the river's banks (De Rosa and Fredduzzi, 2019). The tool's primary output is a polygon which represents the bankfull width along the river; the user must then measure the width of the polygon generated in order to obtain bankfull width values (De Rosa and Fredduzzi, 2019). A third automatic method of bankfull-width detection is the USGS Stream Channel and Floodplain Metric Toolbox, which identifies bankfull river width from the break in slope at the channel boundary on high-resolution DEMs (Hopkins et al., 2018).

Unlike measurements taken in the field, remotely derived measurements are easy to obtain and require little investment due to publicly available datasets and open-source software. Although remote sensing techniques can be very efficient, they introduce new problems. Some of these problems include LiDAR being reflected off the water surface, image distortion from clouds and associated initial costs in addition to many other issues (Vetter et al., 2009). In addition, methods that use DEMs as an input for remotely estimating bankfull width have trouble in wetlands with poorly defined banks as well as in locations with point bars or log jams (Hladik et al., 2012). Despite these limitations, estimating bankfull width from LiDAR-generated DEMs has proven to be an efficient and reliable method for various rivers across the United States (Hofle et al., 2009).

## 1.5 Research Goals

This project aims to use remote sensing to produce accurate and continuous estimates of bankfull widths within New England rivers. In particular, the project looks to quantify the accuracy of automatic bankfull width determination using the USGS Stream Channel and Floodplain Metric Toolbox with LiDAR-derived DEMs in New England rivers; quantify channel width change longitudinally downstream in response to differences in bed and bank material as well as dams; and determine the influence of bank and bed materials on channel width in similarly sized rivers.

## Chapter 2: Methods

### 2.1 Study Area

This project focused on six rivers located throughout New Hampshire and Vermont that had high-resolution DEMs and previously conducted geomorphic assessments (Figure 3). During previous geomorphic assessments, rivers were divided up into segments called reaches ranging from 0.5 km to 7 km long (Vermont Agency of Natural Resources, 2009). Each reach was given a series of coded letters and numbers that describe both its location and geomorphic properties. Reach numbers decreased from the highest number at the headwaters to reach 1 at the river's mouth. Reaches ranged in size, slope and substrate. Some examples of reach segment breaks were a gorge, dam, waterfall, tributary junction, or sudden change in slope.

River reaches were clustered into larger groups to facilitate geospatial processing (see below). More specifically, due to both the extensive memory demand of the ArcMap 10.8.1 plugin tool and in order to evaluate the influence of the various model input parameters on a smaller scale, the five longest rivers were each split up into clusters of continuous reaches. In total, there were thirteen clusters with an average of five reaches in each cluster. Each of the thirteen clusters had various riparian corridors, watershed areas as well as respective bed and bank materials (Table 1).

#### 2.1.1 Ammonoosuc River

The Ammonoosuc River is a 55-mile-long tributary of the Connecticut River. The Ammonoosuc River originates on the western slope of Mount Washington, NH, and flows through multiple towns, then eventually outflows into the Connecticut River in Woodsville, NH. The Ammonoosuc watershed is primarily forest (83%), development (5%) and a mixture of

wetlands and agriculture (NLCD, 2019). Reaches M21 through M2 were assessed. These reaches consisted of sections of river between Littleton, NH, and Woodsville, NH. The Ammonoosuc riverbanks were primarily composed of boulder/cobble material (92.3%); the remainder was sand, which was primarily located in the impounded reaches. The assessed reaches on the Ammonoosuc River were wholly classified as boulder/cobble bed substrate (100%). The Ammonoosuc had a diverse riparian corridor with forest (53%), cropland/pasture (19%), commercial/industrial (15.4%), and residential (12.5%). The Ammonoosuc River has diverse reaches ranging from steep gorges to large impoundments as well as single and multi-threaded channels. Bankfull field measurements on the Ammonoosuc River ranged from 27 meters to 72 meters near the Woodsville Dam; these were the largest among the study rivers.

#### 2.1.2 Cocheco River

The Cocheco River is a 38-mile-long tributary of the Piscataqua River that begins in Farmington, NH, and runs through Rochester and Dover eventually joining the tidal Salmon Falls River along the Maine border. The composition of the Cocheco watershed is forest (62%), developed (16%), wetlands (9%), agriculture (5%) and the rest a mixture of land cover classifications (NLCD, 2019). Reaches M20 through M12 were assessed. Of the assessed reaches of the Cocheco River, the majority of bank material was composed of sand (66%), with the remaining material boulder/cobble (33%). The bed substrate of the Cocheco River was primarily sand at (66%), with the remaining consisting of bedrock at (33%). While 100% of the Cocheco River riparian corridor was classified as forest, lower reaches of the Cocheco previously assessed have riparian corridors composed of residential and commercial land use. The Cocheco River contained a diverse set of reaches varying from steep-step pool bed forms in

the headwaters to shallower riffle-pool forms in the lower reaches. The Cocheco River had bankfull width measurements ranging from 7 meters in the upper sections to 25 meters near the lower assessed reaches.

### 2.1.3 Dog River

The Dog River is 18 miles long with headwaters beginning in Roxbury, VT. The river eventually flows into the Winooski River near Montpelier, VT. The Dog River is located mainly in a forested watershed (74%), with some agriculture (6%) and little to no development (2.7%; NLCD 2019). The Dog River had a riparian corridor composed mostly of cropland/pasture (56.3%). Watershed land use was primarily forest (31.25%) and commercial/industrial (12.5%). M14 through M1 were completely comprised of boulder/cobble banks. The majority of bed substrate was also boulder/cobble (87.5%), with the remaining material composed of bedrock. The Dog River has a diverse set of reaches. They range from unconfined reaches with gentle slopes to extremely steep bedrock gorges lacking floodplain access.

### 2.1.4 Lamprey River

The Lamprey River is a 50-mile-long river which rises in Northwood, NH, and flows southeast into a saltwater estuary called Great Bay. The composition of the Lamprey watershed is forest (66%), with other important watershed land uses including wetlands (13%) and developed (8%; NLCD, 2019). Reaches M25 through M2 were assessed, and these reaches had a diversity of bank materials including silt/clay (31%), sand (26%), boulder/cobble (26%), and gravel (17%). Bed substrate also varied, including reaches that were boulder/cobble (42%), sand (25%), gravel (11%), silt/clay and bedrock (11%). Lamprey's riparian corridor consisted of

mostly forested cover (84%), with the remainder residential (16%). The Lamprey River had diverse reaches ranging from steep bedrock gorges to large woody wetlands with low lying banks and floodplain access.

#### 2.1.5 Stevens Branch

The Stevens Branch is a 13-mile-long tributary of the Winooski River. The Stevens Branch begins in Williamstown, VT, then flows through the town of Barre, VT, and eventually into the Winooski River. The Stevens Branch is located in an area with diverse land coverage including forest (50%), developed (19%), wetlands (13%), and agriculture (11%; NLCD, 2019). Reaches M11 through M15 were assessed during the summer of 2022, and these reaches contained a mixture of boulder/cobble and gravel banks, comprising 50% and 40% of the material respectively. The Stevens Branch consisted of boulder/cobble (60%) bed material with the remainder gravel (40%). The Stevens Branch had moderate bank slopes throughout all of the assessed reaches.

#### 2.1.6 Sugar River

The Sugar River is a 27-mile-long tributary of the Connecticut River. Its headwaters originate from Lake Sunapee, NH, then it eventually meets the Connecticut River in Claremont, NH. This river has numerous dams which act as both reservoirs for town drinking supplies as well as a source of power for much of the region. The composition of the Sugar watershed is primarily forest (74%), development (8%), wetlands (5%) and open water (4%; NLCD, 2019). Reaches M25 through M18 were assessed, and 100% of these reaches had boulder/cobble bank and bed material as their primary substrate. These reaches also had a riparian corridor consisting

of forest (94%) and residential (6%). Bankfull width measurements were taken in reaches M39. The Sugar River also consisted of low-lying reaches with undefined banks in some of the upper reaches near Newport, NH.

## 2.2 Field Measurements of Bankfull Width

Each of the six study rivers (Ammonoosuc, Cocheco, Dog, Lamprey, Stevens Branch, and Sugar) was assessed in the Summer of 2022 using established methods in which dominant vegetation type, bank material, bed material, revetment type, riparian corridor type and bankfull width were visually assessed and recorded along each reach (Vermont Agency of Natural Resources, 2009).

During the Summer of 2022, bankfull width was measured at 150 locations throughout the six study rivers at locations varying in width, bed material, and bank material (Figure 4). At each location, bankfull width was identified using one or more of the following indicators: flat top of developing point and lateral bars, location of change on bank from steep to gentler slope above the inflection point, and the lower extent of persistent woody vegetation (Vermont Agency of Natural Resources, 2004). When bankfull indicators conflicted with each other, the persistence of woody vegetation was used as the primary indicator. The bankfull elevation was first identified on the bank with more obvious indicators, then the horizontal distance to the opposite bank was visually sighted with a Vortex Crossfire HD 1400 rangefinder (uncertainty  $\pm 0.1$  meters for measurements under 200 meters). A GPS point was obtained using a Garmin eTrex 10 (uncertainty  $\pm 3$  meters) at each of the locations where bankfull width measurements were taken.

Field bankfull width was preferentially measured at locations with strong bankfull indicators. Locations were not distributed randomly throughout reaches; rather, they tended to be located at sites with clearly defined alluvial banks. Where possible, measurements were obtained at locations of previous bankfull measurements from 2008 to 2014 (Vermont Department of Natural Resources, 2009).

### 2.2.1 Assessing Quality of Field Bankfull Measurements

Several criteria were developed in order to evaluate the quality of the field bankfull width measurements for purposes of comparison to remote sensing. More specifically, field bankfull width measurements used for accuracy assessment met the following criteria. First, measurements were farther than 5 meters from a tributary that causes a noticeable widening in the hydro-flattened water surface (Figure 5). Hydro-flattening is the process of artificially lowering cells in a DEM to form a continuous water surface, thus removing artifacts from the DEM surface (USGS, 2014). Second, measurements were not taken in a region where one or both banks are poorly defined due to wetlands or bedrock outcrops (Figure 6). Third, measurements were not taken in locations where there is a major error with hydro-flattening of the DEM, which occurred for two tiles (4 km<sup>2</sup>) in the Stevens Branch (Figure 7). Fourth, measurements were taken in locations where bankfull width change among three adjacent cross sections was less than 5 meters (Figure 8). Fifth, the position of both riverbanks changed by less than 5 meters as seen on satellite imagery between the time of LiDAR flight and field measurements (Figure 9). Sixth, the GPS point corresponding to the bankfull measurement was closer than 5 meters from the riverbank seen on satellite imagery (Figure 10). Lastly, measurements were obtained in single threaded channels only (Figure 11). Out of the 150

bankfull width measurements taken in the field, 88 satisfied the previous criteria and were therefore accepted for comparison to remote sensing.

### 2.2.2 Evaluating Uncertainty in Field Bankfull Width Measurements

Measuring bankfull width in the field can be challenging and is prone to multiple sources of error ranging from the subjective nature of where bankfull is located to the measuring of the distance across the channel. To assess the accuracy of the bankfull width field data, including an upper bound on potential channel change between the time of LiDAR flight and the most recent field surveys, measurements taken from prior geomorphic assessments (2008-2014) were compared to 2022 measurements. If the horizontal locations of two bankfull field measurements in these two different surveys were closer than 5 meters to each other, then they were considered comparable. The survey error was calculated as the root mean square error (RMSE) between the bankfull widths from both field surveys:

$$1) \text{ RMSE (m)} = \frac{1}{N} \sqrt{\sum_{i=1}^N (O_i - F_i)^2}$$

where  $O_i$  indicates each old (2008-2011) bankfull width,  $F_i$  indicates each new (2022) field bankfull width and  $N = 19$  is the total number of overlapping observations. Total error on field measurements was estimated by adding in quadrature the range finder uncertainty (0.1 m) and the survey error (2.95 m), producing a total estimated error of 2.95 meters.

### 2.3 Bankfull Regression Equation

Hydraulic geometry regression equations capture the expected relationship between watershed area and river size based on both the local geology and geomorphology of a particular region. The following regression equation between bankfull width and drainage area was

developed using channel measurements from Massachusetts and the seacoast New Hampshire region (Bent and Waite, 2013):

$$2) W \text{ (ft)} = 15.0418(A)^{.4038}$$

where  $W$  is the bankfull width in feet and  $A$  is the watershed area in square miles. This regression equation is the geographically closest published equation to the study rivers and is similar, though not identical, to an equation based on the entire Northeastern US as well as a provisional equation for New Hampshire (Bent and Waite, 2013).

The watershed area was calculated using the USGS Stream Stats tool at each bankfull field measurement location. Watershed area at intermediate locations along each study reach were estimated by the watershed area of the nearest bankfull field measurement location.

Because the primary input for bankfull regression equations is the watershed area, points taken in larger watersheds had higher bankfull regression widths.

## 2.4 Remote Sensing of Bankfull Width

### 2.4.1 Remote Data Sources

Calculating bankfull width remotely from DEMs requires high-resolution topography. In 2014, LiDAR was flown over the Dog River and Stevens Branch, while in 2015, flights were conducted over the Ammonoosuc, Sugar, and upper Cochecho Rivers. In addition, both the Lamprey River and lower reaches of the Cochecho River were flown in 2019. All LiDAR was acquired when the rivers were at low flow. All of the DEMs had a resolution of 0.7 meters or finer, with the Lamprey having a resolution of 0.3 meters. High-resolution hydro-flattened bare-earth DEMs were downloaded from both Vermont and New Hampshire state databases (Vermont

Center for Geographic Information-VCGI, 2017; New Hampshire Granit GIS Database, 2019).

The tiles in the datasets each had an area of 2 square kilometers.

#### 2.4.2 Manually Preprocessing DEMs

As part of this study, bare-earth hydro-flattened DEMs tiles for each cluster were merged and clipped using a 250-meter buffer around the USGS flowline (Figure 12a). DEMs were preprocessed for each cluster using the Whitebox GAT within ArcMap 10.8.1 to enable automatic detection of continuous river channels (Lindsay, 2016). The Breach Depressions tool was run to remove topographic depressions and dams in the DEM by artificially lowering the elevation between cells to create a continuous stream network (Figure 12b). The Pit Remove tool from the Tau DEM toolbox was then run on the previously breached DEMs in order to remove artifacts that interfere with flow processing across the DEM by artificially raising the elevation of areas surrounded by high terrain.

Once the preprocessing was complete, the Tau DEM toolbox (Tarboton, 2007) was used within ArcMap 10.8.1 to calculate D8 flow directions, generating the direction of steepest descent from each grid cell (east, southeast, south, southwest, *etc.*) represented using the numbers 1–8 (Figure 12c). The tool D8 Contributing Area was then used to calculate the number of grid cells draining to each cell within the cluster. These outputs were fed into the Stream Definition by Threshold tool to generate a stream raster grid (Figure 12d). Because this study focuses on the main channels of rivers, a large threshold value of 100,000 cells was used to limit the stream raster grid to the largest flow paths. This tool created single threaded channels even when multiple threads were present. In multithreaded reaches, the tool chose the largest channel. Finally, the Stream Reach and Watershed tool and the Tau DEM Postprocessor were used within

ArcMap 10.8.1 to vectorize the stream raster grid to create a continuous streamline along the main channel (Figure 12e ).

#### 2.4.3 Bank Detection and Floodplain Analysis Calibration

The locations of bankfull riverbanks were identified using the Bank Detection and Floodplain Analysis Tool, which is part of the USGS Stream Channel and Floodplain Metric Toolbox (Hopkins, 2018). Specifically, this tool identifies the elevation of the channel banks by examining the DEM topography along cross sections placed orthogonal to the channel centerline (Figures 14f and 15). Along each cross section, the channel banks were placed where the channel expands onto the floodplain, causing a sudden decrease in bank slope. In multithreaded reaches, bankfull locations were only identified for the primary channels. All geospatial processing was completed in ArcMap 10.8.1.

The Bank Detection and Floodplain Analysis Tool required the selection of several parameters for each cluster. The first parameter, channel cross section linear fit, was used to create cross sections along the previously generated streamline. Large values of this parameter will result in smoother cross sections that are less sensitive to channel meanders. A value of 30 meters was used for each of the 13 clusters. Values larger than 30 meters resulted in cross sections being placed diagonally on meander bends, and values lower than 30 meters resulted in cross sections placed diagonally on straightened channels. The next parameter, channel cross section length, was used to determine the length of each of the cross sections used to identify bank locations. The channel cross section length was set to 25% greater than the largest field bankfull measurement for each cluster. The next parameter, point spacing between cross sections, is the spacing of points along each cross section, used to extract DEM elevation values.

This metric is based on the resolution of the DEM. The resolution of all DEMs was 0.7 meters so the spacing was set to 0.7 meters. The next parameter, slope break vertical increment, was set based on the vertical accuracy of the DEM which was 0.1 meters for all clusters. This parameter sets the vertical interval at which the slope break is evaluated at each cross section. The next parameter, spacing between cross sections, sets the interval between cross sections. Based on preliminary investigation, a value of 4 meters was found to be the smallest spacing (highest spatial accuracy) that did not produce computer memory issues. Values lower than 4 meters resulted in a substantial increase in the number of cross sections returned resulting in memory issues. A value of four meters was selected for all clusters.

The next parameter, the bank detection slope break ratio, is utilized to identify the location of breaks in the channel banks at each vertical increment. This is achieved by comparing the width of the channel at a given increment to the width of the channel at the next higher increment. If the ratio of these two widths is greater than the slope break ratio value, then the tool will search for a slope indicating the location of a slope break (Figure 13). Larger values of this parameter require greater changes in channel width to identify channel banks. Preliminary investigation determined that values less than 0.25 meters or greater than 2 meters produced unreasonable bank positions.

The next parameter, the bank detection slope break percentage, is used to identify the specific locations of the channel banks by measuring the slope between points along the cross section. To determine this parameter, the vertical change detected from the slope break ratio is divided by the difference between the width values and the resulting value is multiplied by 100 to obtain the slope as a percentage (Figure 13). If the slope percentage exceeds the user-specified

value, the tool will identify the points as the channel banks. The USGS toolbox manual recommends values between 1% and 7%.

As discussed above, the optimal values of many of these parameters (including the spacing between cross sections, point spacing along cross sections and channel slope break vertical increment) are solely based on the quality and resolution of the DEM. Other parameters (channel cross section length and channel cross section linear fit) can be set based on the characteristics of the river. The remaining two parameters (bank detection slope break ratio and bank detection slope percentage) could not be determined prior to the bank determination process and were instead selected based on model calibration and validation (see below) for each of the thirteen clusters.

#### 2.4.4 Calibration Model and Data

Calibration techniques were used to find the best values for two model parameters (bank detection slope break ratio and bank detection slope percentage) by comparison to field bankfull width measurements. Of the 88 high-quality field measurements of bankfull width, 60% (chosen randomly within each reach) were used to calibrate the model between the thirteen different clusters. More specifically, the Bank Detection and Floodplain Analysis Tool was used to find the bankfull widths along each of the thirteen clusters with each of ten different bank detection slope break ratio values ranging from 0.25 to 2.0 meters while the slope break percentage was fixed at 3%. Separately, the same tool was used to find bankfull widths along each of the thirteen clusters with each of seven different integer values of the slope break percentage chosen from the interval 1-7%, while the slope break ratio was held constant at 1 meter.

A python script was used to evaluate bankfull width output. All scripting was completed in python version 2.7. The script calculated the following three metrics for each of the various candidate bank detection slope break ratio values and the bank detection slope break percentage parameter values for each cluster. First, the script determined the number of widths greater than zero, which represents the number of widths generated using remote sensing for a particular cluster. Second, the script calculated the number of reasonable widths, which were remote sensing widths that fell within the range of 25% less than the smallest field measurement and 25% greater than the largest field measurement for each of the clusters.

Third, the script matched up each field width measurement to the remote sensing values by spatially joining the field GPS point to the three closest remote bankfull widths, then finding the average of the three remote widths. The script then calculated the RMSE between the field and remote bankfull widths for each cluster:

$$3) \text{ RMSE (m)} = \frac{1}{N} \sqrt{\sum_{i=1}^N (F_i - P_i)^2}$$

where  $F_i$  indicates each field bankfull width,  $P_i$  indicates the average of the three closest remote bankfull widths identified using a spatial join and  $N$  is the total number of observations for each cluster. The normalized RMSE was also calculated for each of the clusters:

$$4) \text{ Normalized RMSE} = \frac{\text{RMSE}}{F_{max} - F_{min}}$$

where  $F_{max}$  represents the maximum field bankfull width measurement and  $F_{min}$  the minimum field bankfull width measurement for each cluster. The normalized RMSE makes it possible to compare rivers of vastly different sizes.

### 2.4.5 Validation

The optimal values of the slope break threshold ratio and slope break percentage parameters for each cluster were selected as the parameter values that resulted in the lowest RMSE value along with the highest number of returned widths and the highest number of reasonable widths. The 37 field bankfull width measurements from the calibration dataset were compared to the average of the three closest remote widths generated using the optimal parameter values for each cluster. RMSE calculated from the 37 validation widths was considered to be an independent check on model performance.

## 2.5 Statistical Analysis

### 2.5.1 Comparing Field, Remote and Regression Widths

A comparison of field, remote, and regression widths was conducted to assess the accuracy of the remote sensing and regression approaches in estimating bankfull width. High-quality field bankfull widths were plotted against both the remote widths and the widths from bankfull regression (Equation 1). Using the SciPy stats suite in python, both ANOVA and Tukey's Honestly Significant Difference (Tukey's HSD) tests were used to quantify method effectiveness and accuracy of these methods compared across throughout study rivers. A Tukey HSD compares the pairwise differences between all possible combinations of group means to the HSD, which is calculated by multiplying the critical value based on the number of groups compared by the standard error. If the pairwise difference exceeds the HSD, then the two means are significantly different. Tukey tests are a conservative statistical test, meaning they are less likely to detect a significant difference between datasets as well as less likely to identify false positives.

### 2.5.2 Evaluating the Influence of Bed and Bank Material on River Width

Bankfull river widths from remote sensing were compared in order to evaluate the influence of bed and bank materials. Using the SciPy stats suite in python, both ANOVA and Tukey's HSD tests were used to compare field bankfull widths among both bed and bank substrates. Field bankfull widths were compared to bank material and bed material at that location. At the reach scale, average remote sensing bankfull widths were compared to the reach-scale assessment for bank and bed substrates. When bank materials differed on the left and right banks, the larger of the two grain sizes was used for analysis.

The influence of substrate material was assessed on both unnormalized and normalized bankfull widths. Widths were normalized to enable comparison of the influence of substrate material among river reaches of vastly varying sizes. Normalization was accomplished by dividing each of the bankfull field and remotely sensed widths by the corresponding widths from regression based on watershed area:

$$5) \text{ Normalized Width} = \frac{F_i}{R_w}$$

where  $F_i$  represents the field bankfull width measurement and  $R_w$  the bankfull width from the regional regression equation (Equation 2). The normalized width makes it possible to compare reaches of different sizes.

### 2.5.3 Assessing Longitudinal Variation in Bankfull Width

Prior to evaluating spatial trends in bankfull width for each of the six study rivers, a longitudinal smoothing filter was used to reduce the noise in the data generated from the automatic bankfull detection tool, while retaining the natural spatial variability of these alluvial rivers. The Savitzky-Golay filter was chosen for smoothing because it preserves the shape of the

data without producing distortion (Savitzky and Golay, 1964). The specific window size of the filter was selected based on the size of the river. A window size of 41 was used for larger rivers such as the Ammonoosuc, Sugar and Lamprey Rivers, while a window size of 31 was used for the Stevens Branch, Cocheco and Dog Rivers. A polynomial order of two was used for all six study rivers. While the polynomial order chosen was low, it managed to capture large variations in bankfull width resulting from various features such as dams and gorges. This method ensured that both anthropogenic and natural interferences could be accounted for while also producing a smooth line characterizing changes in bankfull width along the river.

## Chapter 3 Results and Discussion

### 3.1 Remote Sensing of Bankfull Width

#### 3.1.1 Calibration Results

Estimated bankfull widths from remote sensing were compared to the 57 high-quality field measurements within the calibration dataset using multiple candidate values for the slope break ratio and slope break percentage parameters. The optimal slope break ratio value for all clusters was one or less (Table 2); slope break ratio values greater than one meter resulted in a monotonic decrease in both the number of widths obtained and the number of reasonable widths, and an increase in the RMSE value (Appendix B). Since there was no improvement for decreasing the slope break ratio below one, a slope break ratio of one was selected for all reaches. The optimal slope break percentage value, selected to minimize RMSE without a large reduction in the number of returned points and the number of reasonable points, varied between 1% and 7% between different clusters (Appendix B). In general, optimal values of this parameter were higher for clusters with steeper banks (Table 2). Overall, the calibration bankfull widths had a RMSE value of 5.11 meters, and 51% of remotely sensed calibration widths were within 2.95 meters of the field measurements (Figure 14).

#### 3.1.2 Validation Results

Following calibration to determine optimal model parameters, the remote sensing algorithm with optimal parameter values were used to determine the bankfull width throughout the study rivers. Comparison of remotely sensed bankfull widths to 37 validation field measurements revealed an RMSE of 6.77 meters. Only 46% of widths estimated during

validation were within 2.95 meters of the field measurements (Figure 15). Remote sensing widths from validation tended to be less accurate than remote sensing widths from calibration due to parameter selection being finely tuned to match the calibration measurements in the dataset (Bessar et al., 2020). Regardless, the independent validation process revealed reasonable agreement between the remote sensing estimates and field measurements.

### 3.1.3 Bankfull Widths from Remote Sensing, Field Measurements and Regression

Automatic bankfull detection from remote sensing was used to obtain 26,800 bankfull width measurements along 134 km of study rivers, which were processed in thirteen different clusters. Following the completion of calibration, analyst involvement was minimal in the processing of each cluster. Combining data from all clusters, the remote bankfull widths closely matched measurements collected in the field. Estimated error on the field measurements was 2.95 meters. Of the combined calibration and validation remote bankfull widths, 49% were within 2.95 meters of field measurements (Figure 16).

The RMSE between each of the clusters varied, with the Stevens Branch having the smallest RMSE of 2.95 meters (Table 3). However, the Stevens Branch had the highest normalized RMSE due to its small width (Table 3). Previous studies have suggested that bankfull detection from remote sensing is most successful when river width is at least ten times the resolution of the DEM (De Rosa, 2019), a condition that is violated for the Stevens Branch, which has a DEM resolution of 0.7 meters and is narrower than 7 meters in multiple locations.

The Massachusetts regression equation results in widths that are too wide in large rivers and too small in small rivers is consistent with the 2005 New Hampshire provisional curves, which results in widths that are wider than the MA curves for drainage area greater than 10

square miles and smaller for drainage areas less than 10 square miles (Bent and Waite, 2013). An RMSE value of 10.13 meters was found between the field bankfull widths and the values derived from the regional equation (Equation 1). Only 16% of the regressed bankfull widths were within 2.95 meters of field widths (Figure 17 and Figure 18). In addition, there was a significant difference between remote and regressed bankfull widths evaluated at the location of field measurements ( $p < 0.1$ ). Regression relationships are the least accurate method of estimating bankfull width for study rivers, though they may be appropriate in channelized portions of rivers free from anthropogenic influences and human development (Anning, 2011). Previous studies have also found that New England regional regression equations tend to be less accurate than other regions throughout the United States (Bieger et al., 2015).

## 3.2 Bankfull Width for Study Rivers

### 3.2.1 Ammonoosuc River

The Ammonoosuc River had the highest average field width, highest remote width and the largest regression width among the study rivers (Table 4). In general, bankfull widths on the Ammonoosuc increased downstream, illustrating the positive relationship between drainage area and bankfull width (Figure 19). Bankfull widths on the Ammonoosuc were locally increased upstream of three large dams. For example, the largest bankfull width on the Ammonoosuc is located in one of the middle reaches above the Lisbon Dam (Figure 20).

### 3.2.2 Cocheco River

The Cocheco River had the second smallest field width, remote width and regression width (Table 4). Only the upper and middle reaches of the Cocheco were assessed, so the river

tended to be relatively narrow (Figure 21). In general, widths were smallest in the bedrock reaches in the headwaters, then increased moving downstream into the alluvial middle reaches (Figure 22). Regressed bankfull widths tended to be more than five meters higher than both the remote and field values (Table 4), possibly due to regression equations not accounting for the steep and rocky conditions in the upper Coheco.

### 3.2.3 Dog River

The Dog River exhibited a large variation in bankfull width (Figure 23). Most reaches in the Dog River had an average bankfull width of 35 meters, slightly increasing in size as the river flows into the Winooski. Large widths were present upstream of the Northfield Mills Dam and the bedrock gorge in M19; the smallest widths of approximately 8 meters were found within the bedrock gorge (Figure 24). The regressed bankfull widths tended to be more than 5 meters higher than both the remote and field values (Table 4), likely due to the complex nature of the Dog River.

### 3.2.4 Lamprey River

The majority of assessed reaches of the Lamprey River had similar geomorphic composition. The average regression, remote and field bankfull widths were all within a meter of each other for the Lamprey River (Table 4), likely due to the relatively stable nature of the Lamprey, as well as the fact that the Lamprey River had the most recent DEM data from 2019 and therefore the shortest interval to the 2022 field assessment. The Lamprey River's longitudinal profile reveals the river slowly increases in size as it flows downstream, with

smaller fluctuations compared to other study sites (Figure 25). Reaches upstream of the Wiswall Dam impoundment are wide, then width decreases downstream of the dam (Figure 26).

### 3.2.5 Stevens Branch

The Stevens Branch longitudinal profile illustrates bankfull width slightly increasing downstream (Figure 27). Since only 7 km was assessed, width was not observed to substantially change (Figure 28). No dams were included in the assessed reaches, but the watershed had the most development. The Stevens Branch had the second largest difference between regression and field bankfull width despite being the smallest study river (Table 4). Simple regression equations cannot account for local geomorphology and sediment characteristics, thus leading to a large discrepancy between estimated widths.

### 3.2.6 Sugar River

The Sugar River's longitudinal profile illustrates a highly variable river, with bankfull widths as high as 80 meters upstream of the hydroelectric dams in Newport, NH, with widths decreasing to as low as 15 meters directly below the dams (Figure 29). Width then increased slightly through the rest of the assessed reaches (Figure 30). The Sugar River had the largest difference between regression and field bankfull widths among the six study rivers (Table 4). This was possibly due to a large number of multithreaded channels and therefore mismatch between field measurements, which focused on the larger channel, and regression equations, which provided the sum of all channels.

### 3.3 Effect of Bed and Bank Substrate on Bankfull Width

Bankfull width varied spatially within and among the study rivers, but substrate material was not observed to control this variability. Bed and bank substrate materials were compared to unnormalized and normalized bankfull width both at field measurement locations and at the reach scale (Appendix A). At the reach scale, no significant relationships were found between reach-averaged remotely sensed bankfull width and both bed and bank substrate ( $p > 0.05$  for all rivers).

At field measurement locations, no significant relationships between bank material and width were found. No significant relationships were found between bed material and width for five out of the six study rivers. Significant differences were found in both unnormalized bankfull width and normalized bankfull width among different bed substrates in the Ammonoosuc River. Specifically, the unnormalized bankfull width of sandy reaches was higher than boulder reaches within this river (Appendix A;  $p=0.0127$ ). The normalized bankfull width of sandy reaches was larger than bedrock or boulder reaches within this river (Appendix A;  $p=0.009$  and  $p=0.02$ ).

Previous studies have found an inverse relationship between bed substrate size and river width, typically because bed material becomes finer downstream where widths are generally higher (Costigan et al., 2014). However, the two largest bankfull widths on the Ammonoosuc are located near the Lisbon Dam impoundment, which is located in the middle of the assessed portion of the river but happens to be one of the few sandy locations on the river.

### 3.4 Spatial Variability in Bankfull Width

Bankfull widths exhibited large spatial variability over short longitudinal distances. Some variability resulted from anthropogenic sources such as impoundment construction and bank

armorings (Figure 31). Variability was also found in natural reaches as a result of river meander processes (Figure 31). It is likely that methodological limitations contributed to the fine-scale variations, but spatial variability in bankfull width was still present in all six study rivers even after smoothing. Sub-reach-scale variability in width is not detectable in sparse field measurements and is only revealed through the continuous measurements possible with remote sensing. Regression equations also cannot account for this spatial variability, because they do not include anthropogenic influences such as dams as well as natural heterogeneity from bedrock geology.

The largest observed influence on the bankfull width was artificial dams, which caused a local increase in widths in upstream impoundments (Figure 32). Average bankfull widths were larger upstream of dams when compared to downstream ( $p = 0.03$ , Table 5). In other studies, impoundments have also been shown to create an artificial increase in bankfull width (Casado et al., 2016). Natural changes in bed control, such as bedrock gorges, also contributed to changes in bankfull width.

## Chapter 4: Conclusion

### 4.1 Automatic Bankfull Width Detection in New England

This study produced reasonable, remotely derived bankfull widths for six different rivers throughout New Hampshire and Vermont. Bankfull widths were estimated for 134 river kilometers with more accuracy than possible with regional regression equations. This study found that remotely derived bankfull widths are comparable to field bankfull widths among several types of rivers, bed material and bank material in New England. This thesis did not find many strong relationships between width or normalized width among various bed and bank materials, likely due to the small number of field measurements and the coarse resolution of the reach-scale data. Results from this study can be used by planners for both habitat assessment, river restoration, and flood model construction.

### 4.2 Method Limitations and Suggestions for Future Research

Determining bankfull width from remote sensing relies on algorithms that identify a break in slope at channel boundaries within DEMs. Natural and anthropogenic variability in river bankfull width make it challenging for any single choice of algorithm input parameters to produce reasonable values along the length of a river. Results from this thesis suggest that optimal model parameters among rivers exhibit spatial variation. Assessing model parameters on shorter reaches would require more field validation and more computational resources but would most likely lead to a more accurate output.

New England has complex and highly variable geology, geomorphology and anthropogenic influences, resulting in more varied widths than other regions with simpler

geology and minimal human development. Regions that contain rivers with clearly defined banks, without wetlands and bedrock outcrops, are likely to be especially amenable to the remote determination of bankfull positions. Further study is warranted in order to compare bankfull widths between LiDAR and field-based measurements outside of New England regions, as it would be valuable to understand the similarities and differences at the regional scale.

Validation of remote sensing estimation of river widths was performed by a comparison to field width observations, which are also prone to error. Uncertainty inherent in field bankfull width measurements depends on the reliability of the bankfull indicator as well as the particular equipment used to take the measurement (Johnson and Heil, 1996). Rangefinders tend to be more accurate than traditional measuring tape. However, most rangefinder uncertainty increases with distance due to both the equipment error as well as the influence of a slight change in the angle of the shot. In this study, field error was minimized by choosing measurement locations with strong bankfull indicators in confined reaches where floodplain access was minimal. Only one field measurement was obtained at each location, though it is recommended that future studies average together multiple field bankfull measurements at each location. In addition, a hypsometer rangefinder could be used to determine the slope of the banks in the field. A hypsometer rangefinder is capable of calculating the height difference between the top and bottom of the bank, as well as the horizontal distance, enabling the generation of bank slope values for each bankfull field width measurement.

Neither remote sensing nor field measurements can reliably estimate bankfull channel characteristics in regions where the bankfull channel is poorly defined. Areas with poorly defined banks such as wetlands and bedrock outcrops already have high uncertainty associated with field bankfull widths due to the subjectivity associated with weaker bankfull indicators. In addition,

these poorly defined banks are challenging to detect on DEMs, resulting in inaccurate bank point placement.

In areas with rapid channel change or avulsion, bankfull widths change over time so cannot easily be compared between measurements obtained at different times. In particular, if notable change has occurred along a river between the time of field data collection and LiDAR acquisition, then the field measurements do not provide an appropriate validation for the remote sensing data. In this study, field measurements were only used for calibration and validation in regions where limited channel change was observed. In future studies, it is suggested that field surveys be conducted simultaneously with LiDAR collection.

The use of LiDAR is a relatively new technology that has only recently been made available for large swaths of New England. So far, few watersheds have repeat LiDAR datasets. Moreover, where historic LiDAR data exist, resolution and quality are poor. For example, a LiDAR dataset for the Stevens Branch is available from 2008, but this previous LiDAR was poor quality (Q3) and the resulting DEM had 3-meter resolution, which was too coarse to evaluate bankfull width on the narrow Stevens Branch. Future studies will have greater access to repeated high resolution LiDAR datasets and therefore will be able to evaluate channel change over time.

High-resolution topography collected using UASs could supplement the current poor temporal resolution between aerial LiDAR flights. High-resolution topography from UASs includes visual (typically structure-from-motion) techniques in regions with limited bank vegetation and clear sight lines, or UAS-mounted LiDAR systems (Jugie et al., 2018; Palace et al., 2018). Repeat high-resolution UAS topography could also be used investigate short-term channel change in a limited reach, such as change during a dam removal or in response to a forecast flood. While the use of UASs could increase both the spectral and temporal resolution of

high-resolution datasets, UAS battery technology currently limits their range to only a few square kilometers.

Higher resolution DEMs generated from UASs would increase the computing cost of the USGS toolbox. Thus, decreasing the number of widths generated from each cluster making the toolbox's ability to generate continuous widths along a river negligible. However, higher resolution DEMs would most likely result in more accurate bankfull width measurements. Previous studies have found that higher resolution DEMs resulted in more accurate flow directions and channel placement thus leading to more accurate bankfull width measurements (Hernández et al., 2022).

Bankfull widths extracted from LiDAR-derived DEMs complement methods based on visual imagery. LiDAR-derived DEMs have been found to be more reliable for estimating bankfull width than visual techniques that use RGB imagery to detect bankfull (Li et al., 2021). LiDAR pulses can penetrate vegetated areas, enabling slope-break detection algorithms to identify bankfull conditions in areas that traditional visual techniques cannot. However, the historical record of RGB imagery is longer and has a higher temporal resolution, enabling the detection of long-term changes in river width. Bankfull widths delineated manually from aerial imagery can be used to provide important historical context for studies of modern channel change (Yang et al., 2019).

This study was limited in its comparison between bankfull width and bed and bank materials by the limited number of available point measurements and the coarse resolution of reach-scale substrate assessment. No significant difference was found between the various bed and bank materials and the average bankfull width on the reach scale. Only one significant relationship was observed between substrate and bankfull width at the point scale. It is likely that

the high variability in substrate within each reach limited the ability to quantify the influence that bed and bank material had on width. Future work could include greater amounts of field measurements to characterize substrate material within a river reach. In addition, remote sensing of grain size distribution holds great promise for producing high-resolution maps of bed and bank materials, which could elucidate the relationship between width and substrate material (Caruso et al., 2019).

#### 4.3 Contributions to River Science

Bankfull measurements generated from remote sensing techniques can provide continuous width measurements throughout river corridors. With the increase in accessibility of high resolution DEMs throughout the world, automatic bankfull width detection is more relevant than ever. Instead of using highly inaccurate regional bankfull regression equations, automatic bankfull width detection from LiDAR-derived DEMs can provide a more accurate baseline for traditional stream restoration projects and habitat assessment. While remote sensing tools and techniques are not a replacement for traditional field surveys, these measurements can augment widely spaced field measurements, as well as provide baseline information for rivers lacking field data. The ability to obtain remotely derived bankfull widths from rivers of varying sizes and substrate compositions allows for effective management over multiple spatial scales by scientists, engineers, and city planners to assess aquatic habitat, restore rivers and design infrastructure.

## Figures

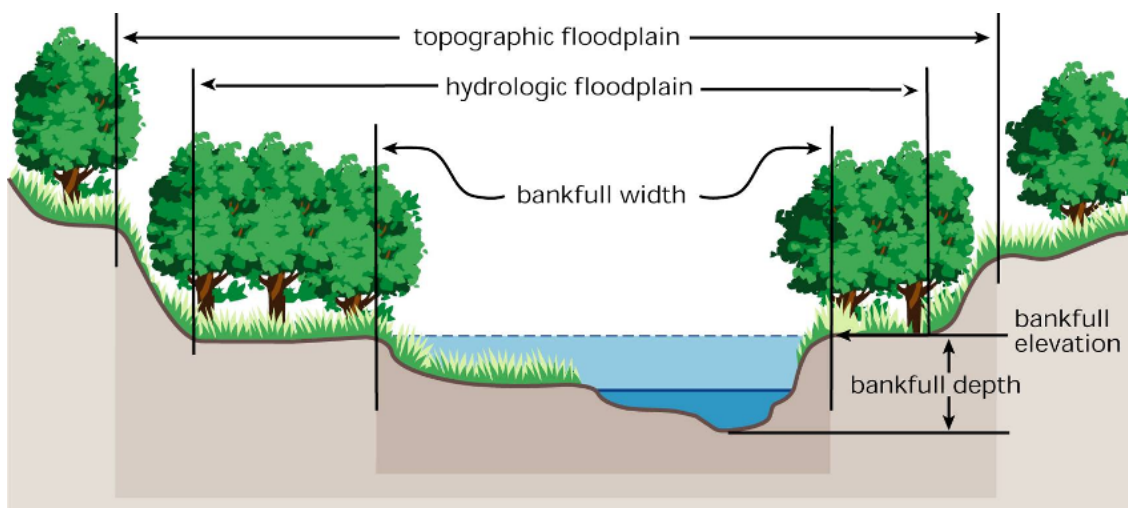


Figure 1. Typical cross section showing various hydrological measurements. Bankfull width depicted in light blue; active channel width depicted in dark blue (Federal Interagency Stream Restoration Working Group).

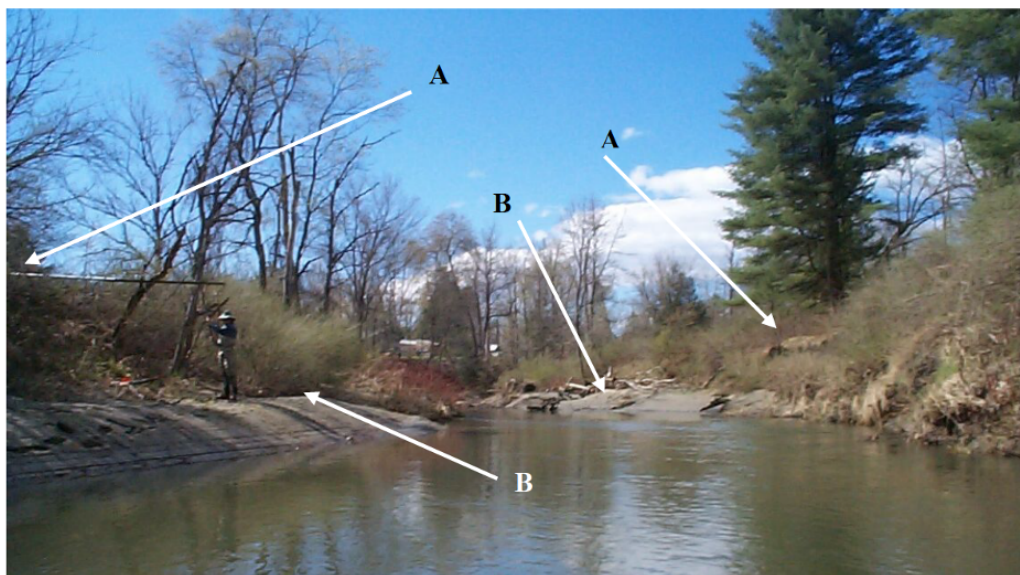


Figure 2 In the field, bankfull location is determined by the presence of permanent vegetation. Arrow A is pointing to the elevation of the abandoned floodplain above the current bankfull stage and arrow B shows the active floodplain indicating current bankfull stage (Stream Geomorphic Assessment Handbooks).

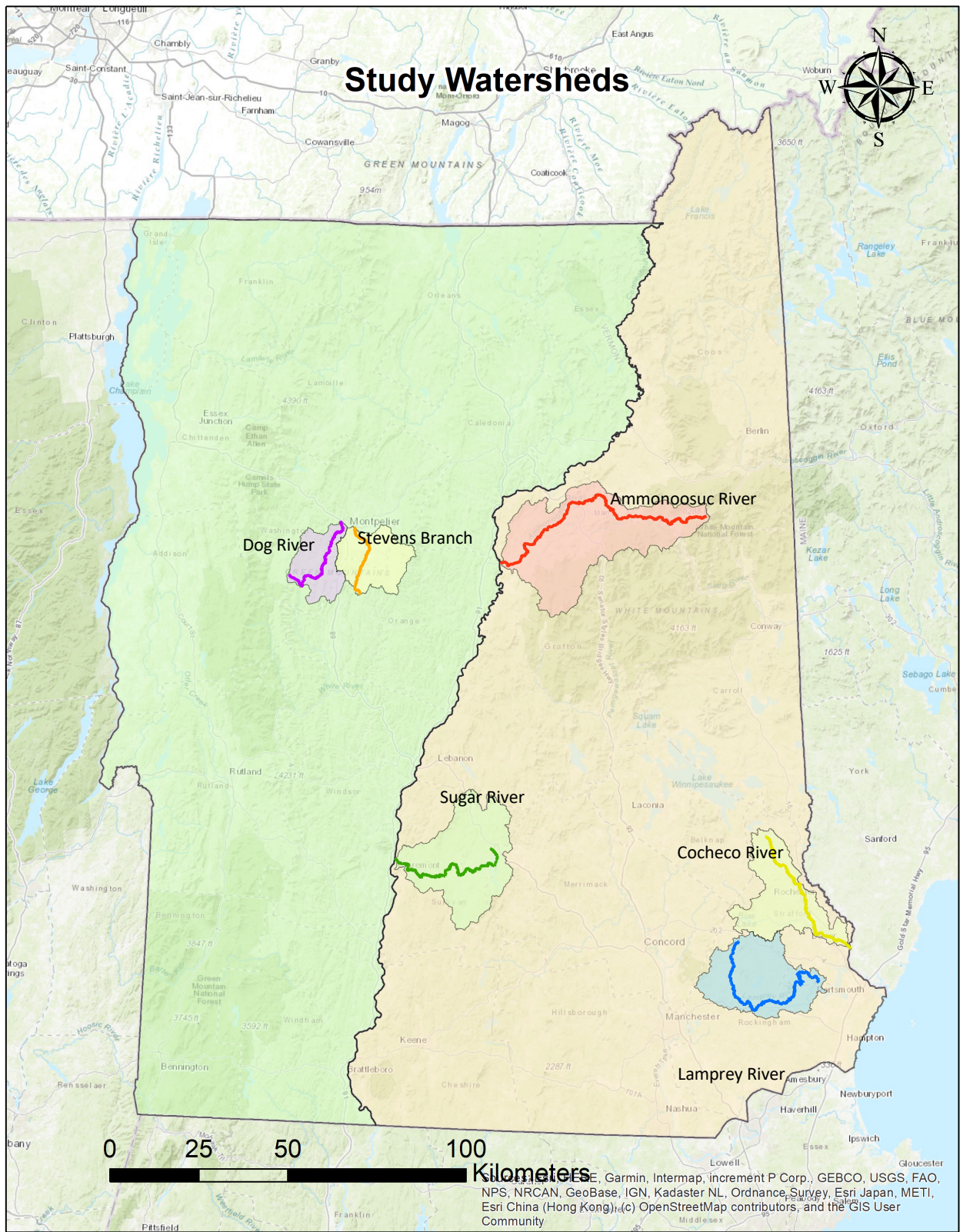


Figure 3. Study rivers and corresponding watersheds.



Figure 4. Examples of different bed and bank materials encountered on study rivers. (a) Sandy bank and cobble bed on the Dog River. (b) Bedrock bank and bed on the Dog River. Undercut sandy banks and bed Lamprey River (Bottom Left), Boulder bed and bank material Sugar River (Bottom right).

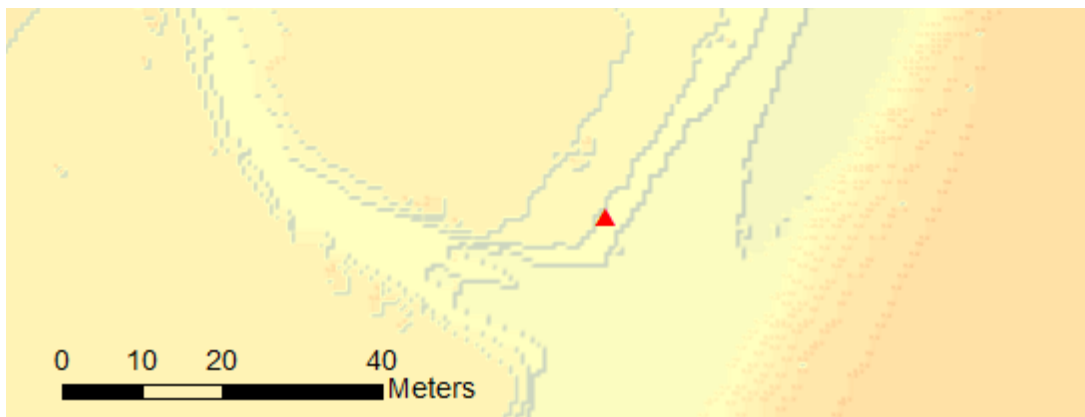


Figure 5. Example of field bankfull width measurement taken closer than 5 meters to a tributary that causes a noticeable widening in the hydro-flattened water surface, which influences cross section placement.

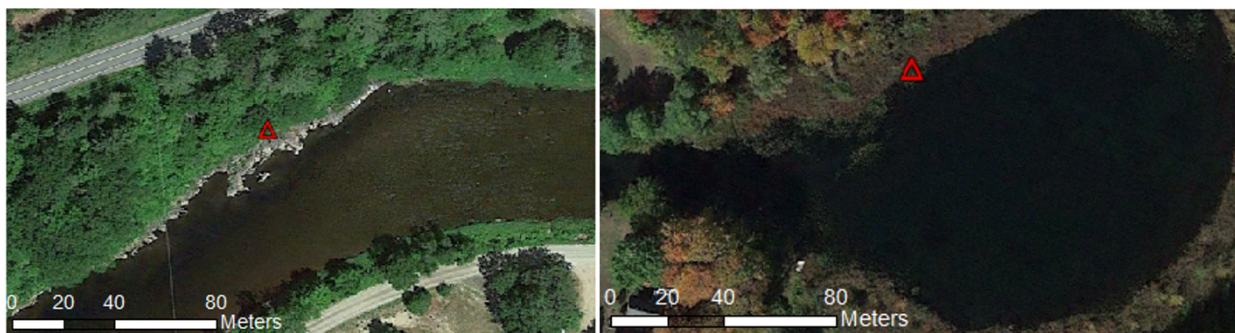


Figure 6. Example where field bankfull width measurement was taken is in a region where banks are poorly defined due to bedrock outcrop (a) or wetlands (b).

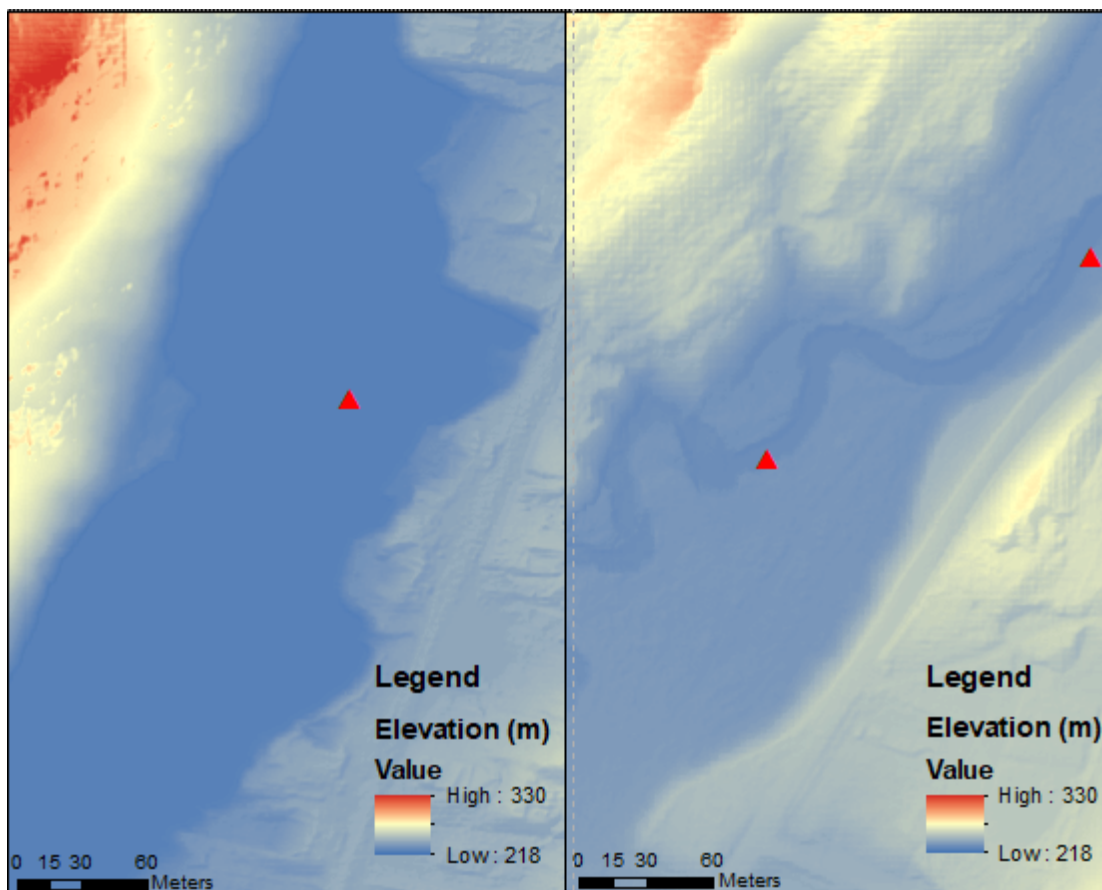


Figure 7. Example of measurement taken in location where there is a major error with hydro-flattening of the digital elevation model (DEM) for the Stevens Branch (a). Typical DEM near a bankfull measurement on the Stevens Branch (b).

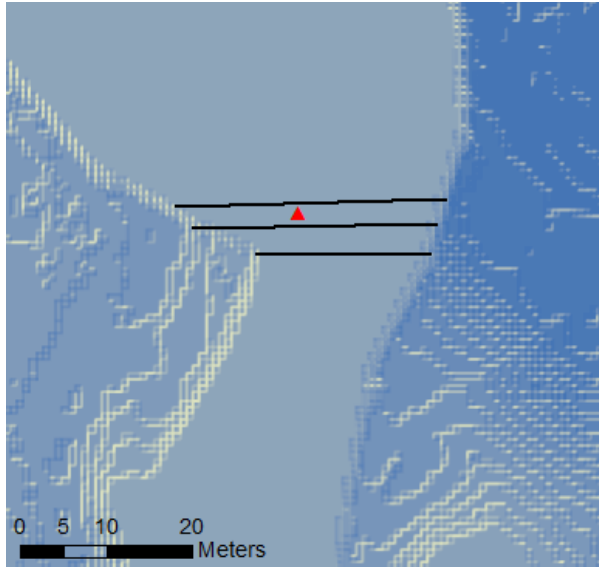


Figure 8. Example from the Lamprey River of a field width measurement obtained in a location where the bankfull width change among 3 adjacent cross sections is greater than 5 meters. Blue shading shows riverbanks.



Figure 9. Example from the Dog River of a region with rapid channel change. (a) Satellite imagery from 2015, which is close to the time of LiDAR flights for most study rivers. (b) Satellite imagery of the same reach in 2021, which is close to the 2022 field measurements, showing a change of more than 5 meters, which would lead to the exclusion of any field measurements in this reach.



Figure 10. Example from the Cocheco River of a location in which the GPS point corresponding to a bankfull width measurement is farther than 5 meters from the riverbank, likely as a result of the continuous tree cover interfering with the GPS signal.



Figure 11. Example from the Ammonoosuc River of a bankfull width measurement at a location within a multithreaded channel.

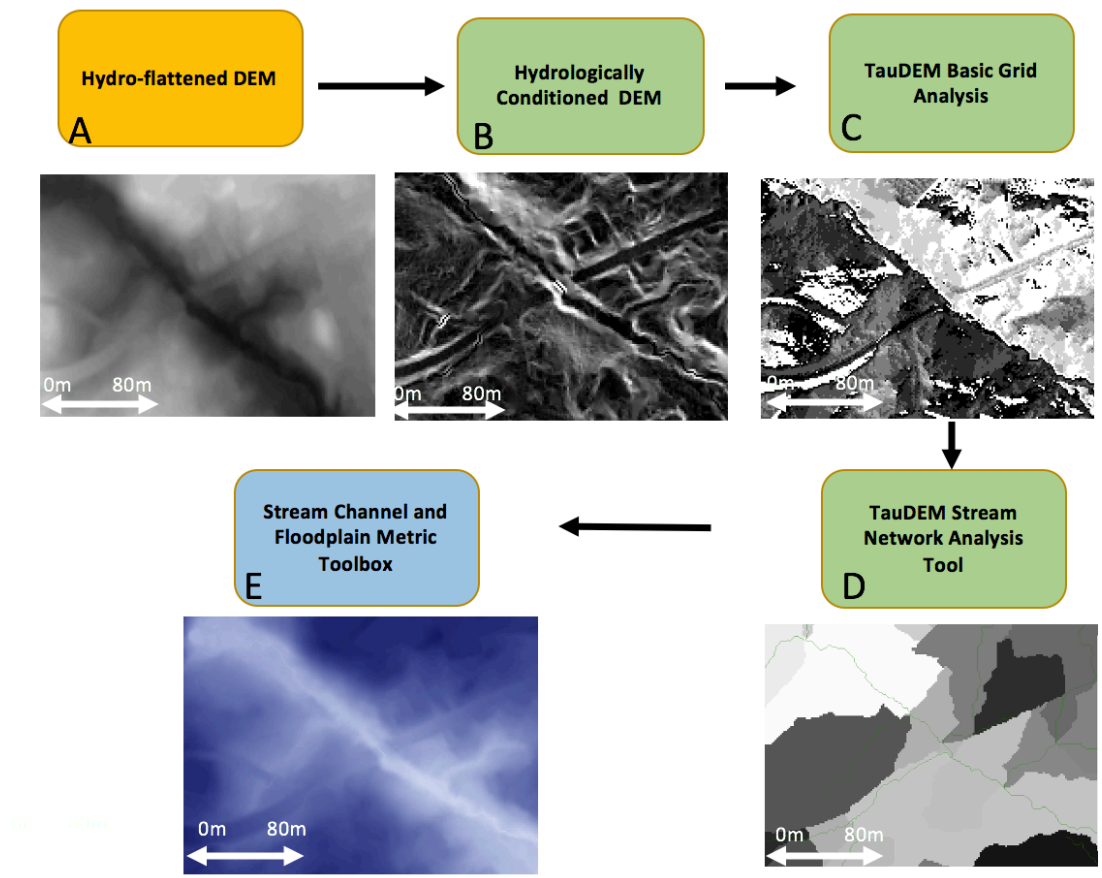


Figure 12. Outputs of GIS methods for automatic bankfull width analysis preprocessing. Hydro flattened DEM (a), Hydrologically conditioned DEM (b), D8 flow directions grid (c), conditioned stream network (d) and post processed DEM with vectorized stream network (e).

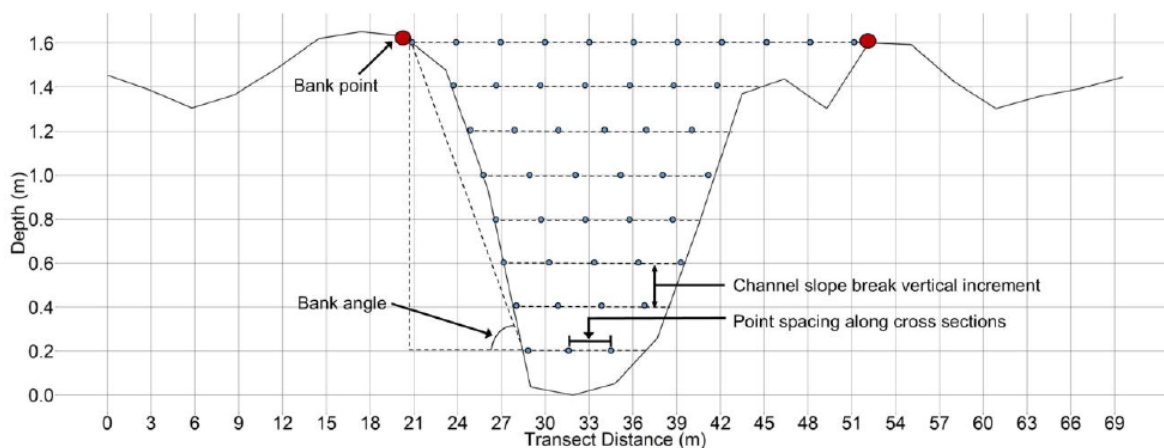


Figure 13. Example cross section used to determine the bankfull point locations within a stream channel. Bank points in red are derived from the slope break ratio and slope break percentage by dividing the width of the channel by the width of the next highest increment and searching for a slope percentage value greater than user specified value (USGS toolbox).

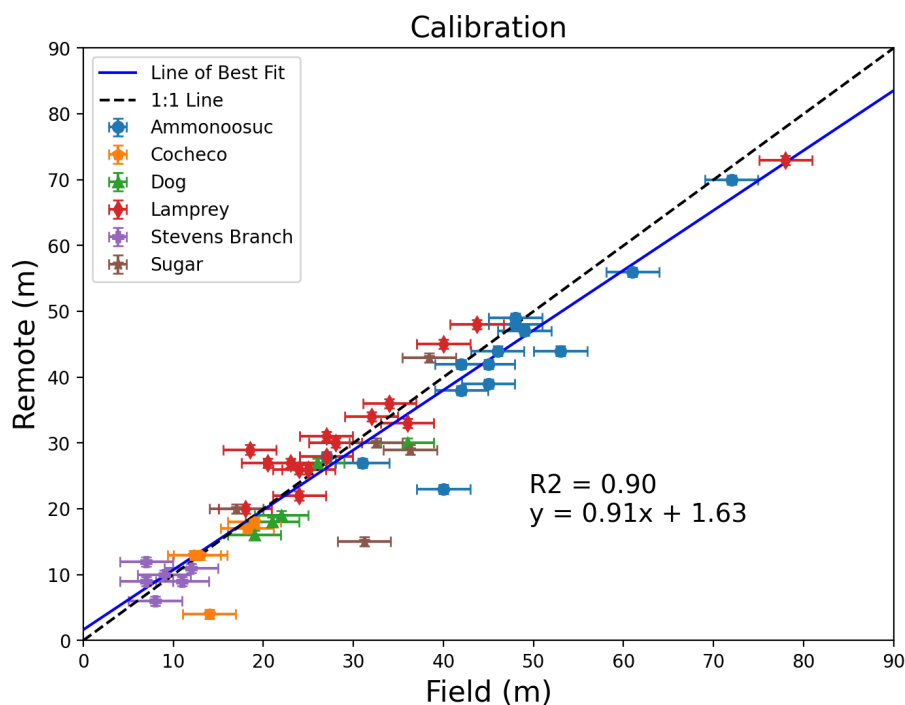


Figure 14. Field measurements of bankfull width compared to the average of the three closest remotely sensed widths for all calibration locations in all of the study rivers. The equation and squared correlation coefficient for the best-fit straight line are shown on the plot. Horizontal bars indicate field uncertainty. Vertical bars indicate resolution uncertainty.

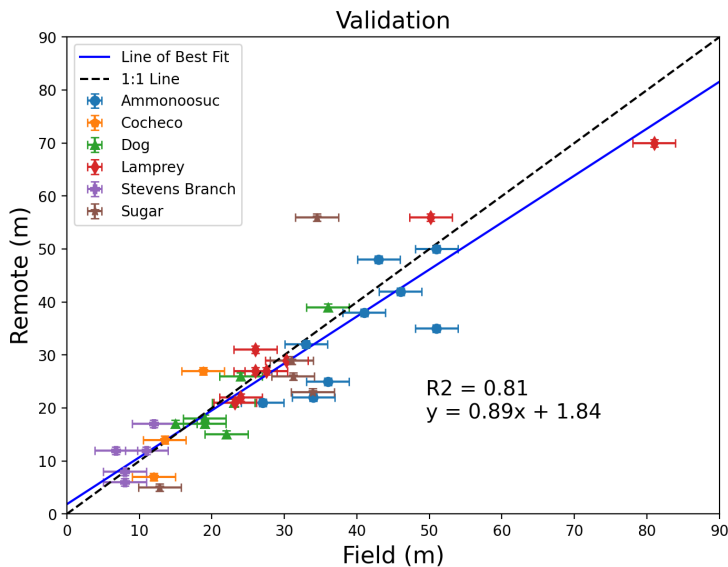


Figure 15. Field measurements of bankfull width compared to the average of the three closest remotely sensed widths for all validation locations in all of the study rivers. The equation and squared correlation coefficient for the best-fit straight line are shown on the plot. Horizontal bars indicate field uncertainty. Vertical bars indicate resolution uncertainty.

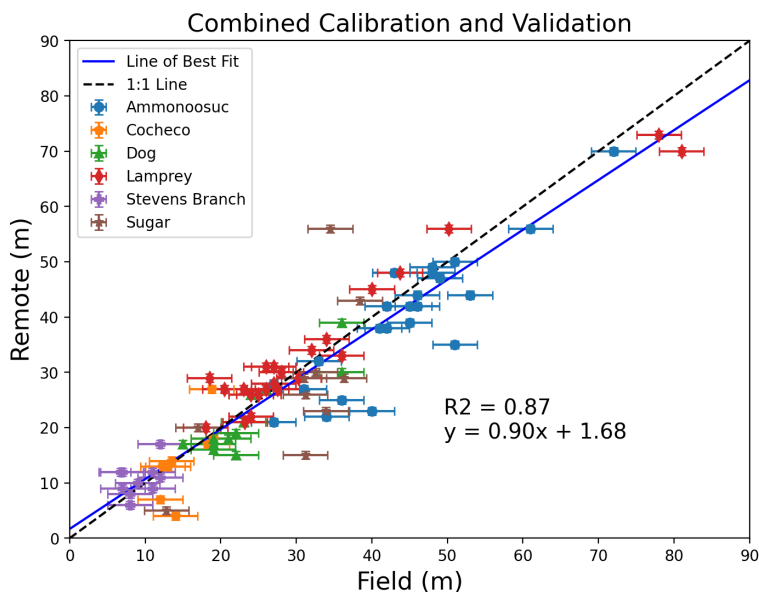


Figure 16. Field measurements of bankfull width compared to the average of the three closest remotely sensed widths for both calibration and validation locations in all of the study rivers. The equation and squared correlation coefficient for the best-fit straight line are shown on the plot. Horizontal bars indicate field uncertainty. Vertical bars indicate resolution uncertainty.

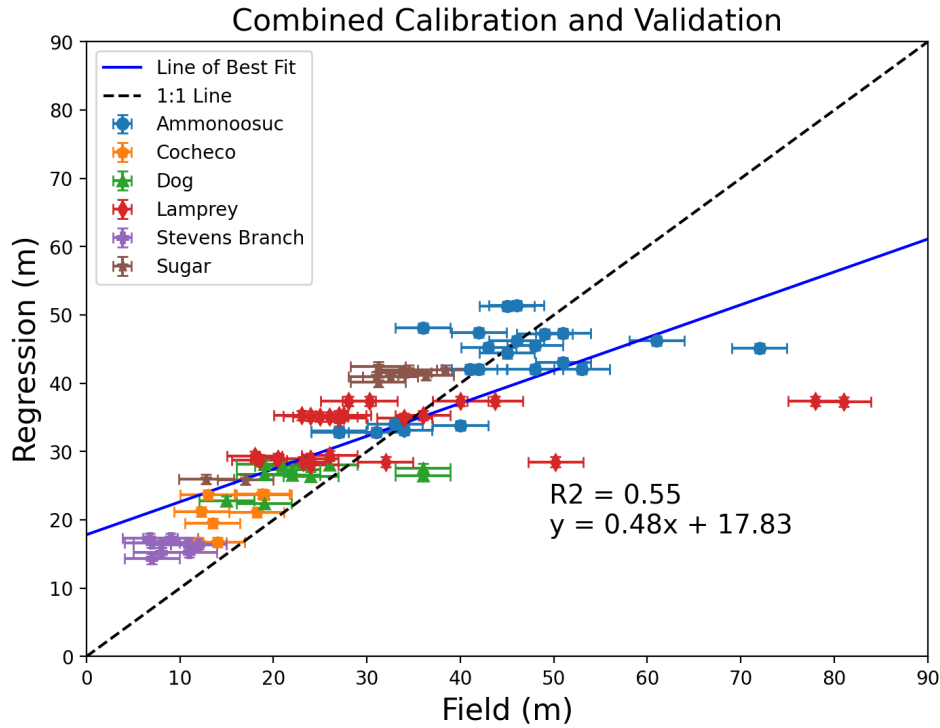


Figure 17. Field measurements of bankfull width compared to regression widths for both calibration and validation locations in all of the study rivers. The equation and squared correlation coefficient for the best-fit straight line are shown on the plot. Horizontal bars indicate field uncertainty. Vertical bars indicate resolution uncertainty.



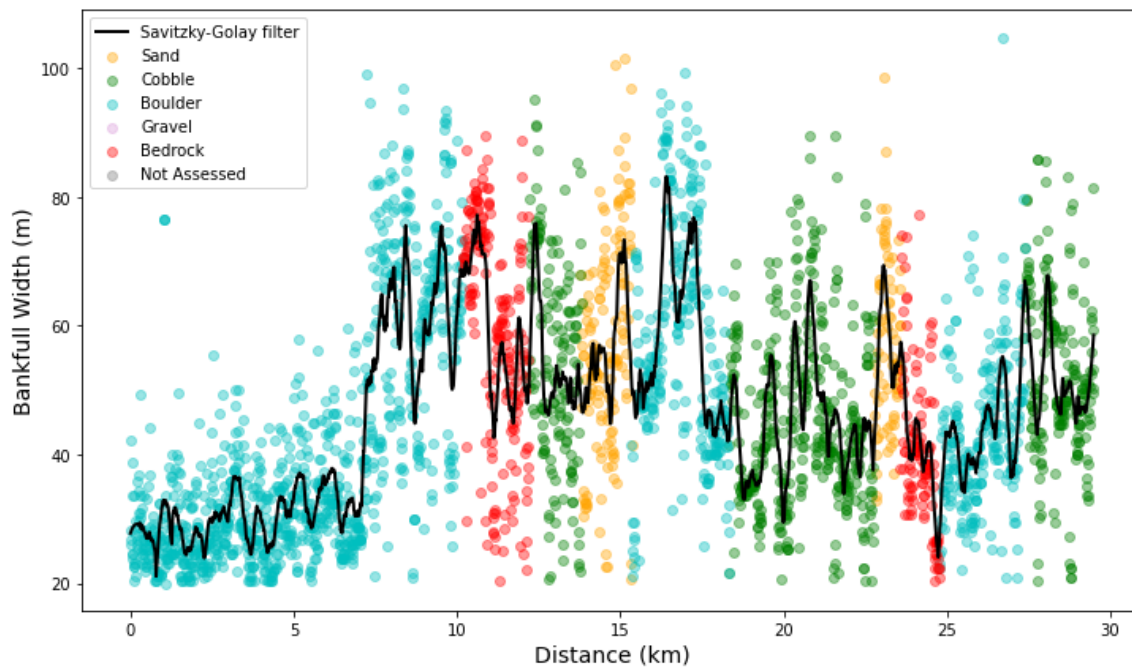


Figure 19. Ammonoosuc River longitudinal profile with raw and smoothed remotely sensed bankfull widths as a function of distance downstream of the Beacon Street Bridge, Littleton, NH. Colors indicate bed substrate.

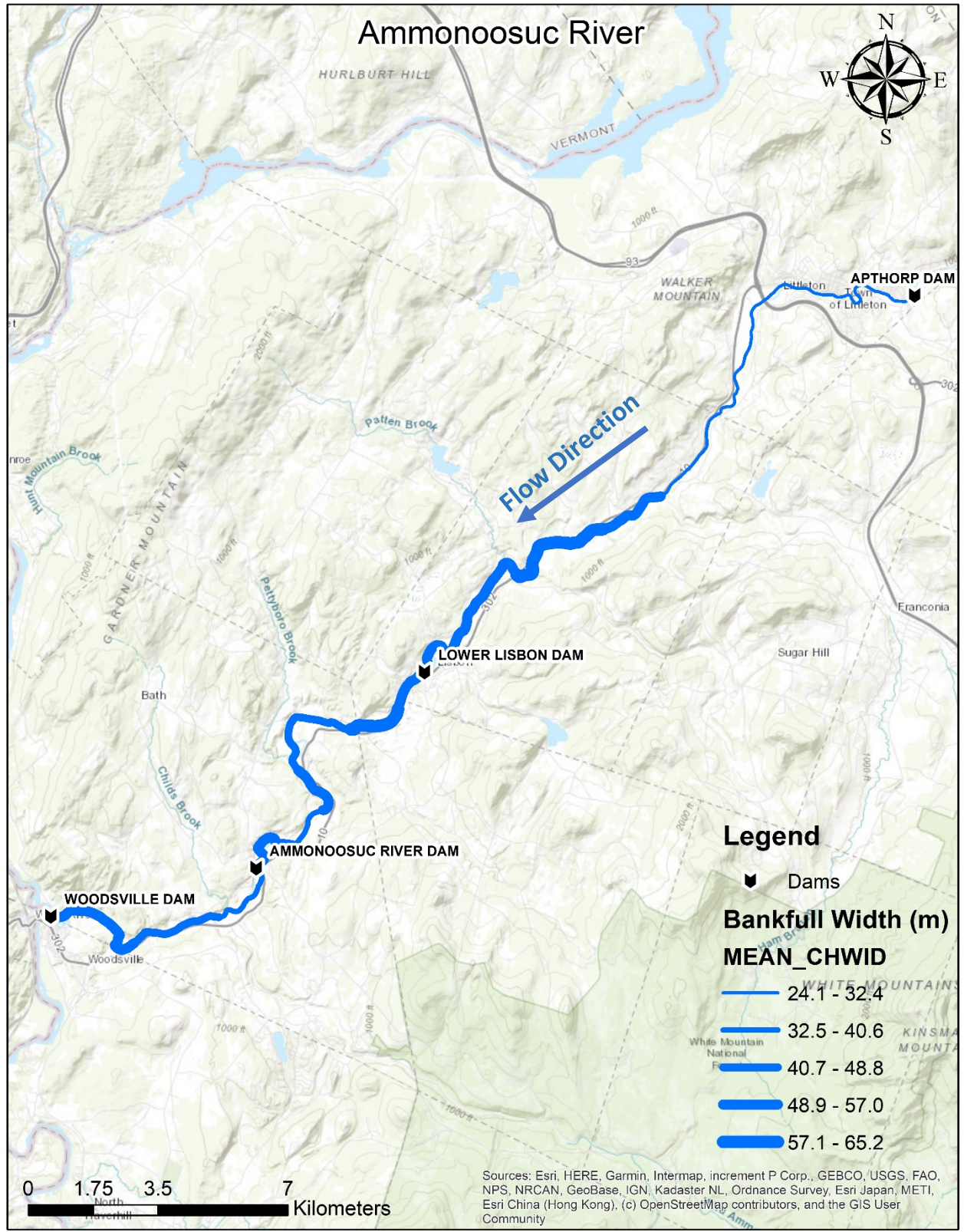


Figure 20. Mean remotely sensed bankfull width for reaches M21–M2 on the Ammonoosuc River.

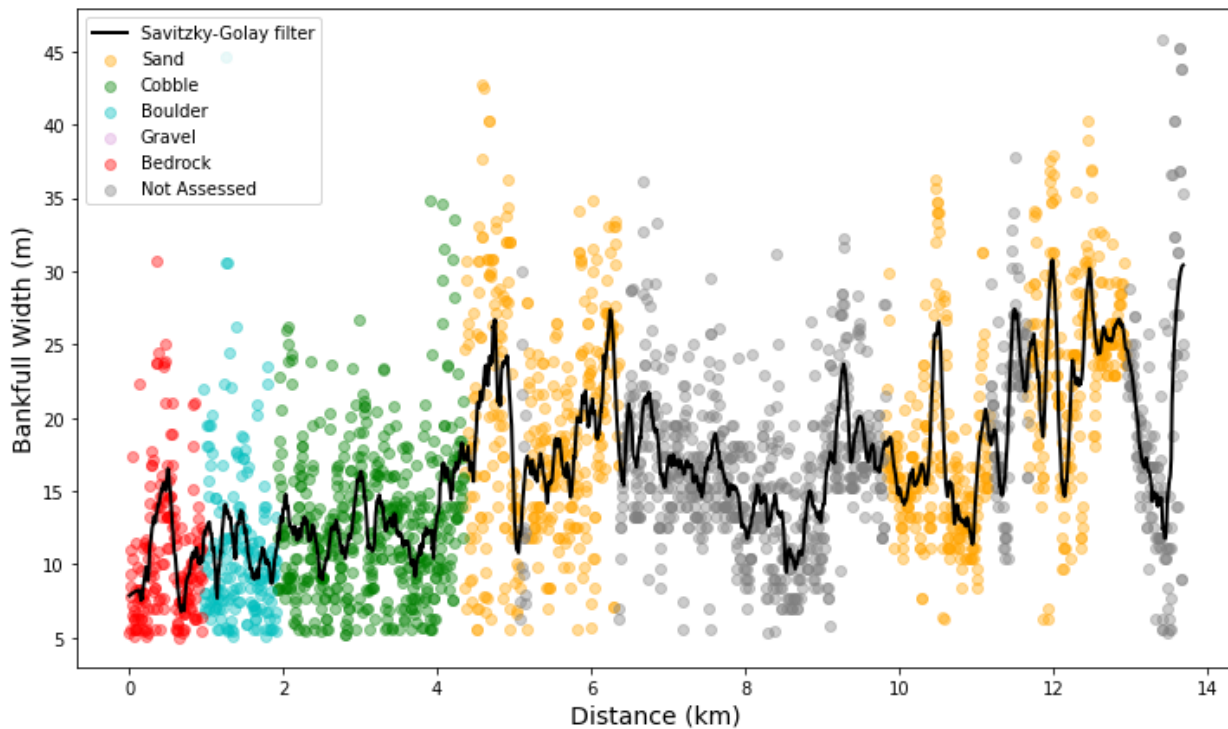


Figure 21. Cochecho River longitudinal profile with raw and smoothed remotely sensed bankfull widths as a function of distance downstream of the Bay Road Bridge, Farmington, NH. Colors indicate bed substrate.

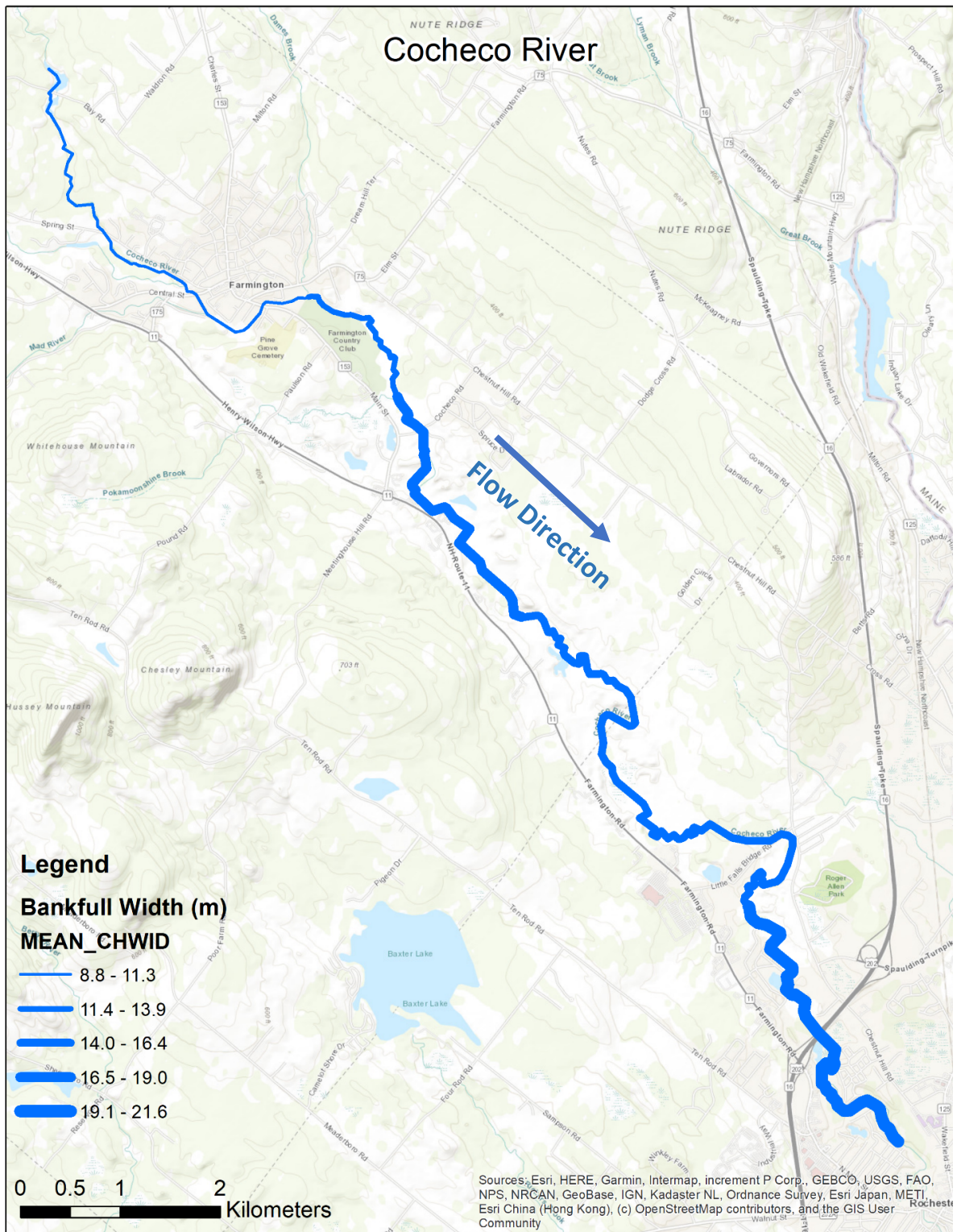


Figure 22. Mean bankfull width along reaches M20–M12 on Cocheco River. The Cocheco flows from north to south.

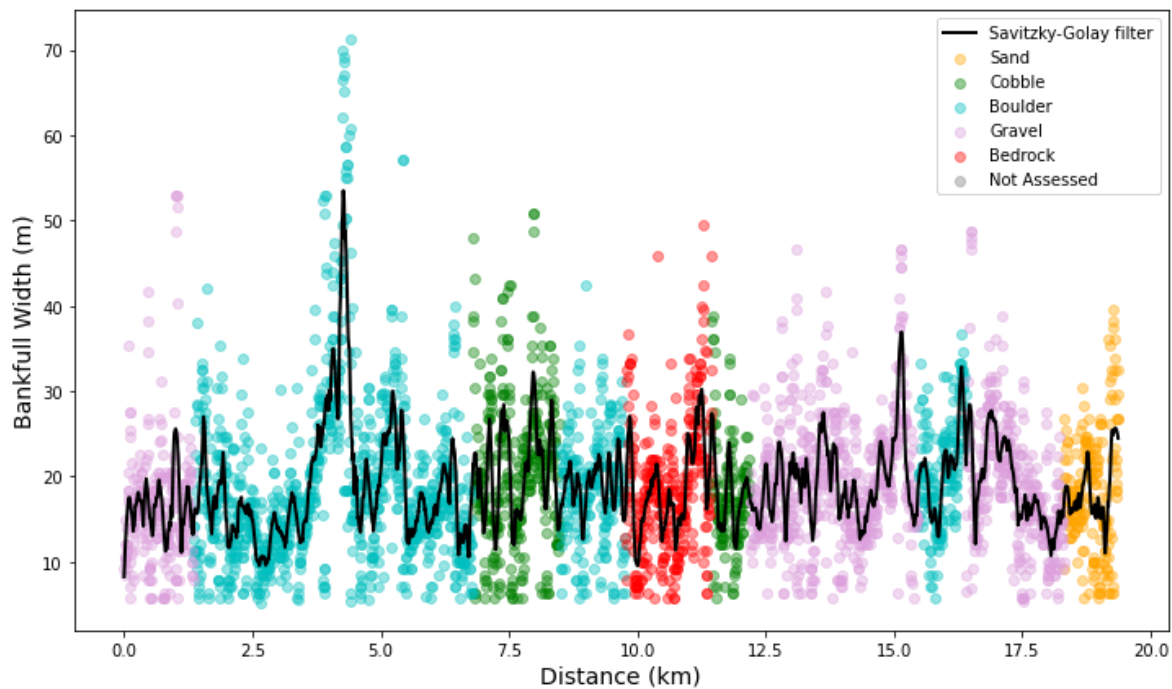


Figure 23. Dog River longitudinal profile with raw and smoothed remotely sensed bankfull widths as a function of distance downstream of the Stony Brook Road Bridge, Northfield, VT. Colors indicate bed substrate.

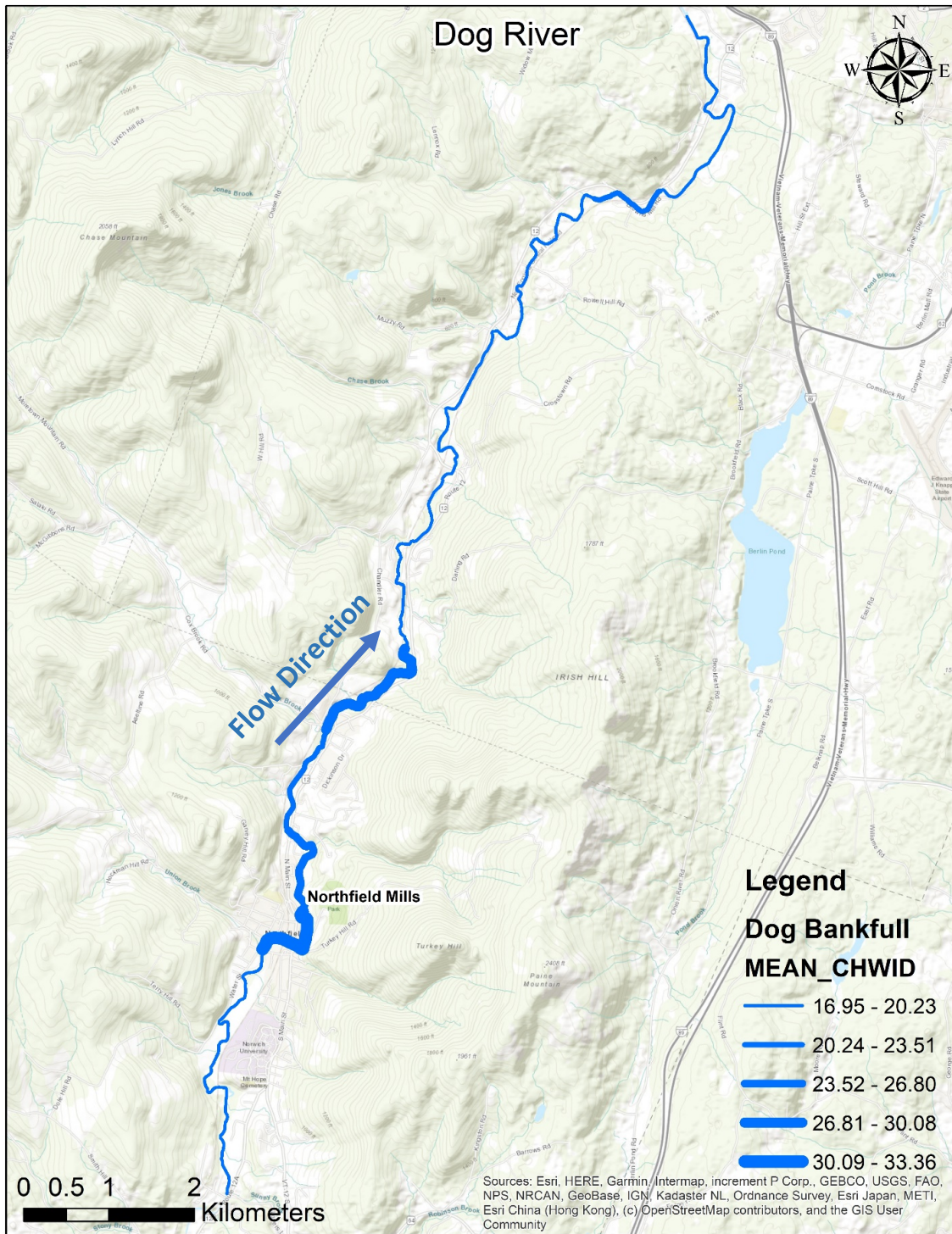


Figure 24. Mean bankfull width along reaches M14–M1 on Dog River. Flow was from south to north.

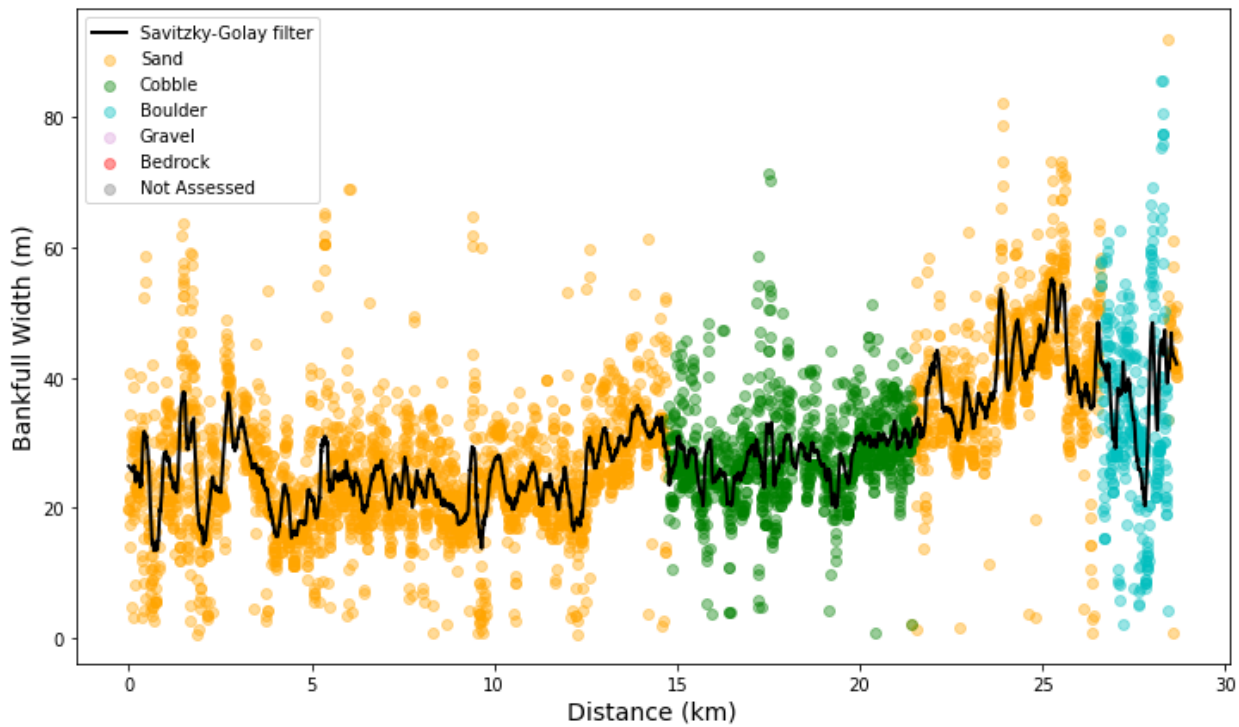


Figure 25. Lamprey River longitudinal profile with raw and smoothed remotely sensed bankfull widths as a function of distance downstream of the Route 125 Bridge, Epping, NH. Colors indicate bed substrate.

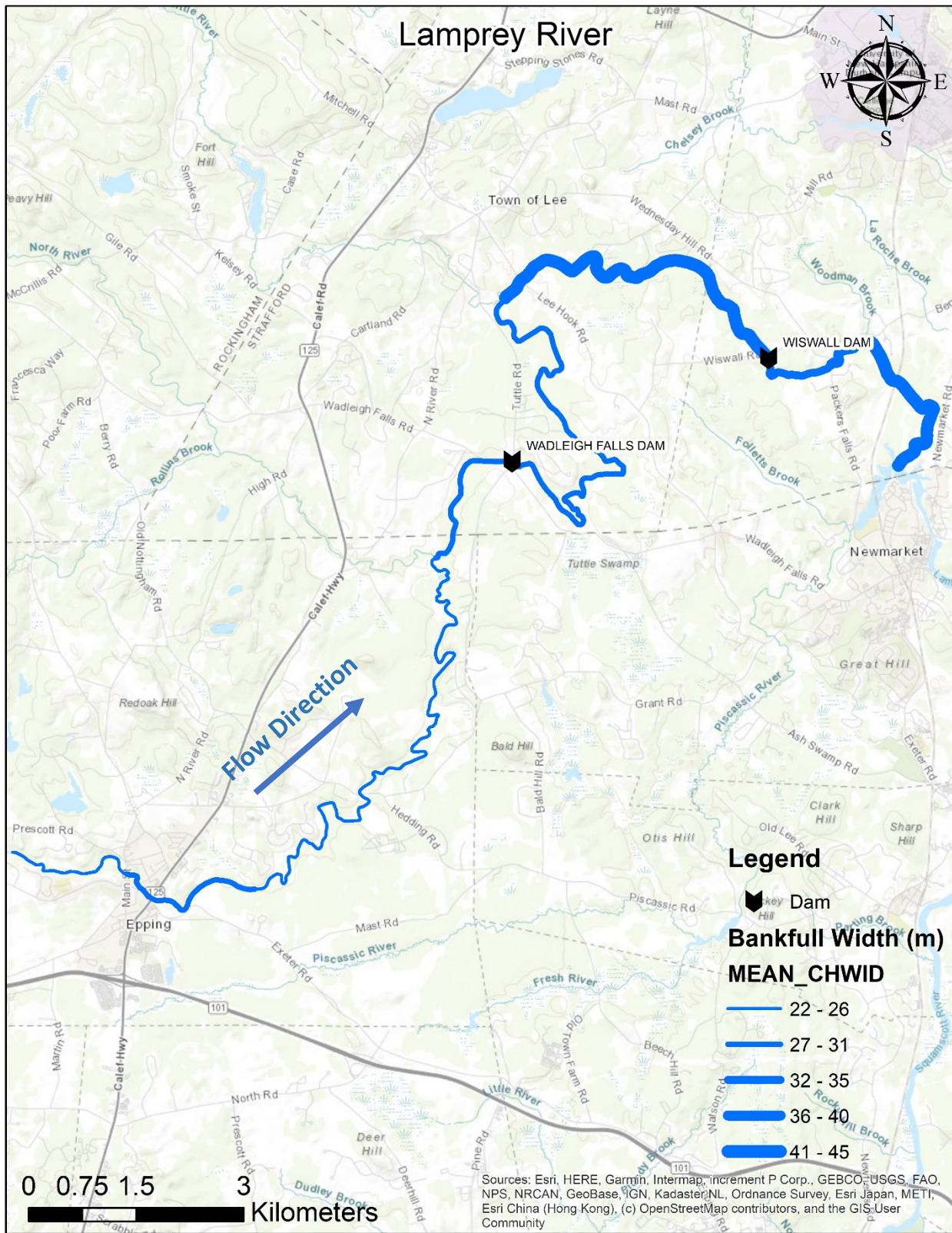


Figure 26. Mean bankfull width along reaches M12–M2 on Lamprey River. The Lamprey flows from west to east.

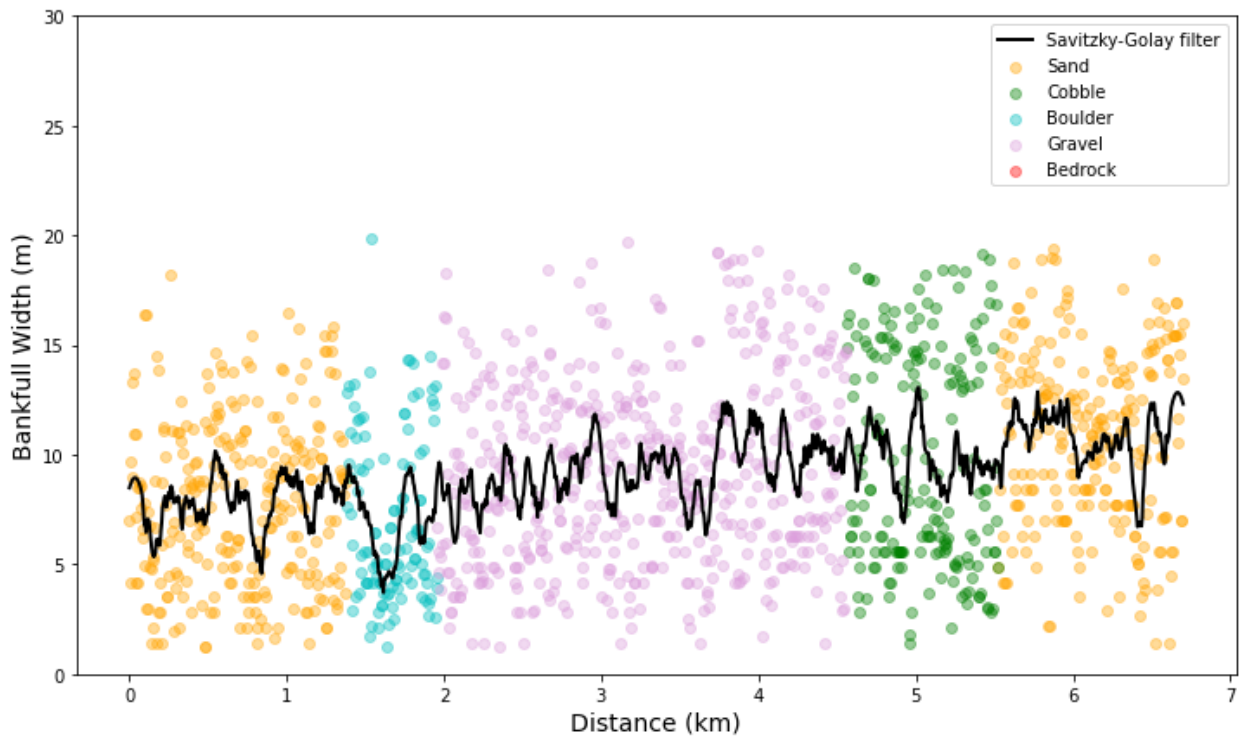


Figure 27. Stevens Branch longitudinal profile with raw and smoothed remotely sensed bankfull widths as a function of distance downstream of the Old Town Road Bridge, Williamstown, VT. Colors indicate bed substrate.

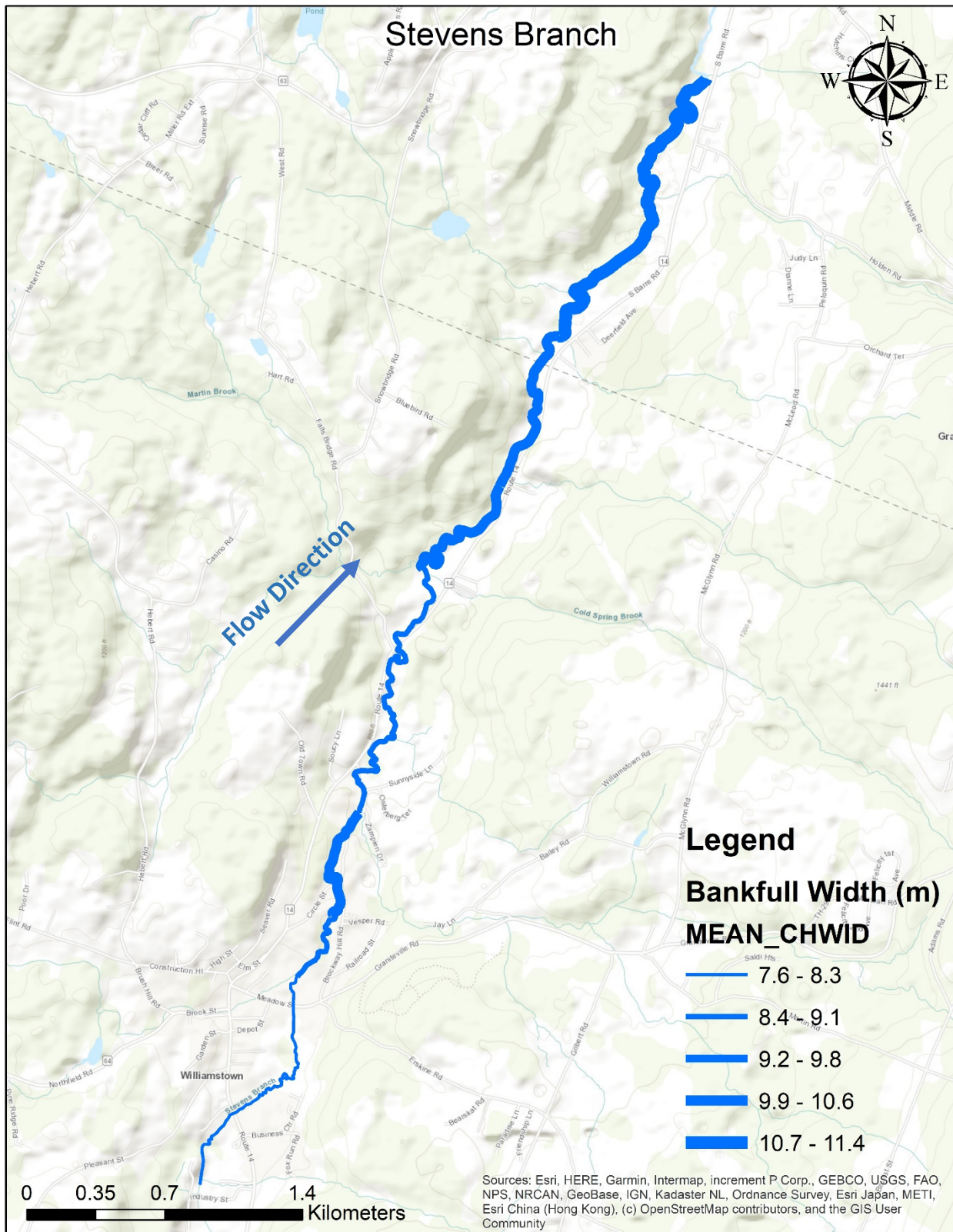


Figure 28. Mean bankfull width along reaches M18–M11 on Stevens Branch. The Stevens Branch flows south to north.

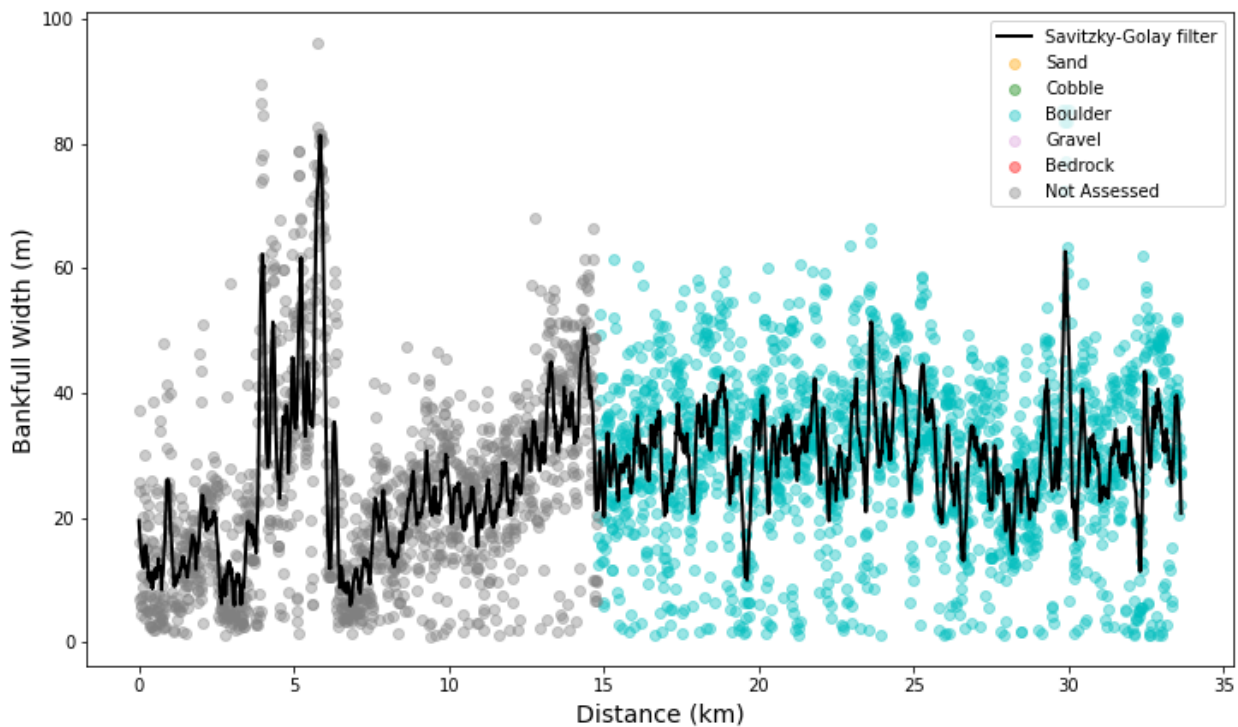


Figure 29. Sugar River longitudinal profile with raw and smoothed remotely sensed bankfull widths as a function of distance downstream of the Treatment Plant Road Bridge, Newport, NH. Colors indicate bed substrate.

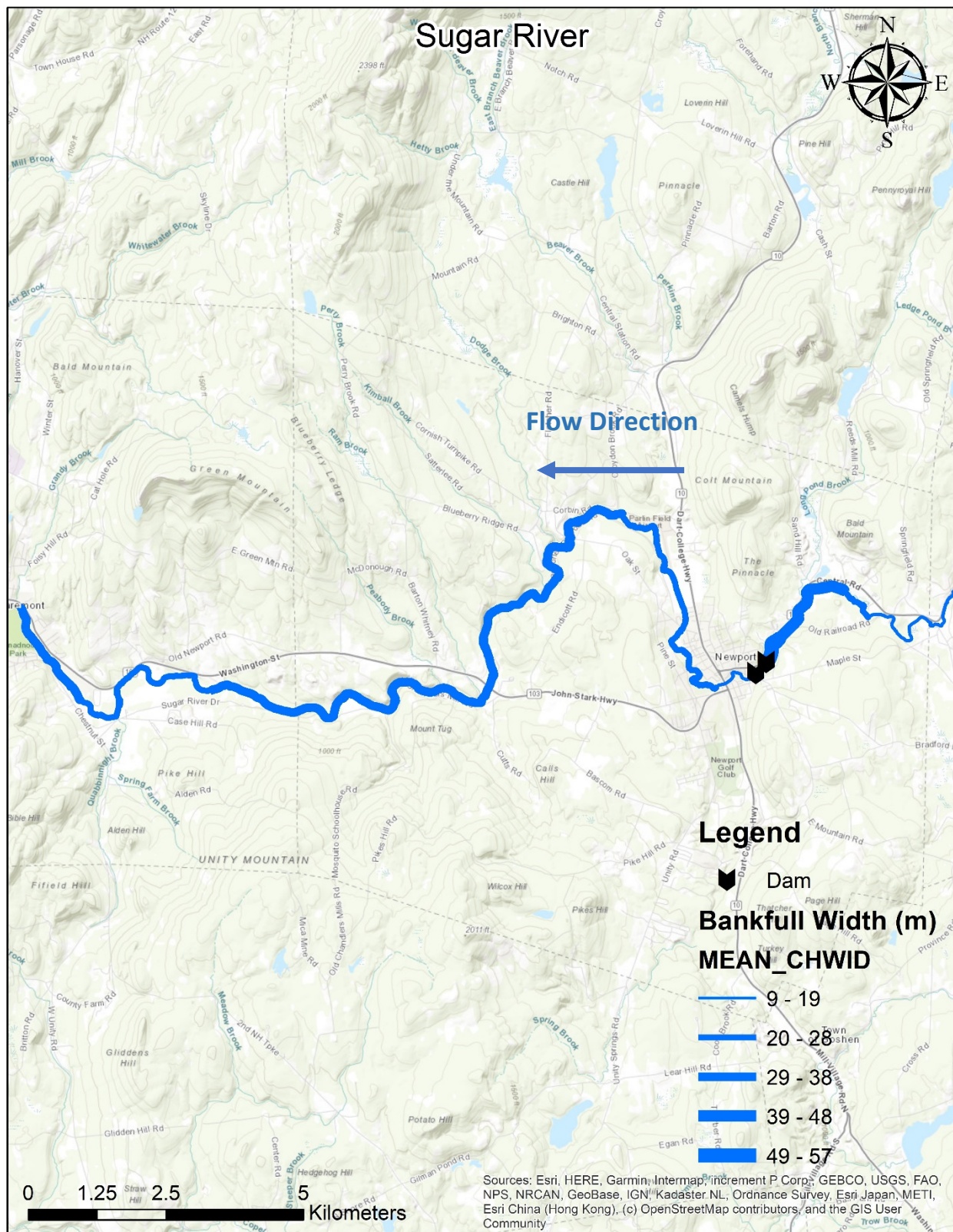


Figure 30. Mean bankfull width along reaches M40–M19 on Sugar River. The Sugar flows east to west.



Figure 31. Satellite photograph of the Sugar River reach M33-M32 with two hydroelectric dams, including remotely derived bankfull channel positions.

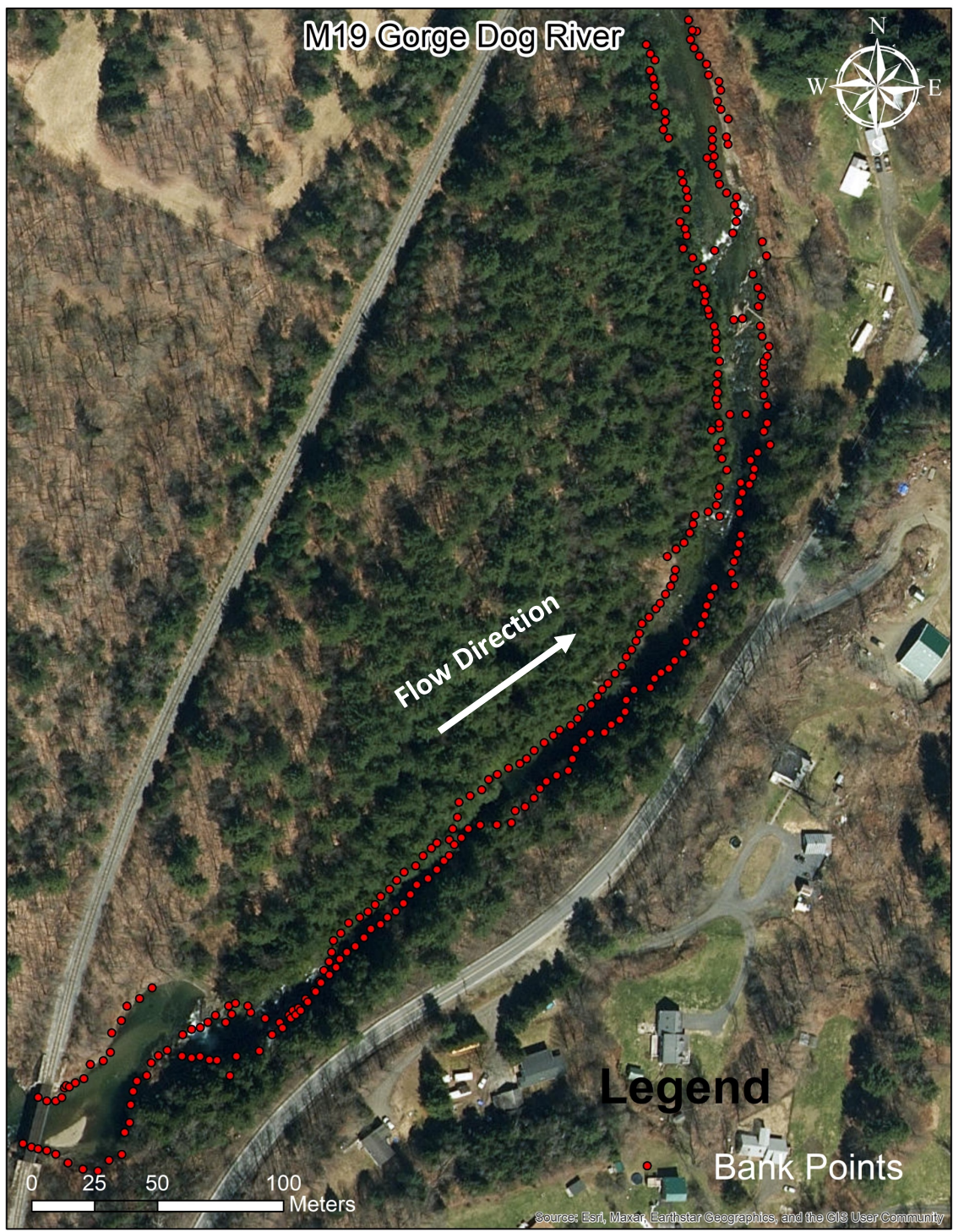


Figure 32. Satellite photograph of the Dog River reach M19B, which passes through a bedrock gorge, including remotely derived bankfull channel positions.

### Tables

Table 1. Assessed clusters representing riparian corridor, watershed area, bank material, and bed substrate.

River name (Cluster)	Reach	Length (km)	Dominant bed substrate	Dominant bank substrate	Riparian corridor	Watershed area ( $km^2$ )
Ammonoosuc(1)	M21-M16	9.1	Boulder	Boulder	Commercial	627
Ammonoosuc(2)	M16-M9	7.1	Boulder	Boulder	Forest	760
Ammonoosuc(3)	M9-M2	14.9	Boulder	Boulder	Forest	1034
Cocheco(1)	M20-M16	3.6	Bedrock	Boulder	Forest	115
Cocheco(2)	M16-M12	10.6	Sand	Sand	Forest	151
Dog(1)	M8-M1	9.7	Boulder	Boulder	Crop/Pasture	239
Dog(2)	M14-M8	4.2	Boulder	Boulder	Residential	198
Lamprey(1)	M12-M10	10.2	Sand	Sand	Forest	250
Lamprey(2)	M10-M7	5.7	Boulder	Boulder	Forest	394
Lamprey(3)	M7-M2	16.8	Boulder	Boulder	Forest	470
Stevens(1)	M18-M11	4.3	Sand	Sand	Residential	63
Sugar(1)	M40-M25	4.6	Boulder	Boulder	Forest	559
Sugar(2)	M26-M19	15.9	Boulder	Boulder	Forest	643

Table 2. Parameter values used as model inputs for automatic bankfull width detection for each river cluster. Optimal values for slope break ratio and slope percentage were selected based on calibration.

River name (Cluster)	Reach	Cross section spacing (m)	Linear fit length (m)	Maximum width (m)	Slope break ratio (m)	Slope percentage (%)	Vertical increment (m)	Point spacing (m)	Calibration points	Validation points
Ammo(1)	M21 - M16	4	30	110	1	1	0.1	0.7	5	3
Ammo(2)	M16 - M9	4	30	110	1	3	0.1	0.7	5	3
Ammo(3)	M9 - M2	4	30	110	1	7	0.1	0.7	5	4
Coheco(1)	M20 - M16	4	30	50	1	6	0.1	0.7	3	3
Coheco(2)	M16 - M12	4	30	50	1	6	0.1	0.7	3	0
Dog(1)	M8 - M1	4	30	80	1	4	0.1	0.7	5	4
Dog(2)	M14 - M8	4	30	80	1	3	0.1	0.7	2	0
Lamprey(1)	M12 - M10	4	30	100	1	4	0.1	0.3	3	2
Lamprey(2)	M10 - M7	4	30	100	1	7	0.1	0.3	4	2
Lamprey(3)	M7 - M2	4	30	100	1	7	0.1	0.3	6	5
Stevens(1)	M18 - M11	4	30	50	1	6	0.1	0.7	5	4
Sugar(1)	M41 - M26	4	30	100	1	1	0.1	0.7	3	0
Sugar(2)	M26 - M19	4	30	100	1	4	0.1	0.7	5	4

Table 3. Root mean square error (RMSE) and normalized RMSE between field and remotely derived estimates of bankfull width for each cluster in the six study rivers.

River name (Cluster)	Combined RMSE (m)	Combined normalized RMSE
Ammonoosuc(1)	9.01	0.20
Ammonoosuc(2)	6.90	0.15
Ammonoosuc(3)	4.74	0.11
Cocheco(1)	5.04	0.28
Cocheco(2)	4.77	0.26
Dog(1)	2.55	0.08
Dog(2)	3.55	0.11
Lamprey(1)	5.18	0.08
Lamprey(2)	3.91	0.06
Lamprey(3)	4.32	0.07
Stevens(1)	2.95	0.48
Sugar(1)	10.52	0.41
Sugar(2)	9.95	0.39

Table 4. Average Field , Remote and Regression point data and total Average Remote reach data for all Rivers

River	Field (m)	Field SD (m)	Remote(m)	Remote SD (m)	Regression(m)	Regression SD (m)	Total Remote(m)	Total Remote SD (m)
Ammonoosuc	43.9	10.4	39.6	11.9	42.4	6.1	37.1	17.4
Cocheco	15.1	3.0	14.1	7.0	20.8	3.0	14.8	7.1
Dog	23.5	6.5	21.9	7.2	26.6	2.0	19.5	8.8
Lamprey	32.8	16.3	34.1	14.3	33.3	3.7	29.1	11.5
Stevens	9.1	2.1	10.1	3.1	16.2	0.9	9.7	4.3
Sugar	29.8	8.3	27.6	14.1	38.3	6.6	27.6	15.2

Table 5. Average remotely derived bankfull widths for the river reaches immediately upstream and downstream of all active dams within study rivers.

River	Dam Name	Mean Upstream Width (m)	Upstream SD (m)	Mean Downstream Width (m)	Downstream SD (m)
Ammonoosuc	Lower Lisbon	56.21	19.1	55.3	18.7
Ammonoosuc	Bath	52.2	18.8	38.6	14.1
Dog	Northfield Mills	33.35	10.8	26.65	9.7
Lamprey	Wadleigh Falls	30.72	6.9	27.7	7.21
Lamprey	Wiswall	40.43	10.41	33.2	12.6
Sugar	Gordon Woolen Mill 1	57.05	21.9	25.05	16.1
Sugar	Gordon Woolen Mill 2	25.05	16.1	9.34	6.2

## Appendix A

Tables in Appendix A represent Tukey test results comparing bankfull width among various substrate materials for all study rivers. This appendix presents results for the following bed and bank substrate materials: BED (Bedrock), BO (Boulder), CO (Cobble), CLA (Clay), G (Gravel) and SA (Sand). In each table, Group 1 and Group 2 represent the groups being compared.

Meandiff represents the mean width difference between the two groups being compared, in units of meters for unnormalized bankfull width and unitless for normalized bankfull width. P-adj represents the adjusted level of significance, which is the probability that there is no difference in width between the groups. Lower and upper represent the bounds in which the true meandiff is expected to fall, in units of meters for unnormalized bankfull width and unitless for normalized bankfull width. Reject represents whether to accept or reject the null hypothesis that there is no difference in width between the groups; the null hypothesis is rejected (True) for p-adj values under 0.05.

Table A-1. Tukey test comparing normalized bankfull width among various bed substrates on the Ammonoosuc River at field measurement locations.

Group1	Group2	meandiff	p-adj	lower	upper	reject
BED	BO	0.1831	0.362	-0.1236	0.4898	FALSE
BED	CO	0.3678	0.0543	-0.0055	0.741	FALSE
BED	SA	0.5245	0.0093	0.1156	0.9334	TRUE
BO	CO	0.1847	0.2162	-0.0726	0.4419	FALSE
BO	SA	0.3414	0.0259	0.0348	0.6481	TRUE
CO	SA	0.1567	0.6328	-0.2165	0.53	FALSE

Table A-2. Tukey test comparing normalized bankfull width among various bed substrates on the Cocheco River at field measurement locations.

Group1	Group2	meandiff	p-adj	lower	upper	reject
BO	CO	-0.1075	0.5722	-0.4349	0.2198	FALSE
BO	SA	0.0174	0.9	-0.3606	0.3954	FALSE
CO	SA	0.1249	0.4839	-0.2024	0.4523	FALSE

Table A-3. Tukey test comparing normalized bankfull width among various bed substrates on the Dog River at field measurement locations.

Group1	Group2	meandiff	p-adj	lower	upper	reject
BED	BO	-0.1708	0.9	-1.16	0.8185	FALSE
BED	CO	-0.0203	0.9	-0.9234	0.8827	FALSE
BED	G	0.0201	0.9	-0.8647	0.9049	FALSE
BO	CO	0.1504	0.8954	-0.5491	0.8499	FALSE
BO	G	0.1909	0.7849	-0.4849	0.8667	FALSE
CO	G	0.0405	0.9	-0.5014	0.5823	FALSE

Table A-4. Tukey test comparing normalized bankfull width among various bed substrates on the Dog River at field measurement locations.

Group1	Group2	meandiff	p-adj	lower	upper	reject
BO	CO	-0.3104	0.5045	-0.9991	0.3783	FALSE
BO	SA	-0.1631	0.6971	-0.6782	0.352	FALSE
CO	SA	0.1473	0.8149	-0.4809	0.7756	FALSE

Table A-5. Tukey test comparing normalized bankfull width among various bed substrates on the Stevens Branch at field measurement locations.

Group1	Group2	meandiff	p-adj	lower	upper	reject
BO	CO	0	0.9	-0.6191	0.6191	FALSE
BO	G	0.117	0.8216	-0.3474	0.5813	FALSE
BO	SA	-0.0602	0.9	-0.6793	0.5589	FALSE
CO	G	0.117	0.8216	-0.3474	0.5813	FALSE
CO	SA	-0.0602	0.9	-0.6793	0.5589	FALSE
G	SA	-0.1772	0.6048	-0.6415	0.2871	FALSE

Table A-6. Tukey test comparing normalized bankfull width among various bank substrates on the Ammonoosuc River at field measurement locations.

Group1	Group2	meandiff	p-adj	lower	upper	reject
BED	BO	0.1937	0.4115	-0.15	0.5374	FALSE
BED	CO	0.3664	0.1461	-0.0918	0.8247	FALSE
BED	SA	0.4166	0.0512	-0.0018	0.8349	FALSE
BO	CO	0.1727	0.5063	-0.171	0.5164	FALSE
BO	SA	0.2229	0.1667	-0.0655	0.5112	FALSE
CO	SA	0.0502	0.9	-0.3682	0.4685	FALSE

Table A-7. Tukey test comparing normalized bankfull width among various bank substrates on the Cochecho River at field measurement locations.

Group1	Group2	meandiff	p-adj	lower	upper	reject
BO	CO	-0.0472	0.9	-0.4125	0.3181	FALSE
BO	SA	-0.1033	0.713	-0.5252	0.3185	FALSE
CO	SA	-0.0561	0.8668	-0.4215	0.3092	FALSE

Table A-8. Tukey test comparing normalized bankfull width among various bank substrates on the Dog River at field measurement locations.

Group1	Group2	meandiff	p-adj	lower	upper	reject
BED	BO	-0.1708	0.9	-1.2844	0.9429	FALSE
BED	CO	-0.0203	0.9	-1.037	0.9963	FALSE
BED	G	-0.067	0.9	-1.117	0.983	FALSE
BED	SA	0.1509	0.9	-0.9628	1.2646	FALSE
BO	CO	0.1504	0.9	-0.6371	0.9379	FALSE
BO	G	0.1037	0.9	-0.7264	0.9338	FALSE
BO	SA	0.3216	0.7029	-0.5877	1.231	FALSE
CO	G	-0.0467	0.9	-0.7412	0.6478	FALSE
CO	SA	0.1712	0.9	-0.6163	0.9587	FALSE
G	SA	0.2179	0.8636	-0.6122	1.048	FALSE

Table A-9. Tukey test comparing normalized bankfull width among various bank substrates on the Lamprey River at field measurement locations.

Group1	Group2	meandiff	p-adj	lower	upper	reject
BO	CLA	-0.3143	0.6848	-1.281	0.6524	FALSE
BO	SA	-0.1083	0.8996	-0.7253	0.5088	FALSE
CLA	SA	0.206	0.796	-0.626	1.0381	FALSE

Table A-10. Tukey test comparing normalized bankfull width among various bank substrates on the Stevens Branch at field measurement locations.

Group1	Group2	meandiff	p-adj	lower	upper	reject
BO	SA	0.1467	0.092	-0.0293	0.3227	FALSE

Table A-11. Tukey test comparing normalized bankfull width among various bank substrates on the Sugar River at field measurement locations.

Group1	Group2	meandiff	p-adj	lower	upper	reject
BO	CO	0.0461	0.9	-0.3585	0.4507	FALSE
BO	SA	-0.0801	0.7164	-0.3836	0.2234	FALSE
CO	SA	-0.1262	0.7035	-0.5897	0.3374	FALSE

Table A-12. Tukey test comparing unnormalized bankfull width among various bank substrates on the Ammonoosuc River at field measurement locations.

Group 1	Group 2	meandiff	p-adj	lower	upper	reject
BED	BO	0.25	0.9	-18.5985	19.0985	FALSE
BED	CO	14.5	0.3914	-10.6313	39.6313	FALSE
BED	SA	15.5	0.2612	-7.4417	38.4417	FALSE
BO	CO	14.25	0.1807	-4.5985	33.0985	FALSE
BO	SA	15.25	0.0611	-0.5614	31.0614	FALSE
CO	SA	1	0.9	-21.9417	23.9417	FALSE

Table A-13. Tukey test comparing unnormalized bankfull width among various bank substrates on the Cochecho River at field measurement locations.

Group 1	Group 2	meandiff	p-adj	lower	upper	reject
BO	CO	2.7	0.6258	-6.3993	11.7993	FALSE
BO	SA	3	0.6447	-7.5069	13.5069	FALSE
CO	SA	0.3	0.9	-8.7993	9.3993	FALSE

Table A-14. Tukey test comparing unnormalized bankfull width among various bank substrates on the Dog River at field measurement locations.

Group 1	Group 2	meandiff	p-adj	lower	upper	reject
BED	BO	-3.5	0.9	-35.1523	28.1523	FALSE
BED	CO	-1	0.9	-29.8944	27.8944	FALSE
BED	G	-2	0.9	-31.842	27.842	FALSE
BED	SA	5.5	0.9	-26.1523	37.1523	FALSE
BO	CO	2.5	0.9	-19.8815	24.8815	FALSE
BO	G	1.5	0.9	-22.0922	25.0922	FALSE
BO	SA	9	0.7126	-16.844	34.844	FALSE
CO	G	-1	0.9	-20.7387	18.7387	FALSE
CO	SA	6.5	0.8145	-15.8815	28.8815	FALSE
G	SA	7.5	0.766	-16.0922	31.0922	FALSE

Table A-15. Tukey test comparing unnormalized bankfull width among various bank substrates on the Lamprey River at field measurement locations.

Group 1	Group 2	meandiff	p-adj	lower	upper	reject
BO	CLA	-17.825	0.4394	-53.7378	18.0878	FALSE
BO	SA	-7.7361	0.667	-30.6587	15.1865	FALSE
CLA	SA	10.0889	0.6829	-20.8199	40.9977	FALSE

Table A-16. Tukey test comparing unnormalized bankfull width among various bank substrates on the Stevens Branch at field measurement locations.

Group 1	Group 2	meandiff	p-adj	lower	upper	reject
BO	SA	2.4833	0.0686	-0.2337	5.2003	FALSE

Table A-17. Tukey test comparing unnormalized bankfull width among various bed substrates on the Ammonoosuc River at field measurement locations.

Group 1	Group 2	meandiff	p-adj	lower	upper	reject
BED	BO	-0.125	0.9	-17.2824	17.0324	FALSE
BED	CO	13.1667	0.3163	-7.7167	34.05	FALSE
BED	SA	21	0.0789	-1.8766	43.8766	FALSE
BO	CO	13.2917	0.0766	-1.1012	27.6845	FALSE
BO	SA	21.125	0.0127	3.9676	38.2824	TRUE
CO	SA	7.8333	0.7014	-13.05	28.7167	FALSE

Table A-18. Tukey test comparing unnormalized bankfull width among various bed substrates on the Cochecho River at field measurement locations.

Group 1	Group 2	meandiff	p-adj	lower	upper	reject
BO	CO	1.25	0.7809	-4.8583	7.3583	FALSE
BO	SA	5.9	0.0899	-1.1532	12.9532	FALSE
CO	SA	4.65	0.119	-1.4583	10.7583	FALSE

Table A-19. Tukey test comparing unnormalized bankfull width among various bed substrates on the Dog River at field measurement locations.

Group 1	Group 2	meandiff	p-adj	lower	upper	reject
BED	BO	-3.5	0.9	-32.3408	25.3408	FALSE
BED	CO	-1	0.9	-27.3279	25.3279	FALSE
BED	G	1	0.9	-24.796	26.796	FALSE
BO	CO	2.5	0.9	-17.8935	22.8935	FALSE
BO	G	4.5	0.8735	-15.202	24.202	FALSE
CO	G	2	0.9	-13.7968	17.7968	FALSE

Table A-20. Tukey test comparing unnormalized bankfull width among various bed substrates on the Lamprey River at field measurement locations.

Group 1	Group 2	meandiff	p-adj	lower	upper	reject
BO	CO	-10.0536	0.6011	-36.2747	16.1675	FALSE
BO	SA	-7.3209	0.6157	-26.9332	12.2914	FALSE
CO	SA	2.7327	0.9	-21.187	26.6524	FALSE

Table A-21. Tukey test comparing unnormalized bankfull width among various bed substrates on the Stevens Branch at field measurement locations.

Group 1	Group 2	meandiff	p-adj	lower	upper	reject
BO	CO	0	0.9	-10.159	10.159	FALSE
BO	G	1.6	0.8915	-6.0193	9.2193	FALSE
BO	SA	-1	0.9	-11.159	9.159	FALSE
CO	G	1.6	0.8915	-6.0193	9.2193	FALSE
CO	SA	-1	0.9	-11.159	9.159	FALSE
G	SA	-2.6	0.6722	-10.2193	5.0193	FALSE

Table A-22 Tukey test comparing unnormalized bankfull width among various bank substrates on the Ammonoosuc River at reach measurement locations.

Group 1	Group 2	meandiff	p-adj	lower	upper	reject
BED	BO	-4.0365	0.9	-33.0725	24.9995	FALSE
BED	CO	-6.8345	0.9	-38.4373	24.7683	FALSE
BED	SA	6.0233	0.9	-31.7492	43.7959	FALSE
BO	CO	-2.798	0.9	-23.171	17.575	FALSE
BO	SA	10.0598	0.7363	-18.9762	39.0958	FALSE
CO	SA	12.8578	0.6431	-18.745	44.4606	FALSE

Table A-23 Tukey test comparing unnormalized bankfull width among various bank substrates on the Cochecho River at reach measurement locations.

Group 1	Group 2	meandiff	p-adj	lower	upper	reject
BED	BO	0.183	0.9	-21.9888	22.3548	FALSE
BED	CO	2.5163	0.9	-16.6851	21.7176	FALSE
BED	SA	11.4245	0.1553	-6.6787	29.5277	FALSE
BO	CO	2.3332	0.9	-16.8681	21.5346	FALSE
BO	SA	11.2414	0.161	-6.8618	29.3446	FALSE
CO	SA	8.9082	0.1602	-5.4036	23.22	FALSE

Table A-24 Tukey test comparing unnormalized bankfull width among various bank substrates on the Dog River at reach measurement locations.

Group 1	Group 2	meandiff	p-adj	lower	upper	reject
BED	BO	1.9258	0.9	-11.5735	15.4251	FALSE
BED	CO	-4.8242	0.7997	-20.4118	10.7634	FALSE
BED	G	-3.7788	0.9	-22.8696	15.3121	FALSE
BED	SA	-4.5467	0.7524	-18.0459	8.9526	FALSE
BO	CO	-6.75	0.4705	-20.2493	6.7493	FALSE
BO	G	-5.7046	0.7688	-23.1321	11.7229	FALSE
BO	SA	-6.4725	0.3333	-17.4946	4.5496	FALSE
CO	G	1.0454	0.9	-18.0454	20.1363	FALSE
CO	SA	0.2775	0.9	-13.2217	13.7768	FALSE
G	SA	-0.7679	0.9	-18.1953	16.6596	FALSE

Table A-25 Tukey test comparing unnormalized bankfull width among various bank substrates on the Lamprey River at reach measurement locations.

Group 1	Group 2	meandiff	p-adj	lower	upper	reject
BO	SA	-7.2224	0.2766	-21.3285	6.8837	FALSE

Table A-26 Tukey test comparing normalized bankfull width among various bank substrates on the Ammonoosuc River at reach measurement locations.

Group 1	Group 2	meandiff	p-adj	lower	upper	reject
BED	BO	-0.0169	0.9	-0.5526	0.5188	FALSE
BED	CO	-0.1778	0.8004	-0.7608	0.4053	FALSE
BED	SA	0.0911	0.9	-0.6058	0.7879	FALSE
BO	CO	-0.1609	0.6106	-0.5367	0.215	FALSE
BO	SA	0.108	0.9	-0.4277	0.6437	FALSE
CO	SA	0.2688	0.5595	-0.3142	0.8519	FALSE

Table A-27 Tukey test comparing normalized bankfull width among various bank substrates on the Cocheco River at reach measurement locations.

Group 1	Group 2	meandiff	p-adj	lower	upper	reject
BED	BO	-0.1433	0.858	-1.0454	0.7588	FALSE
BED	CO	-0.1212	0.8659	-0.9024	0.6601	FALSE
BED	SA	0.1987	0.6213	-0.5378	0.9353	FALSE
BO	CO	0.0221	0.9	-0.7591	0.8034	FALSE
BO	SA	0.342	0.2904	-0.3945	1.0786	FALSE
CO	SA	0.3199	0.2093	-0.2624	0.9022	FALSE

Table A-28 Tukey test comparing normalized bankfull width among various bank substrates on the Dog River at reach measurement locations.

Group 1	Group 2	meandiff	p-adj	lower	upper	reject
BED	BO	0.1812	0.8532	-0.4692	0.8316	FALSE
BED	CO	-0.203	0.8675	-0.9541	0.548	FALSE
BED	G	-0.0122	0.9	-0.932	0.9077	FALSE
BED	SA	-0.2119	0.7716	-0.8623	0.4386	FALSE
BO	CO	-0.3842	0.3284	-1.0346	0.2662	FALSE
BO	G	-0.1934	0.9	-1.0331	0.6463	FALSE
BO	SA	-0.3931	0.1697	-0.9241	0.138	FALSE
CO	G	0.1908	0.9	-0.729	1.1107	FALSE
CO	SA	-0.0088	0.9	-0.6593	0.6416	FALSE
G	SA	-0.1997	0.9	-1.0394	0.64	FALSE

Table A-29 Tukey test comparing normalized bankfull width among various bank substrates on the Lamprey River at reach measurement locations.

Group 1	Group 2	meandiff	p-adj	lower	Upper	reject
BO	SA	-0.0787	0.5306	-0.3488	0.1914	FALSE

Table A-30 Tukey test comparing unnormalized bankfull width among various bed substrates on the Ammonoosuc River at reach measurement locations.

Group 1	Group 2	meandiff	p-adj	lower	upper	reject
BED	BO	-6.0789	0.9	-35.0048	22.8469	FALSE
BED	CO	-2.3411	0.9	-33.824	29.1418	FALSE
BED	SA	6.0233	0.9	-31.6059	43.6526	FALSE
BO	CO	3.7378	0.9	-16.5579	24.0335	FALSE
BO	SA	12.1023	0.6254	-16.8236	41.0281	FALSE
CO	SA	8.3645	0.8608	-23.1185	39.8474	FALSE

Table A-31 Tukey test comparing unnormalized bankfull width among various bed substrates on the Cocheco River at reach measurement locations.

Group 1	Group 2	meandiff	p-adj	lower	upper	reject
BED	BO	0.183	0.9	-21.9888	22.3548	FALSE
BED	CO	2.5163	0.9	-16.6851	21.7176	FALSE
BED	SA	11.4245	0.1553	-6.6787	29.5277	FALSE
BO	CO	2.3332	0.9	-16.8681	21.5346	FALSE
BO	SA	11.2414	0.161	-6.8618	29.3446	FALSE
CO	SA	8.9082	0.1602	-5.4036	23.22	FALSE

Table A-32 Tukey test comparing unnormalized bankfull width among various bed substrates on the Dog River at reach measurement locations.

Group 1	Group 2	meandiff	p-adj	lower	upper	Reject
BED	BO	1.9258	0.9	-11.5871	15.4387	FALSE
BED	CO	-4.8242	0.8002	-20.4276	10.7792	FALSE
BED	G	-4.3088	0.7834	-17.8217	9.2041	FALSE
BED	SA	-4.7303	0.9	-23.8405	14.3799	FALSE
BO	CO	-6.75	0.4713	-20.2629	6.7629	FALSE
BO	G	-6.2346	0.3656	-17.2678	4.7987	FALSE
BO	SA	-6.6561	0.6749	-24.1012	10.789	FALSE
CO	G	0.5154	0.9	-12.9975	14.0283	FALSE
CO	SA	0.0939	0.9	-19.0162	19.2041	FALSE
G	SA	-0.4215	0.9	-17.8666	17.0236	FALSE

Table A-33 Tukey test comparing unnormalized bankfull width among various bed substrates on the Lamprey River at reach measurement locations.

Group 1	Group 2	meandiff	p-adj	lower	upper	Reject
BO	CO	-8.3589	0.6975	-37.9043	21.1866	FALSE
BO	SA	-7.0804	0.5619	-26.1519	11.9911	FALSE
CO	SA	1.2785	0.9	-24.3086	26.8656	FALSE

Table A-34 Tukey test comparing unnormalized bankfull width among various bed substrates on the Stevens Branch at reach measurement locations.

Group 1	Group 2	meandiff	p-adj	lower	upper	Reject
CO	G	-0.3645	0.1	-27.0916	26.3625	FALSE
CO	SA	1.3326	0.1	-29.5292	32.1943	FALSE
G	SA	1.6971	0.1	-25.03	28.4242	FALSE

Table A-35 Tukey test comparing normalized bankfull width among various bed substrates on the Ammonoosuc River at reach measurement locations.

Group 1	Group 2	meandiff	p-adj	lower	upper	Reject
BED	BO	-0.0488	0.9	-0.6058	0.5082	FALSE
BED	CO	-0.1075	0.9	-0.7138	0.4987	FALSE
BED	SA	0.0911	0.9	-0.6335	0.8157	FALSE
BO	CO	-0.0587	0.9	-0.4496	0.3321	FALSE
BO	SA	0.1399	0.8833	-0.4171	0.6969	FALSE
CO	SA	0.1986	0.7654	-0.4077	0.8049	FALSE

Table A-36 Tukey test comparing normalized bankfull width among various bed substrates on the Cocheco River at reach measurement locations.

Group 1	Group 2	meandiff	p-adj	lower	upper	Reject
BED	BO	-0.1433	0.858	-1.0454	0.7588	FALSE
BED	CO	-0.1212	0.8659	-0.9024	0.6601	FALSE
BED	SA	0.1987	0.6213	-0.5378	0.9353	FALSE
BO	CO	0.0221	0.9	-0.7591	0.8034	FALSE
BO	SA	0.342	0.2904	-0.3945	1.0786	FALSE
CO	SA	0.3199	0.2093	-0.2624	0.9022	FALSE

Table A-37 Tukey test comparing normalized bankfull width among various bed substrates on the Dog River at reach measurement locations.

Group 1	Group 2	meandiff	p-adj	lower	upper	Reject
BED	BO	0.1812	0.8699	-0.4926	0.855	FALSE
BED	CO	-0.203	0.8837	-0.981	0.575	FALSE
BED	G	-0.1573	0.9	-0.831	0.5165	FALSE
BED	SA	-0.2306	0.9	-1.1834	0.7223	FALSE
BO	CO	-0.3842	0.3578	-1.058	0.2895	FALSE
BO	G	-0.3385	0.2962	-0.8886	0.2116	FALSE
BO	SA	-0.4118	0.5158	-1.2816	0.4581	FALSE
CO	G	0.0457	0.9	-0.628	0.7195	FALSE
CO	SA	-0.0275	0.9	-0.9804	0.9253	FALSE
G	SA	-0.0733	0.9	-0.9431	0.7965	FALSE

Table A-38 Tukey test comparing normalized bankfull width among various bed substrates on the Lamprey River at reach measurement locations.

Group 1	Group 2	meandiff	p-adj	lower	upper	Reject
BO	CO	-0.1793	0.632	-0.7302	0.3715	FALSE
BO	SA	-0.0661	0.8465	-0.4217	0.2895	FALSE
CO	SA	0.1132	0.7674	-0.3638	0.5903	FALSE

Table A-39 Tukey test comparing normalized bankfull width among various bed substrates on the Stevens Branch at reach measurement locations.

Group 1	Group 2	meandiff	p-adj	lower	upper	Reject
CO	G	0.0084	0.1	-0.9815	0.9983	FALSE
CO	SA	0.0803	0.1	-1.0628	1.2233	FALSE
G	SA	0.0719	0.1	-0.918	1.0618	FALSE

## Appendix B

This appendix presents all of the calibration cluster data showing the percentage of non-zero width values, the percentage of reasonable width values, and the root mean square error (RMSE) between field and remotely sensed widths.

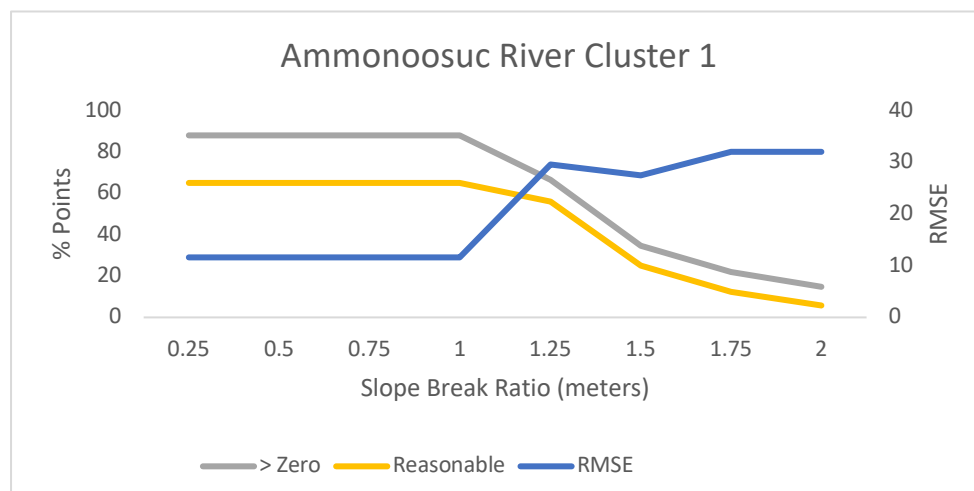


Figure B1. Calibration plot for slope break ratio in Ammonoosuc River cluster 1, showing the percentage of non-zero width values, the percentage of reasonable width values, and the root mean square error (RMSE) between field and remotely sensed widths.

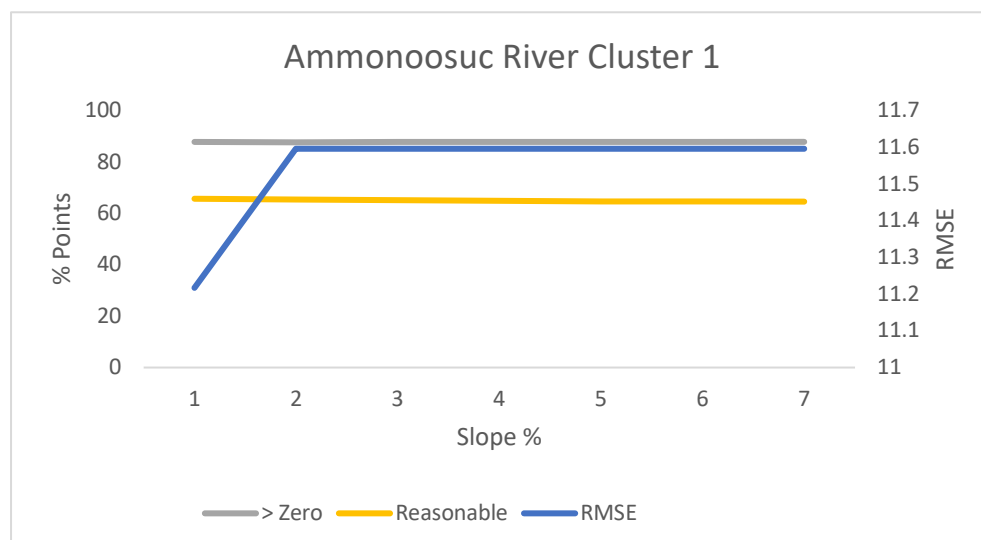


Figure B2. Calibration plot for slope break percentage in Ammonoosuc River cluster 1, showing the percentage of non-zero width values, the percentage of reasonable width values, and the root mean square error (RMSE) between field and remotely sensed widths.

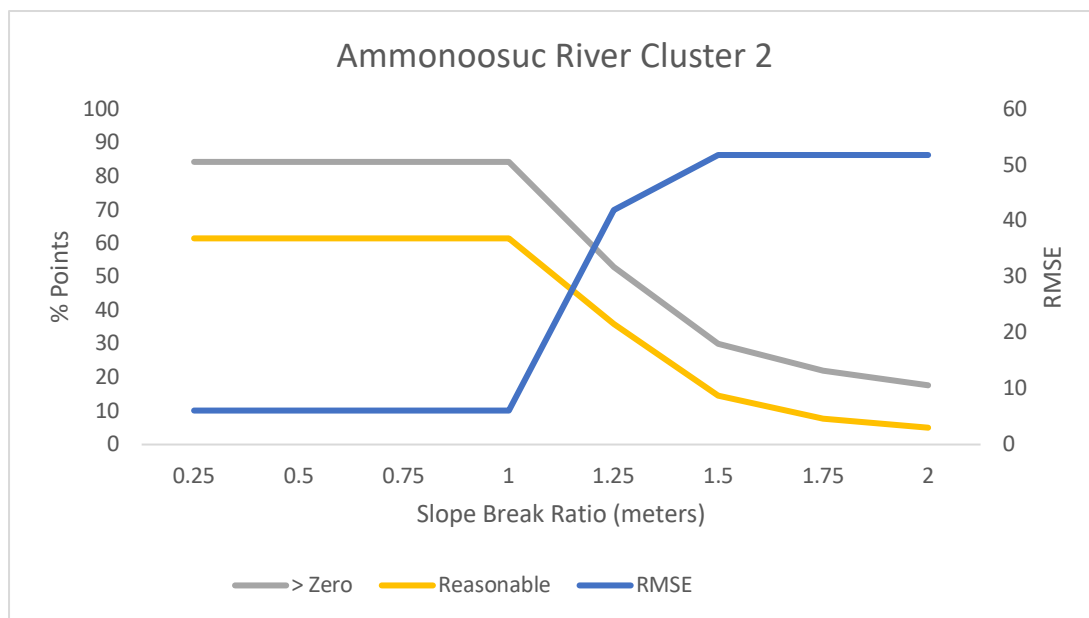


Figure B3. Calibration plot for slope break ratio in Ammonoosuc River cluster 2, showing the percentage of non-zero width values, the percentage of reasonable width values, and the root mean square error (RMSE) between field and remotely sensed widths.

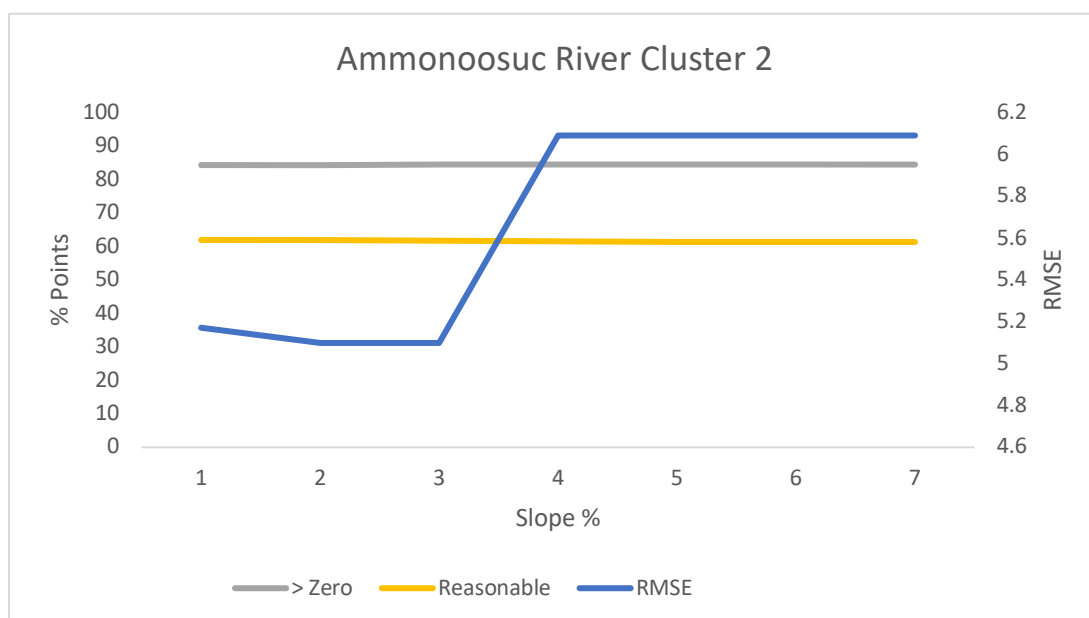


Figure B4. Calibration plot for slope percentage in Ammonoosuc River cluster 1, showing the percentage of non-zero width values, the percentage of reasonable width values, and the root mean square error (RMSE) between field and remotely sensed width.

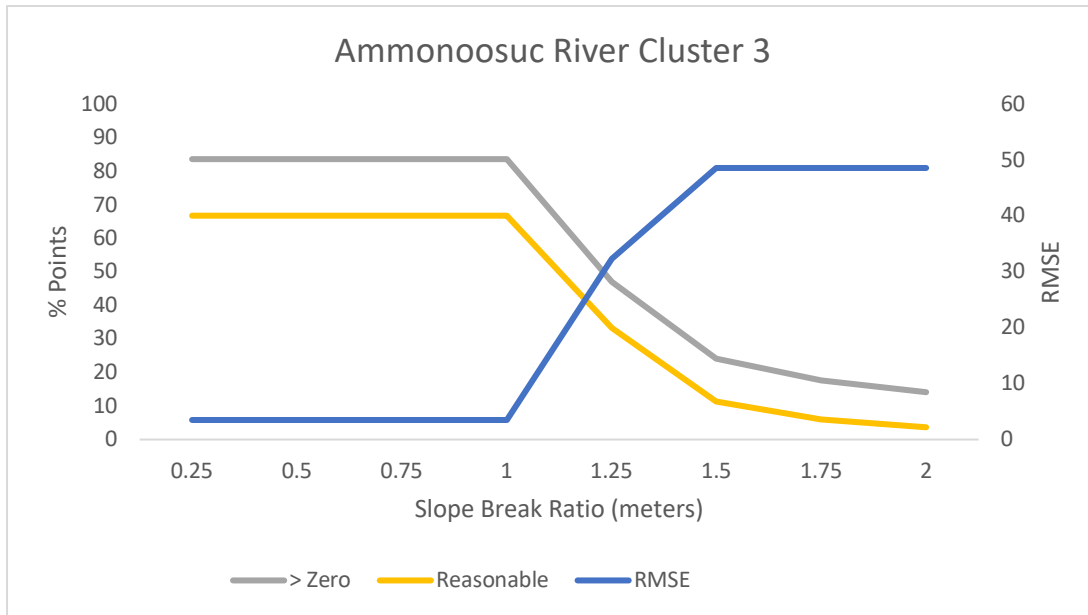


Figure B5. Calibration plot for slope break ratio in Ammonoosuc River cluster 3, showing the percentage of non-zero width values, the percentage of reasonable width values, and the root mean square error (RMSE) between field and remotely sensed widths.

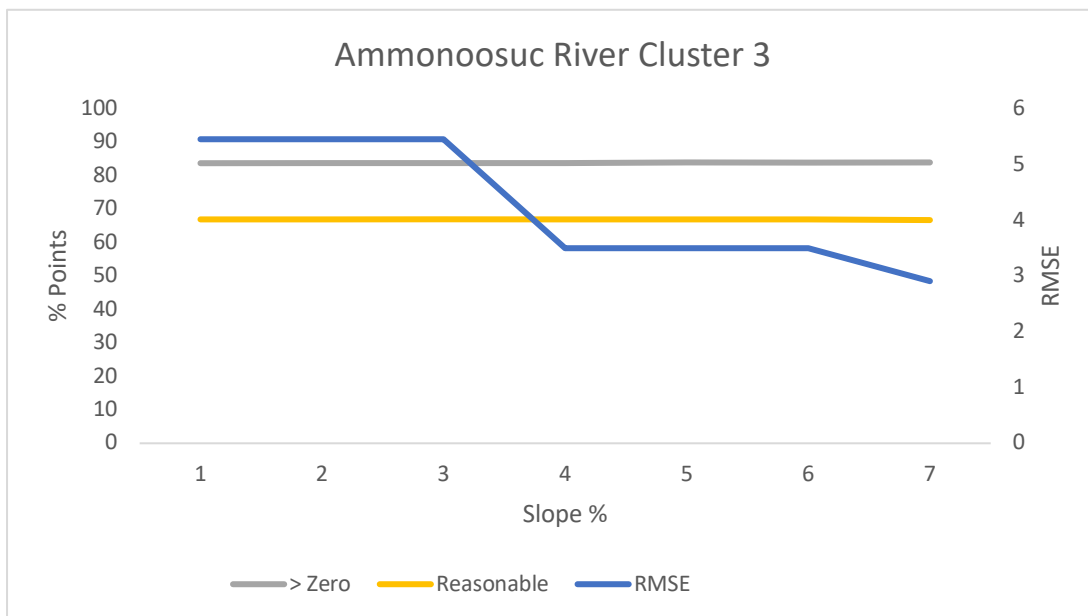


Figure B6. Calibration plot for slope break percentage in Ammonoosuc River cluster 3, showing the percentage of non-zero width values, the percentage of reasonable width values, and the root mean square error (RMSE) between field and remotely sensed widths.

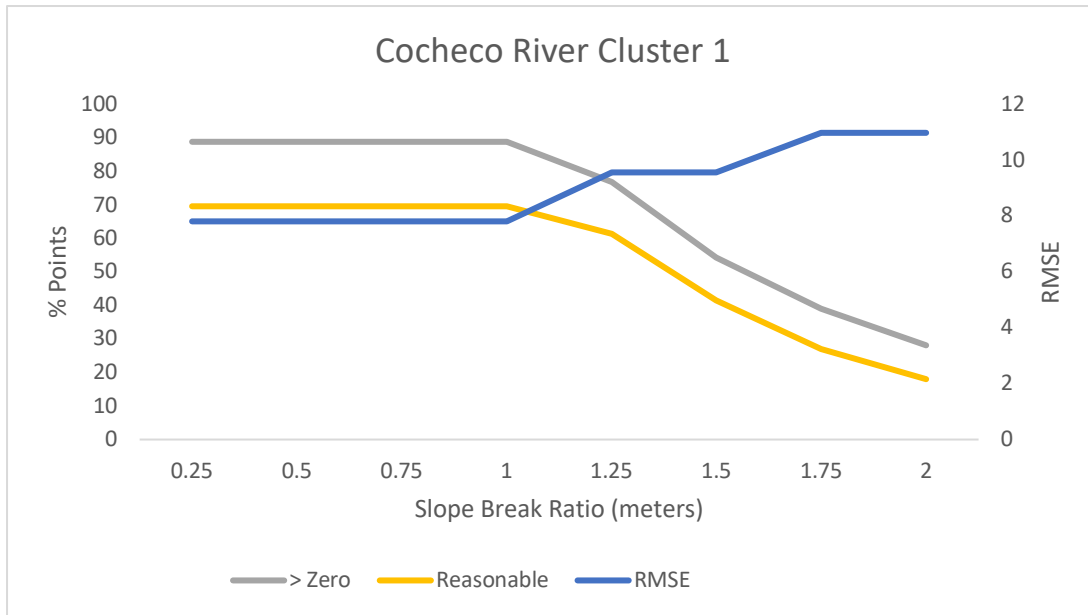


Figure B7. Calibration plot for slope break ratio in Cocheco River cluster 1, showing the percentage of non-zero width values, the percentage of reasonable width values, and the root mean square error (RMSE) between field and remotely sensed widths.

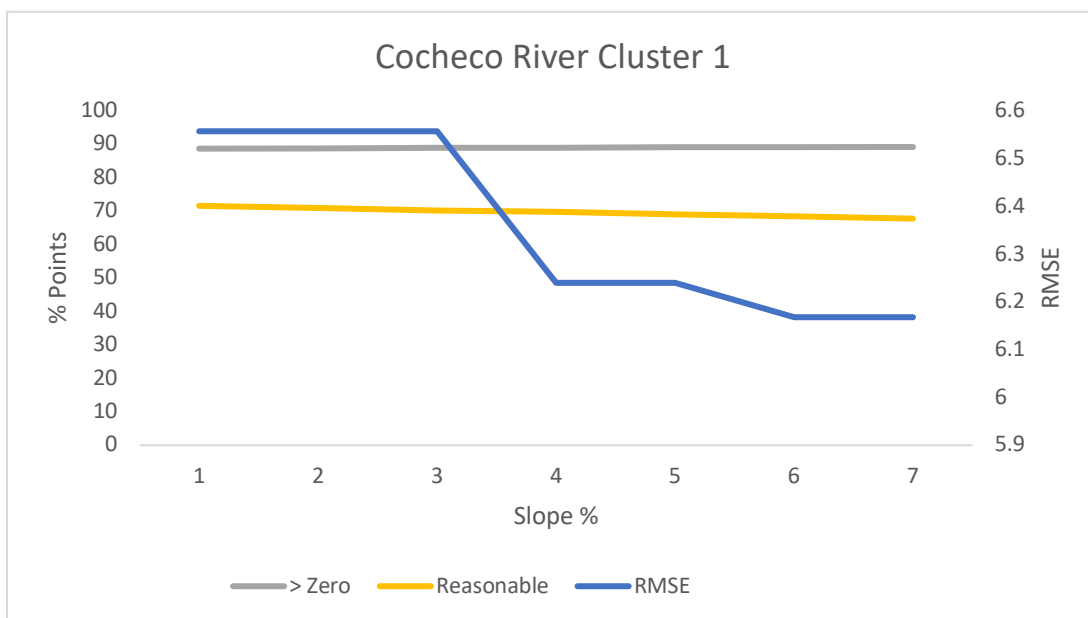


Figure B8. Calibration plot for slope break percentage in Cocheco River cluster 1, showing the percentage of non-zero width values, the percentage of reasonable width values, and the root mean square error (RMSE) between field and remotely sensed widths.

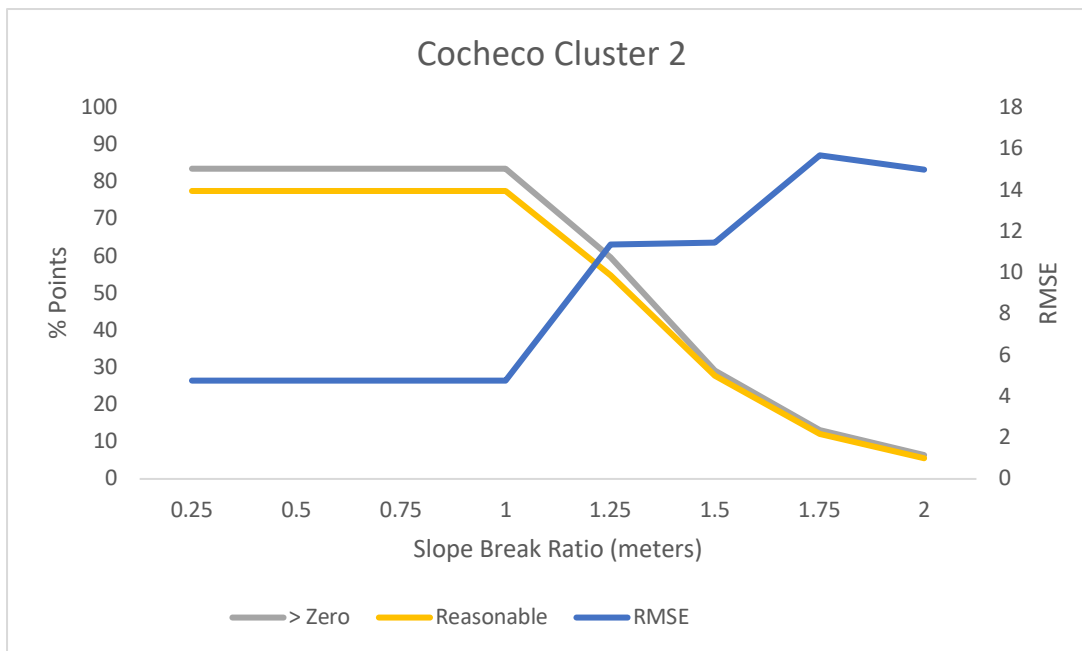


Figure B9. Calibration plot for slope break ratio in Cocheco River cluster 2, showing the percentage of non-zero width values, the percentage of reasonable width values, and the root mean square error (RMSE) between field and remotely sensed widths.

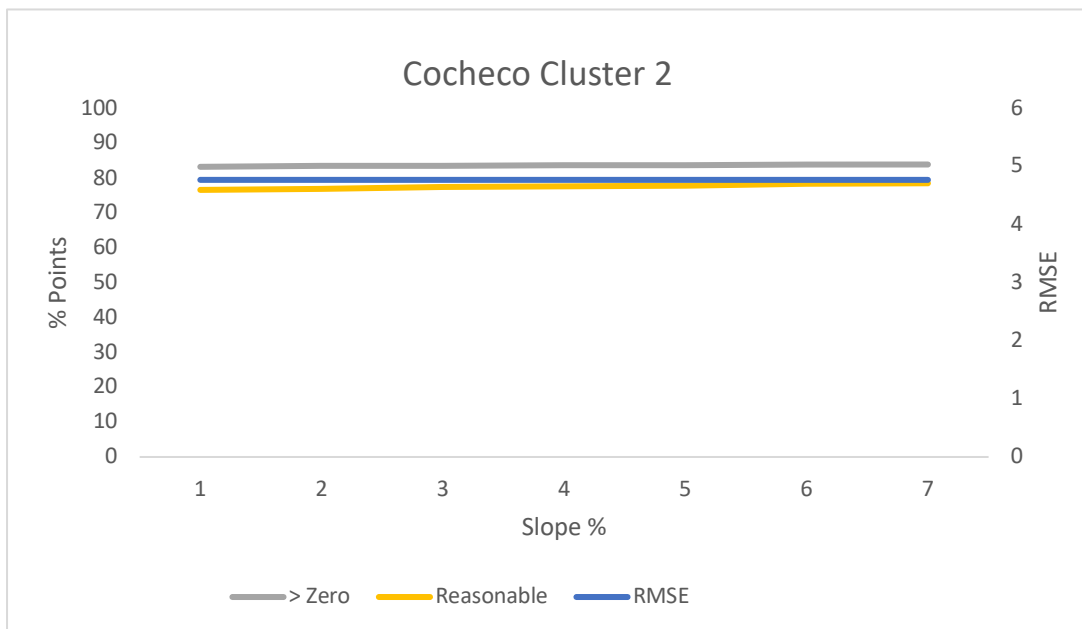


Figure B10. Calibration plot for slope break percentage in Cocheco River cluster 2, showing the percentage of non-zero width values, the percentage of reasonable width values, and the root mean square error (RMSE) between field and remotely sensed widths.

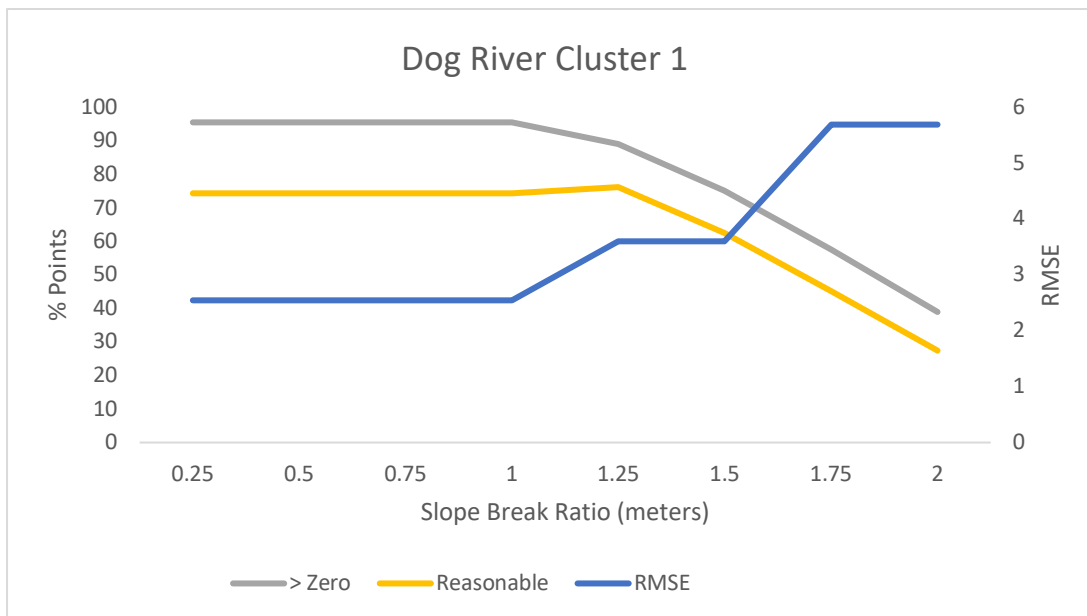


Figure B11. Calibration plot for slope break ratio in Dog River cluster 1, showing the percentage of non-zero width values, the percentage of reasonable width values, and the root mean square error (RMSE) between field and remotely sensed widths.

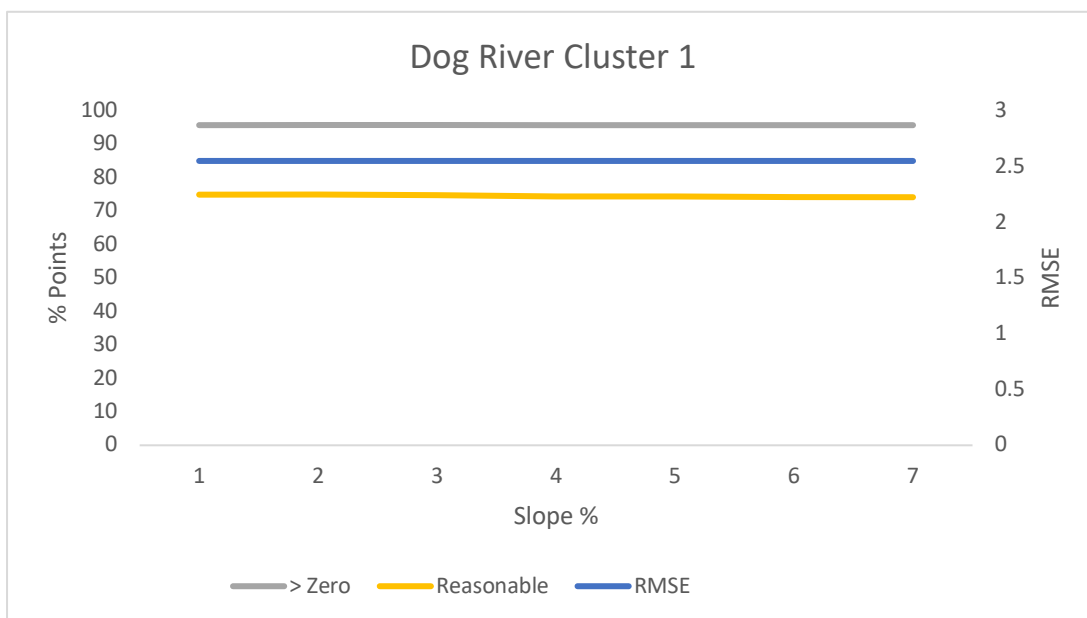


Figure B12. Calibration plot for slope break percentage in Dog River cluster 1, showing the percentage of non-zero width values, the percentage of reasonable width values, and the root mean square error (RMSE) between field and remotely sensed widths.

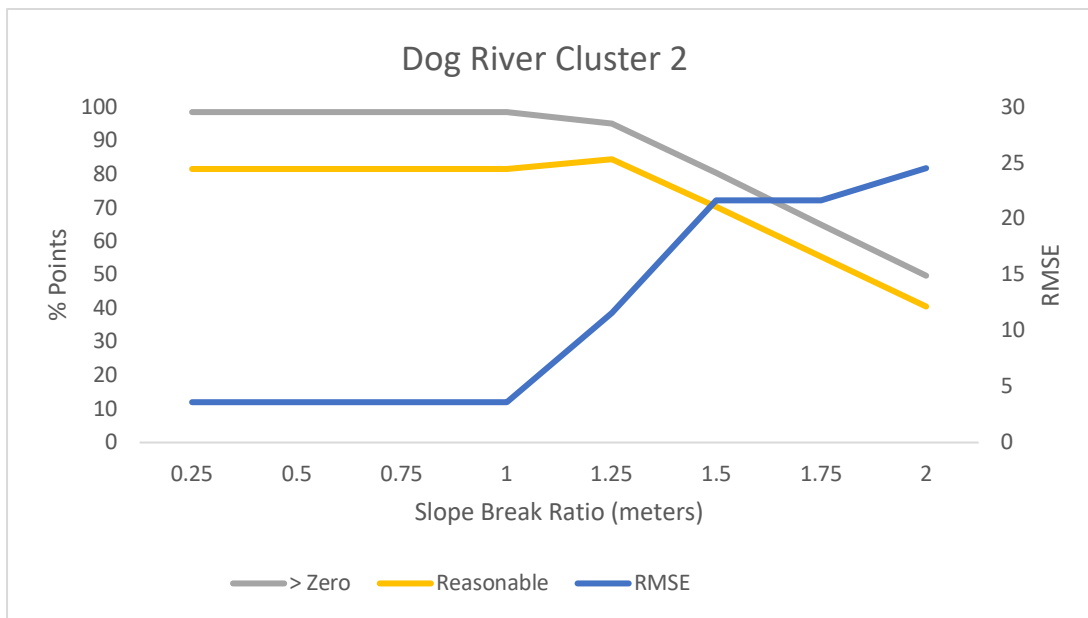


Figure B13. Calibration plot for slope break ratio in Dog River cluster 2, showing the percentage of non-zero width values, the percentage of reasonable width values, and the root mean square error (RMSE) between field and remotely sensed widths.

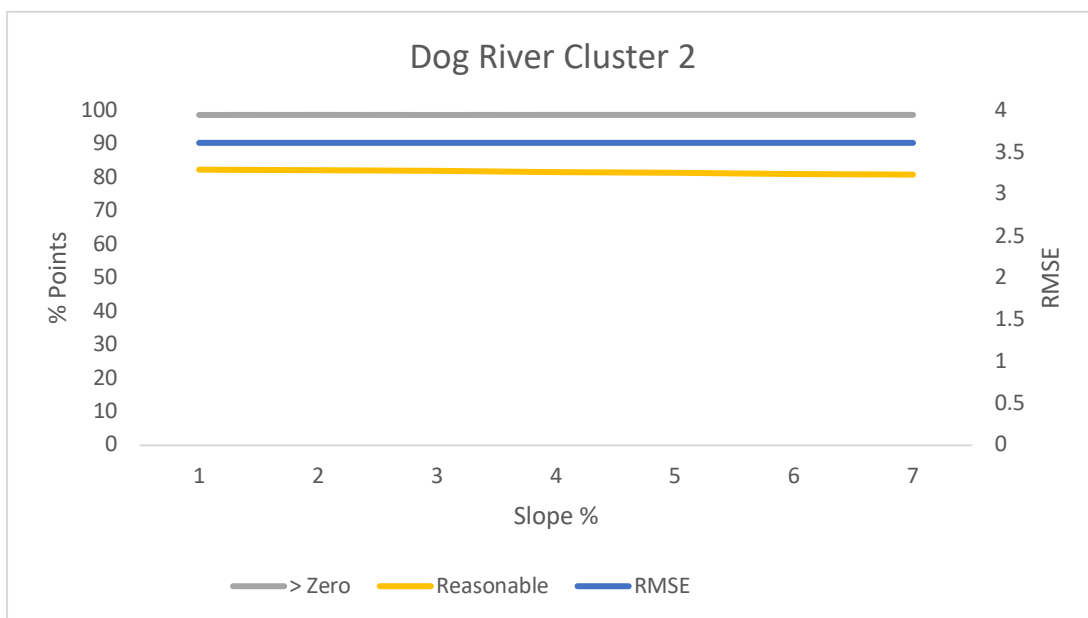


Figure B14. Calibration plot for slope break percentage in Dog River cluster 2, showing the percentage of non-zero width values, the percentage of reasonable width values, and the root mean square error (RMSE) between field and remotely sensed widths.

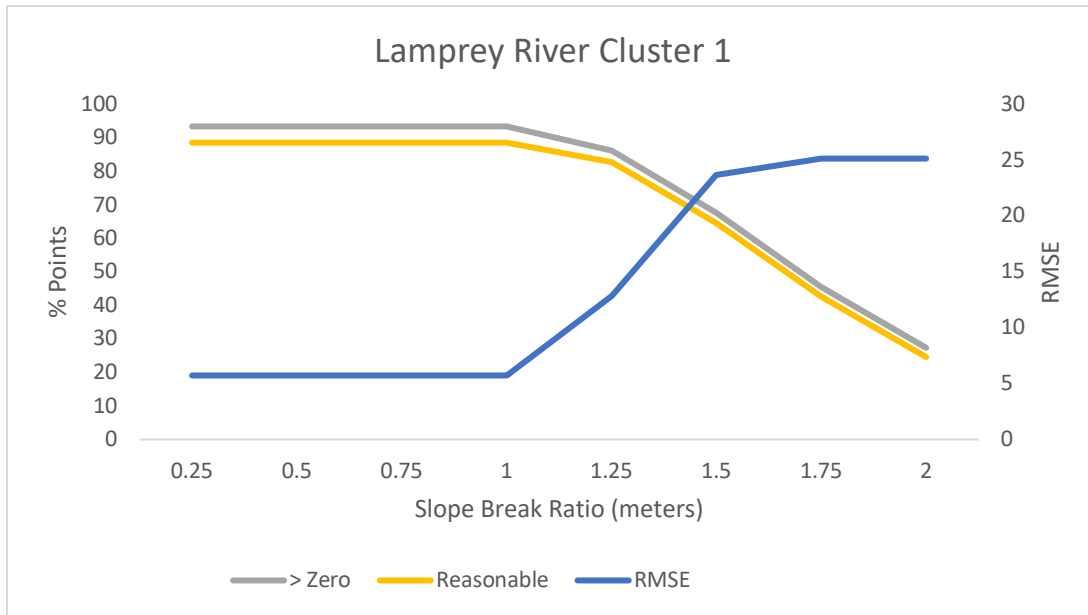


Figure B15. Calibration plot for slope break ratio in Lamprey River cluster 1, showing the percentage of non-zero width values, the percentage of reasonable width values, and the root mean square error (RMSE) between field and remotely sensed widths.

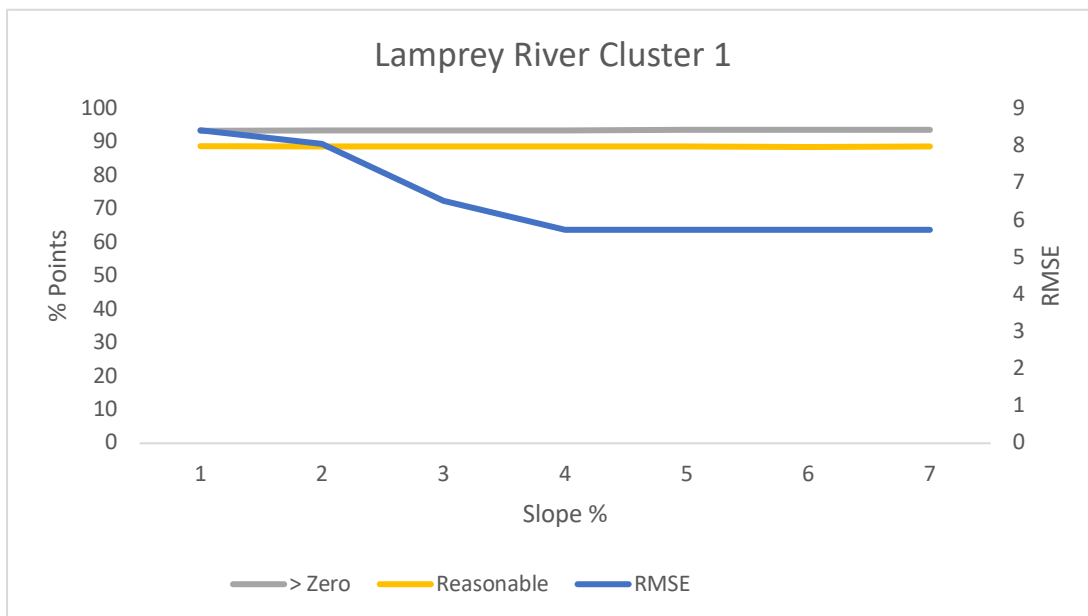


Figure B16. Calibration plot for slope break percentage in Lamprey River cluster 1, showing the percentage of non-zero width values, the percentage of reasonable width values, and the root mean square error (RMSE) between field and remotely sensed widths.

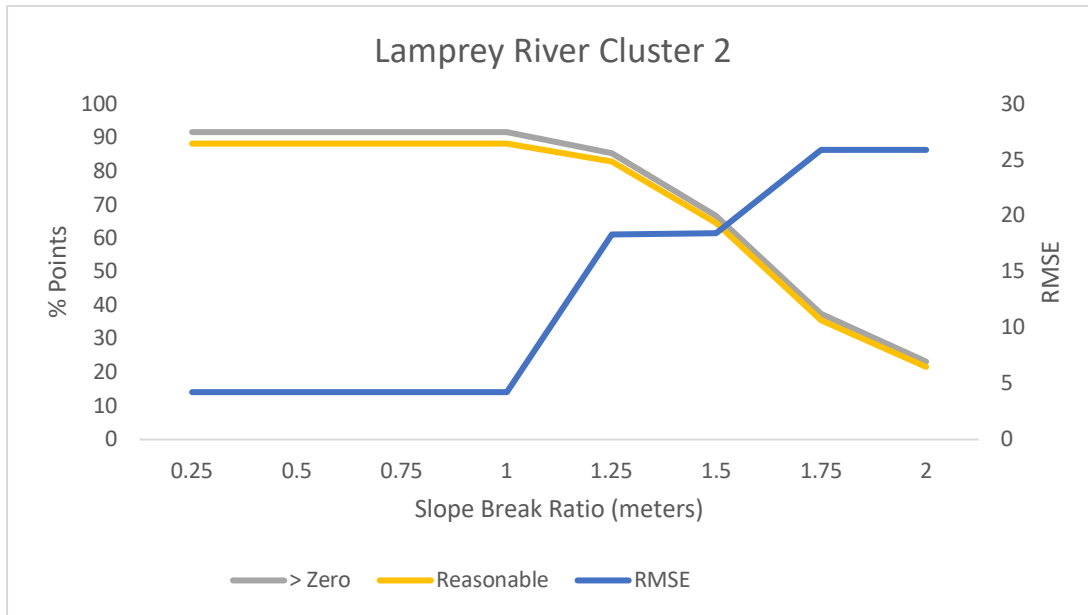


Figure B17. Calibration plot for slope break ratio in Lamprey River cluster 2, showing the percentage of non-zero width values, the percentage of reasonable width values, and the root mean square error (RMSE) between field and remotely sensed widths.

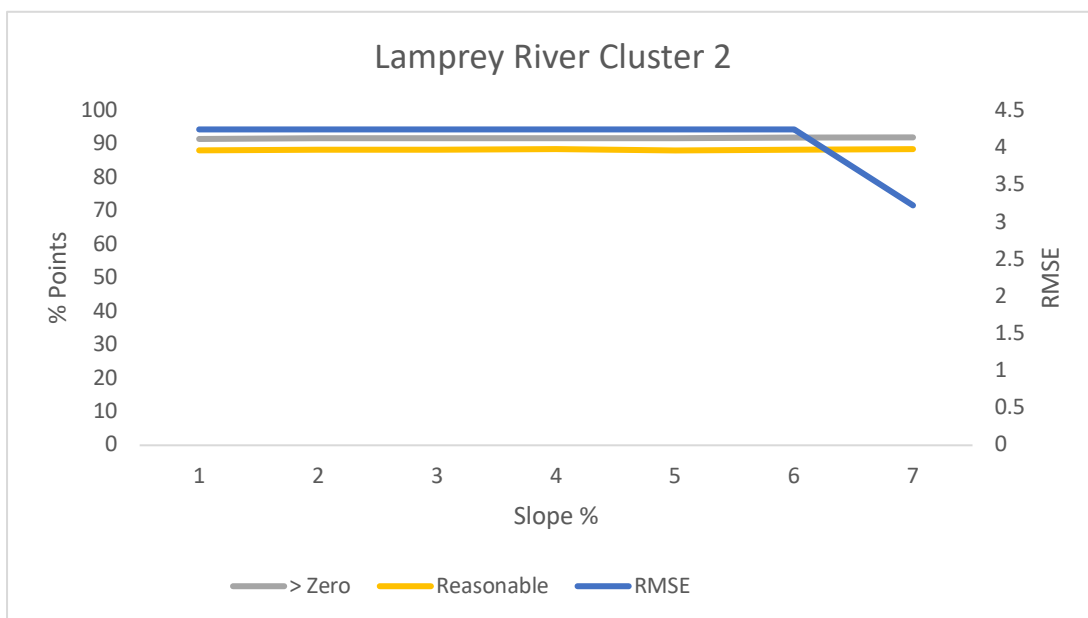


Figure B18. Calibration plot for slope break percentage in Lamprey River cluster 2, showing the percentage of non-zero width values, the percentage of reasonable width values, and the root mean square error (RMSE) between field and remotely sensed widths.

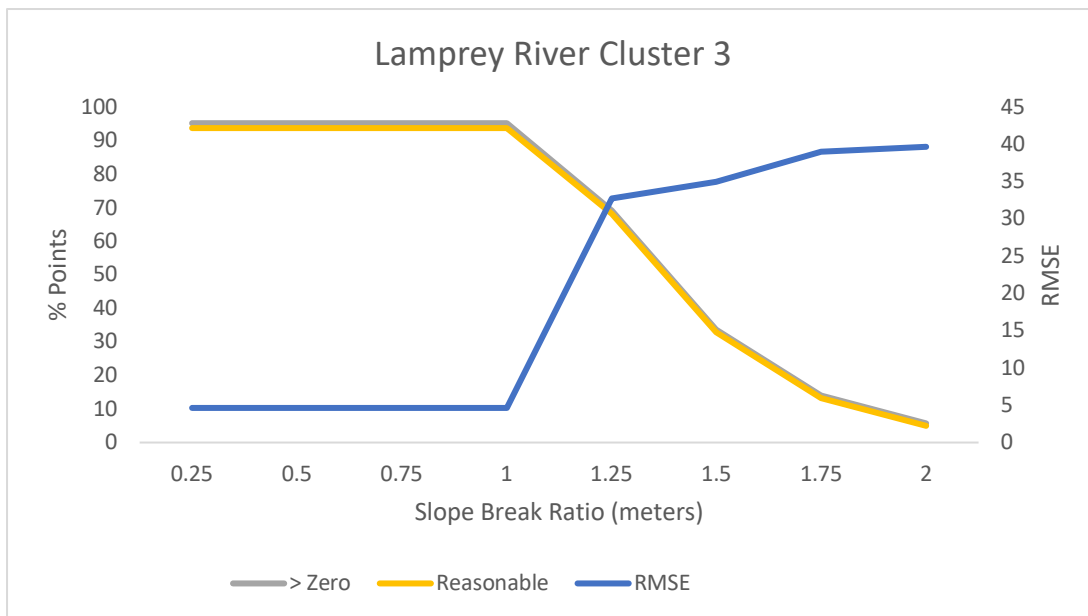


Figure B19. Calibration plot for slope break ratio in Lamprey River cluster 3, showing the percentage of non-zero width values, the percentage of reasonable width values, and the root mean square error (RMSE) between field and remotely sensed widths.

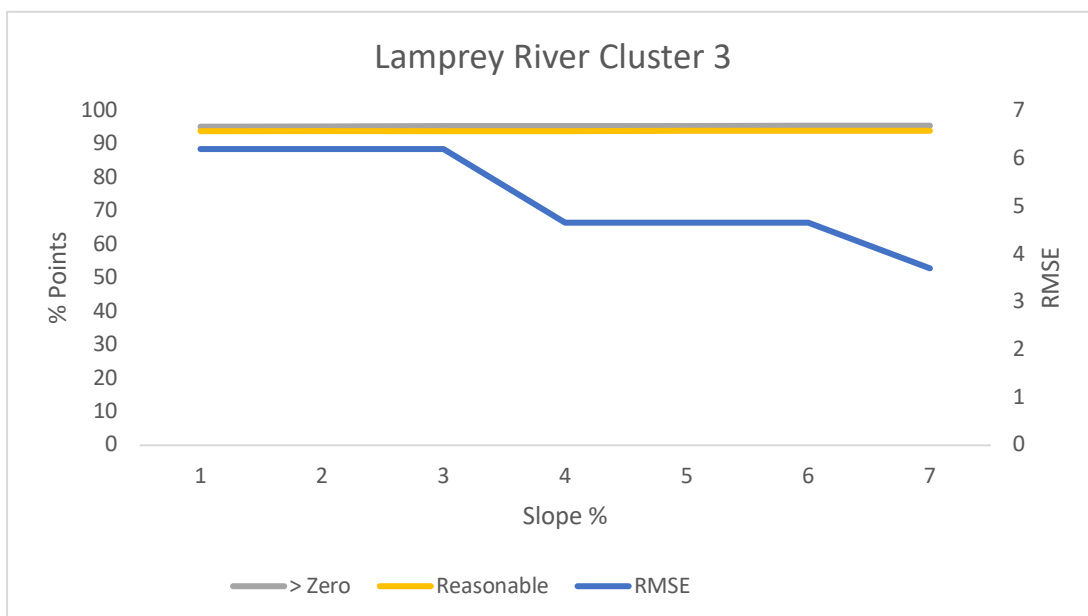


Figure B20. Calibration plot for slope break percentage in Lamprey River cluster 3, showing the percentage of non-zero width values, the percentage of reasonable width values, and the root mean square error (RMSE) between field and remotely sensed widths.

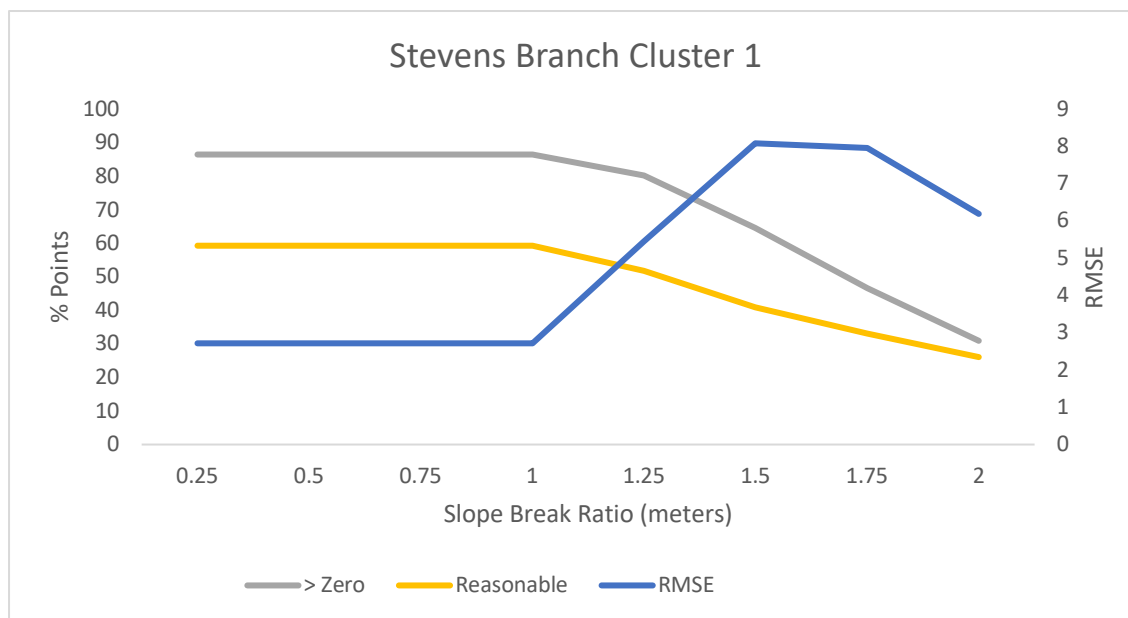


Figure B21. Calibration plot for slope break ratio in Stevens Branch cluster 1, showing the percentage of non-zero width values, the percentage of reasonable width values, and the root mean square error (RMSE) between field and remotely sensed widths.

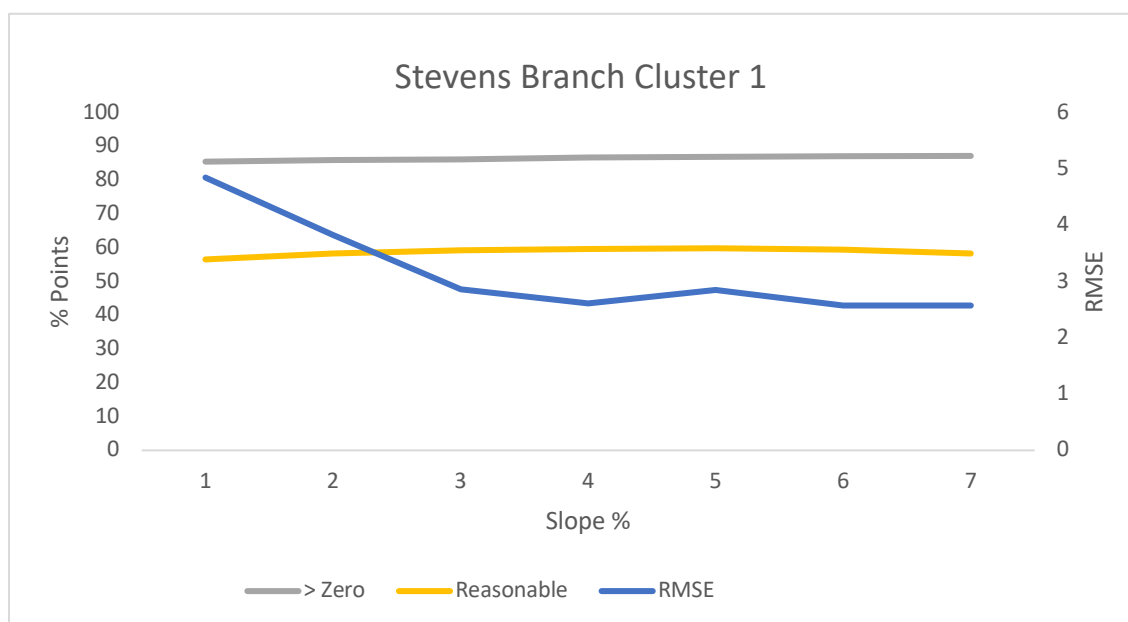


Figure B22. Calibration plot for slope break percentage in Stevens Branch cluster 1, showing the percentage of non-zero width values, the percentage of reasonable width values, and the root mean square error (RMSE) between field and remotely sensed widths.

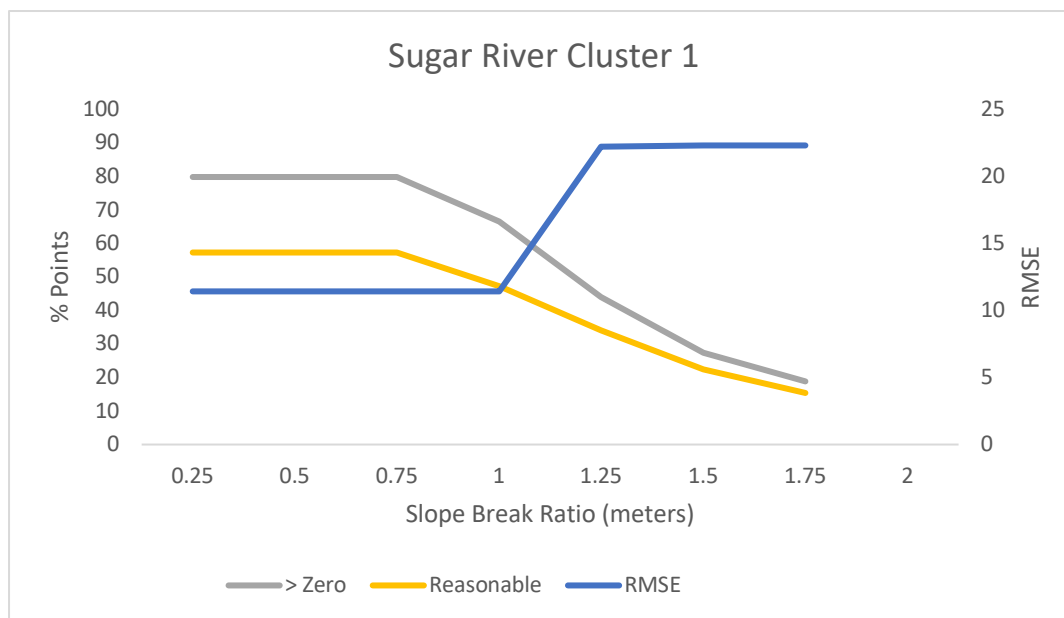


Figure B23. Calibration plot for slope break ratio in Sugar River cluster 1, showing the percentage of non-zero width values, the percentage of reasonable width values, and the root mean square error (RMSE) between field and remotely sensed widths.

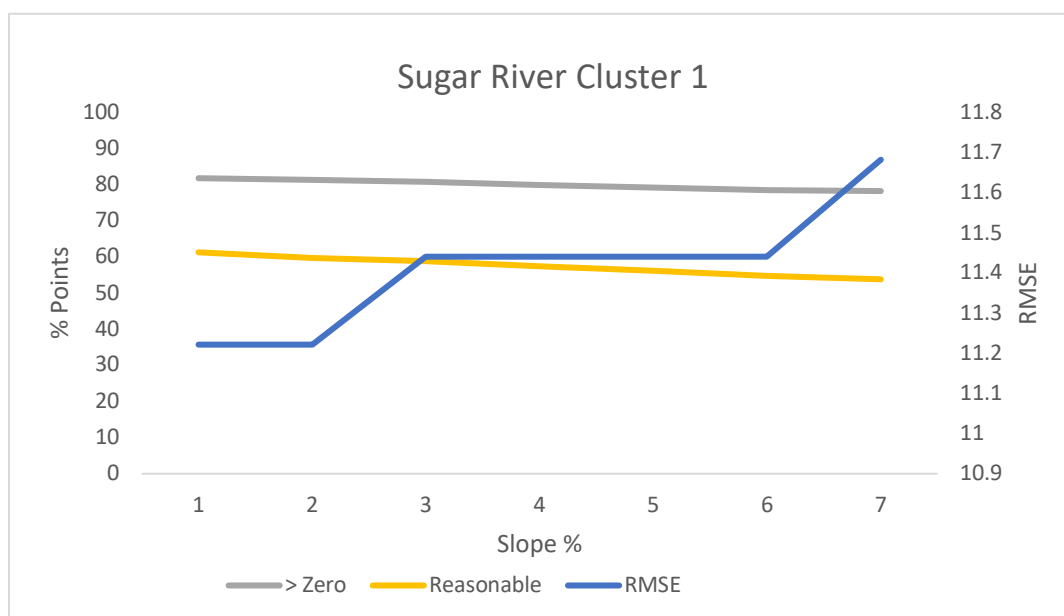


Figure B24. Calibration plot for slope break percentage in Sugar River cluster 1, showing the percentage of non-zero width values, the percentage of reasonable width values, and the root mean square error (RMSE) between field and remotely sensed widths.

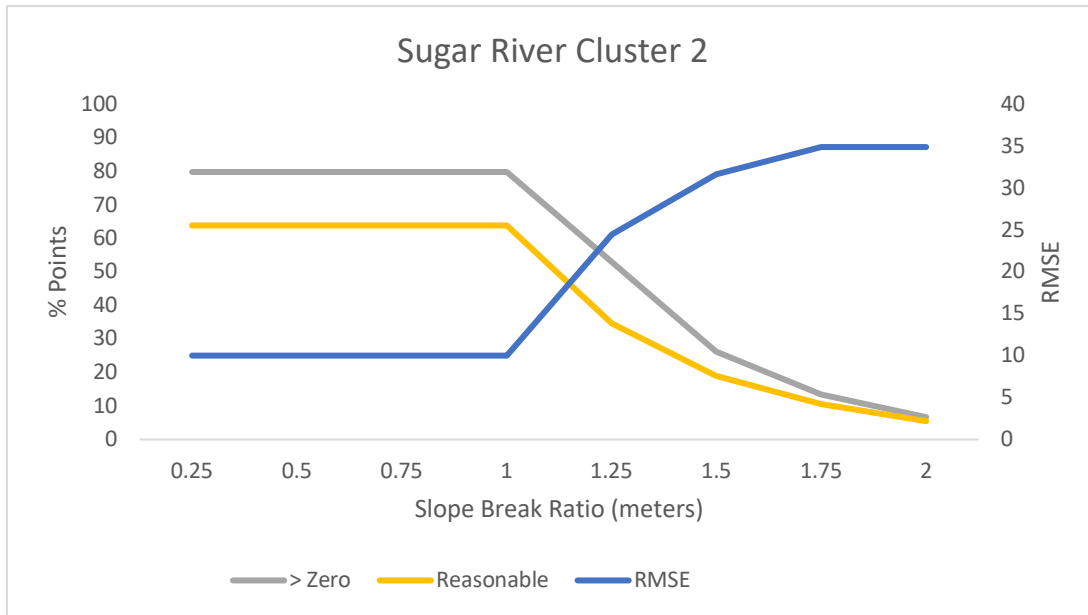


Figure B25. Calibration plot for slope break ratio in Sugar River cluster 2, showing the percentage of non-zero width values, the percentage of reasonable width values, and the root mean square error (RMSE) between field and remotely sensed widths.

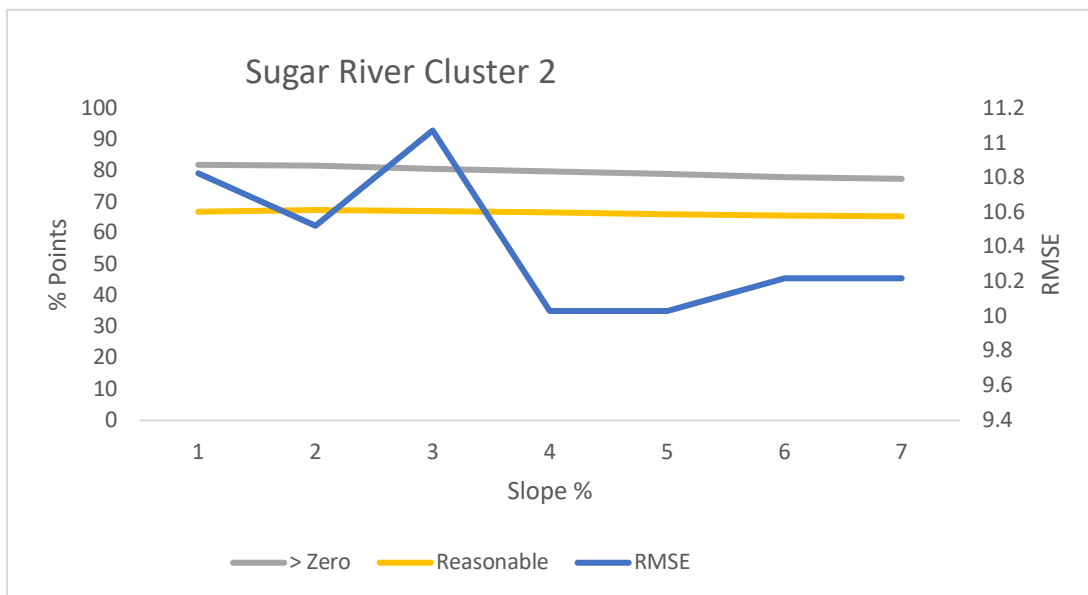


Figure B26. Calibration plot for slope break percentage in Sugar River cluster 2, showing the percentage of non-zero width values, the percentage of reasonable width values, and the root mean square error (RMSE) between field and remotely sensed widths.

## Appendix C

This appendix presents all the longitudinal profiles with smoothed remotely sensed bankfull widths and smoothed normalized bankfull widths as a function of distance, downstream of each site's assessed reaches.

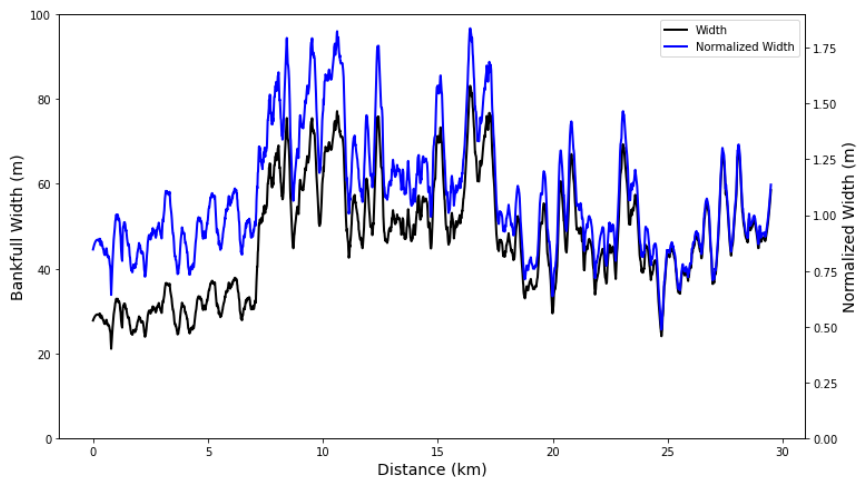


Figure C1. Ammonoosuc River longitudinal profile with smoothed remotely sensed bankfull widths and smoothed normalized bankfull width as a function of distance downstream of the Beacon Street Bridge, Littleton, NH.

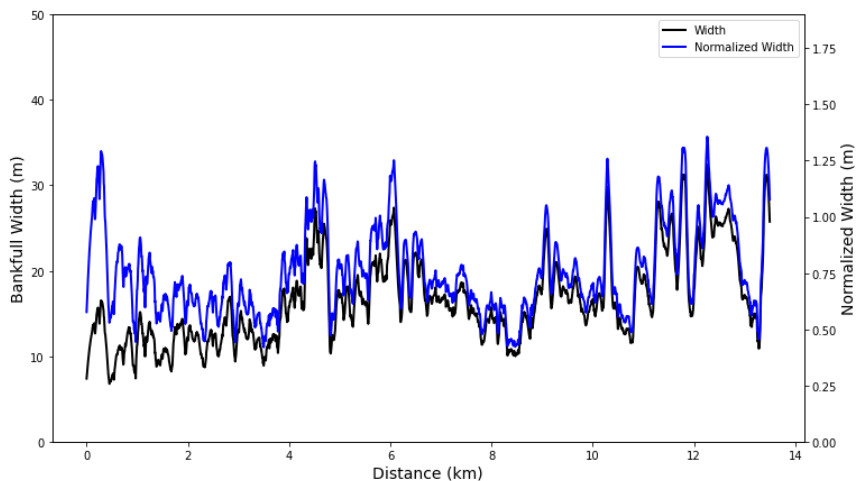


Figure C2. Cocheco River longitudinal profile with smoothed remotely sensed bankfull widths and smoothed normalized bankfull width as a function of distance downstream of the Bay Road Bridge, Farmington, NH.

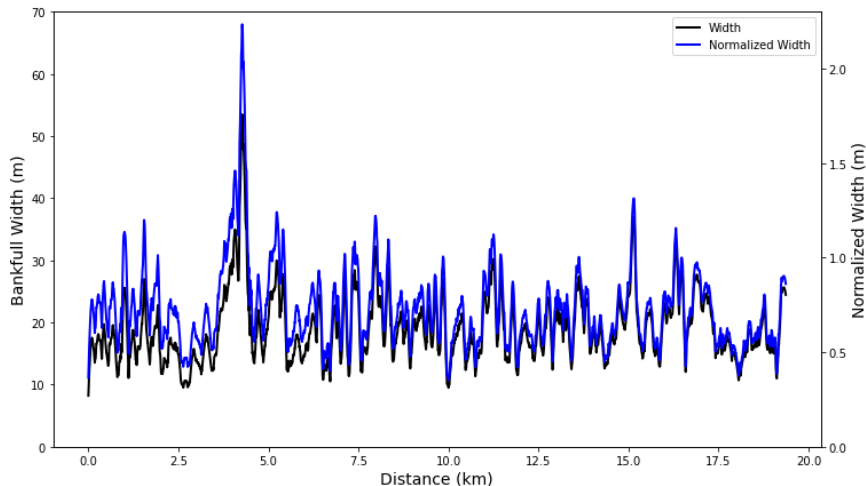


Figure C3. Dog River longitudinal profile with smoothed remotely sensed bankfull widths and smoothed normalized bankfull width as a function of distance downstream of the Stony Brook Road Bridge, Northfield, VT.

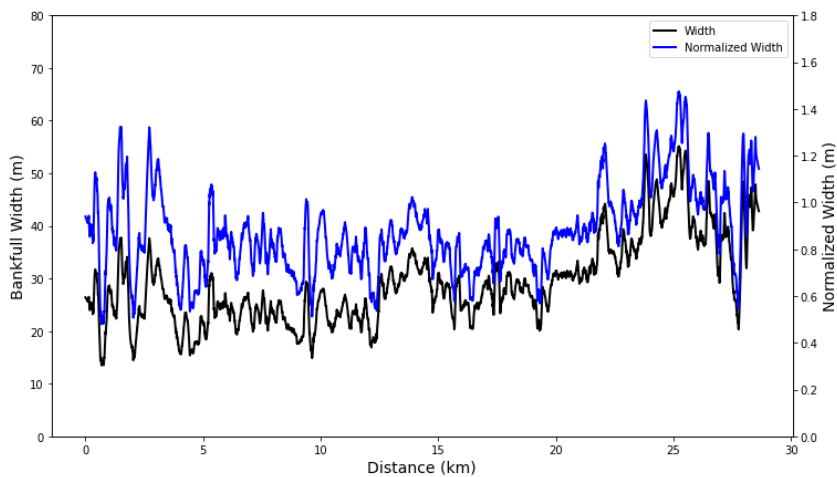


Figure C4. Lamprey River longitudinal profile with smoothed remotely sensed bankfull widths and smoothed normalized bankfull width as a function of distance downstream of the Route 125 Bridge, Epping, NH.

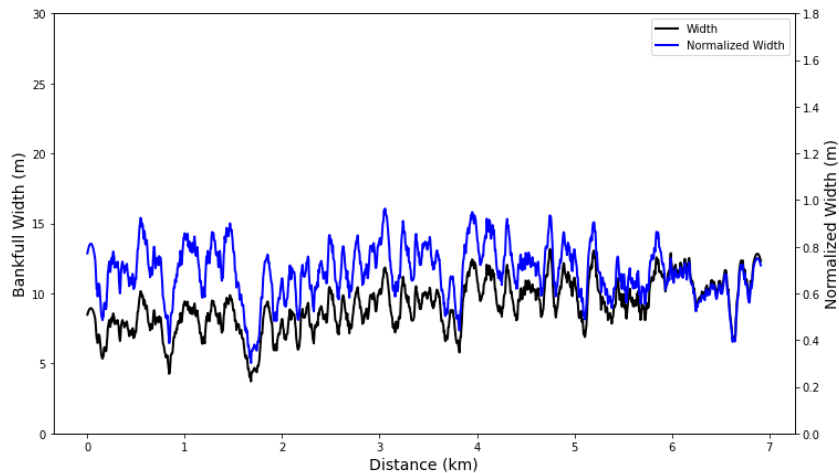


Figure C5. Stevens Branch longitudinal profile with smoothed remotely sensed bankfull widths and smoothed normalized bankfull width as a function of distance downstream of the Old Town Road Bridge, Williamstown, VT.

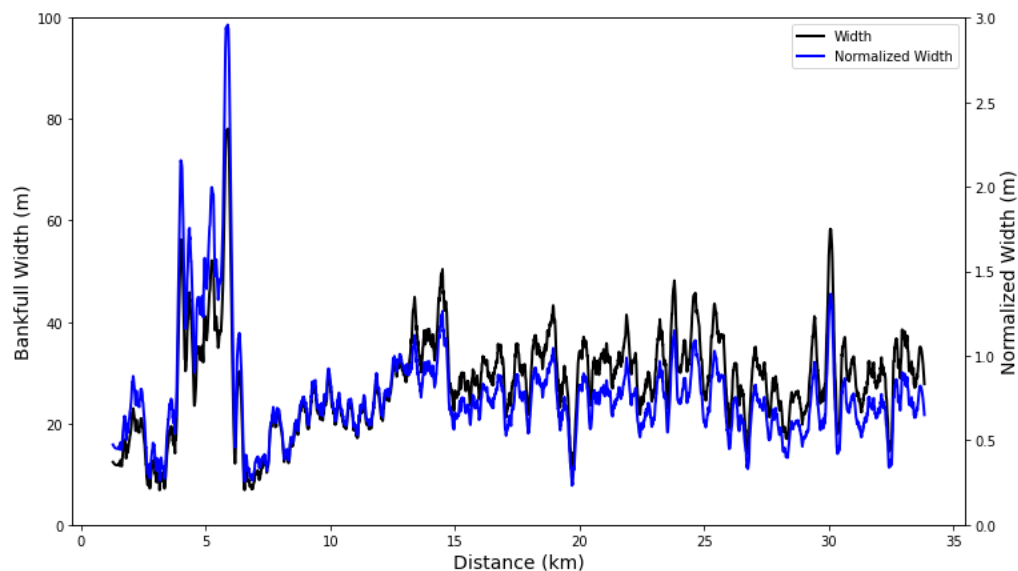


Figure C6. Sugar River longitudinal profile with smoothed remotely sensed bankfull widths and smoothed normalized bankfull width as a function of distance downstream of the Treatment Plant Road Bridge, Newport, NH.

Appendix D

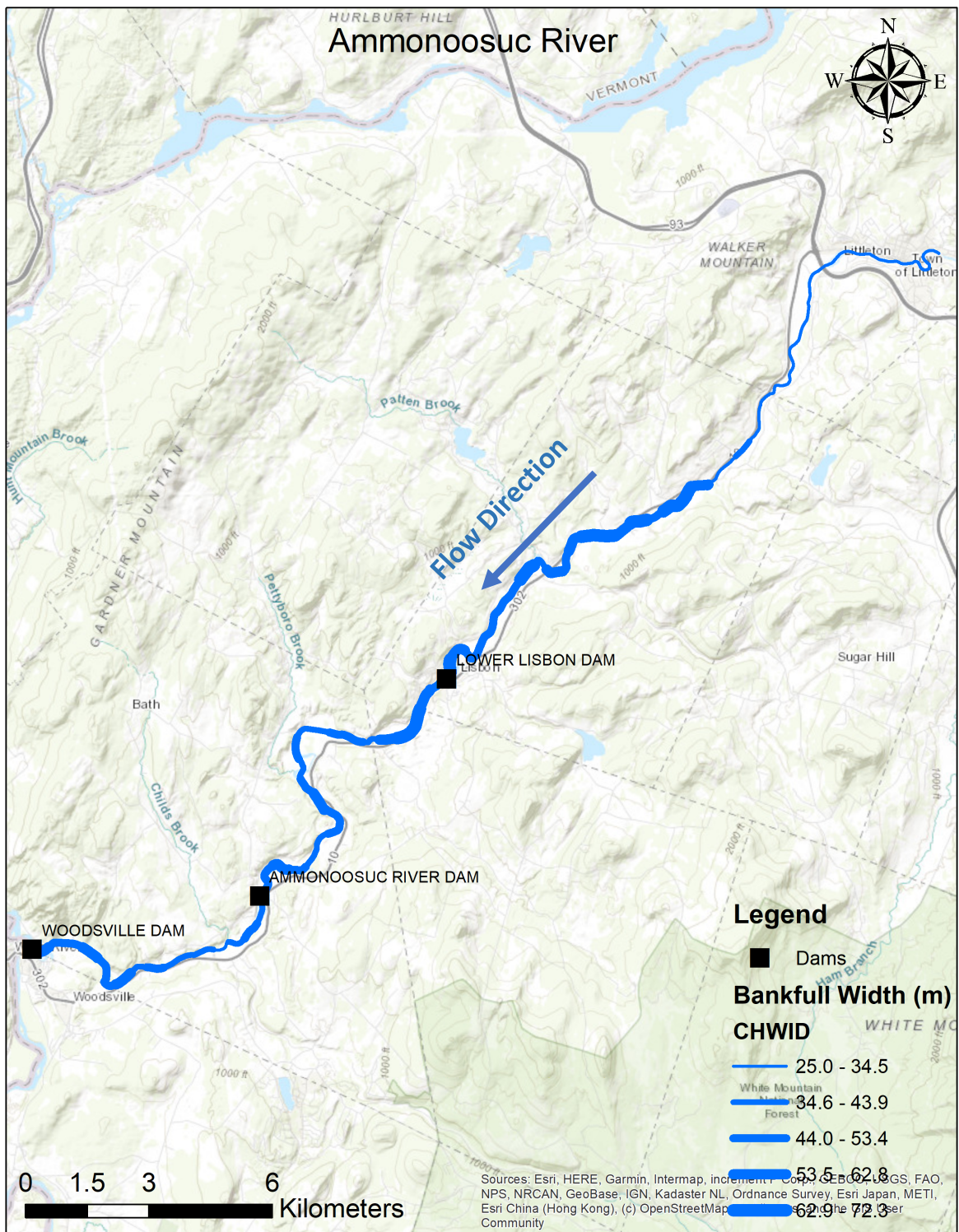


Figure D-1. Mean remotely sensed bankfull width along Ammonoosuc River.

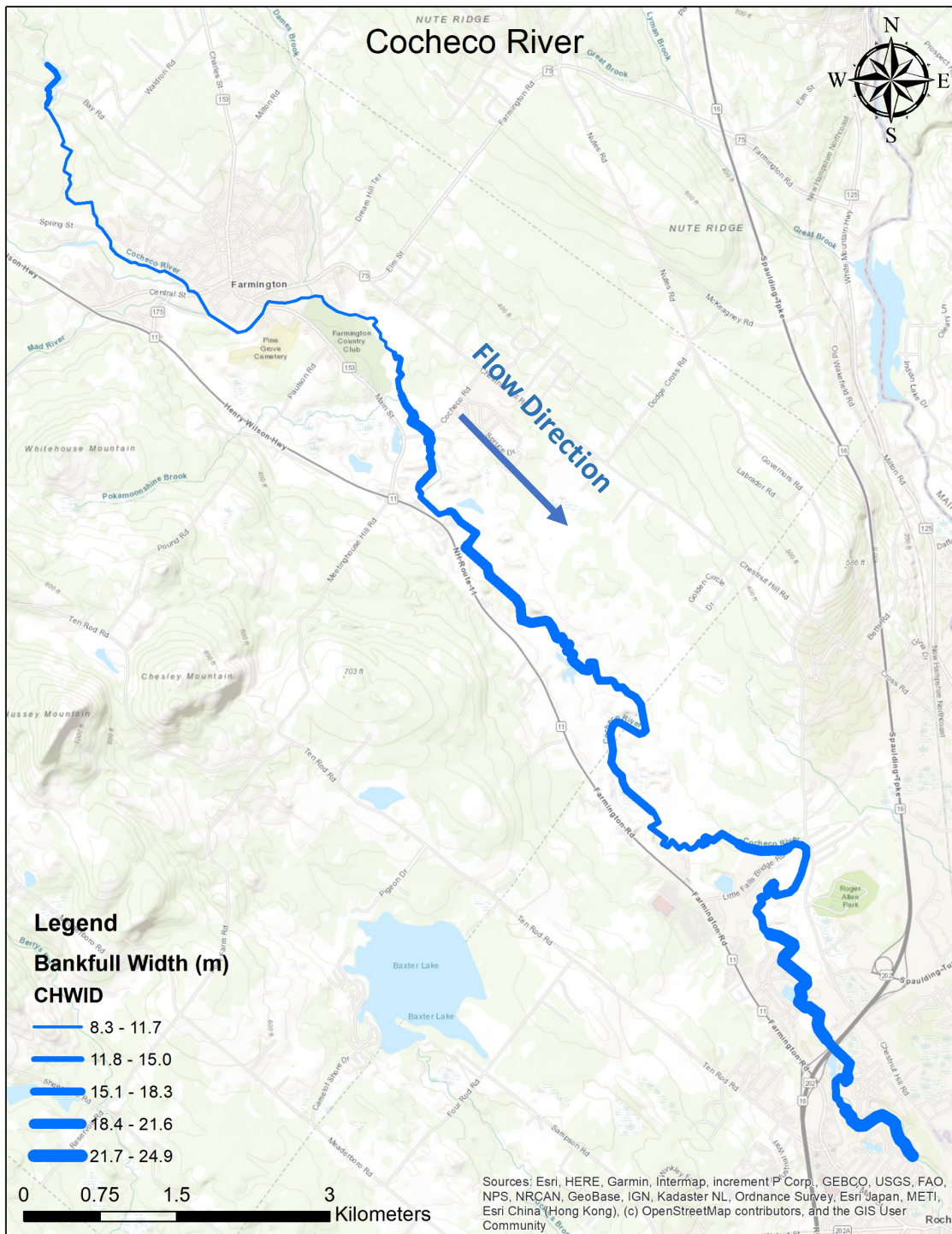


Figure D-2. Mean remotely sensed bankfull width along Cocheco River.

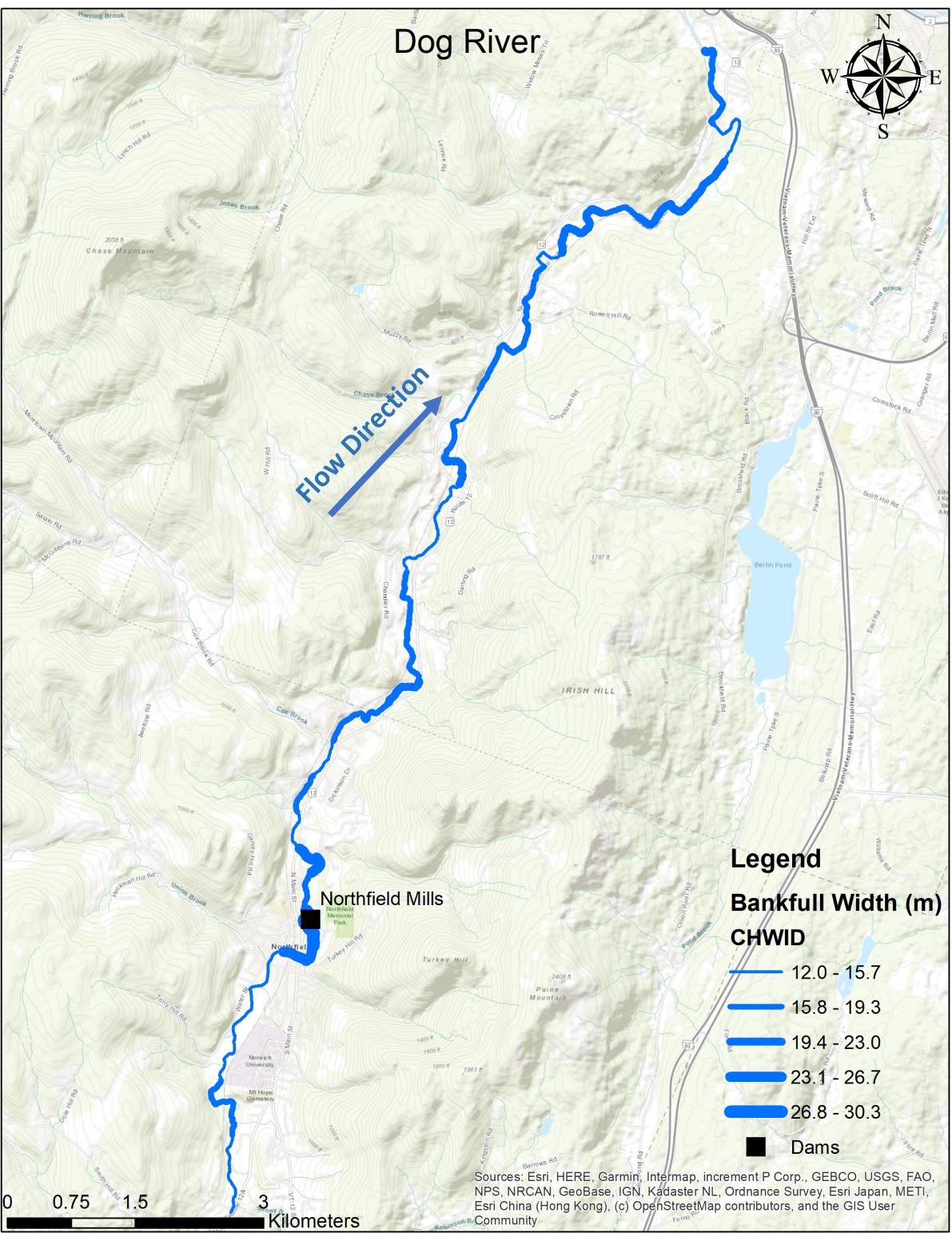


Figure D-3. Mean remotely sensed bankfull width along Dog River.

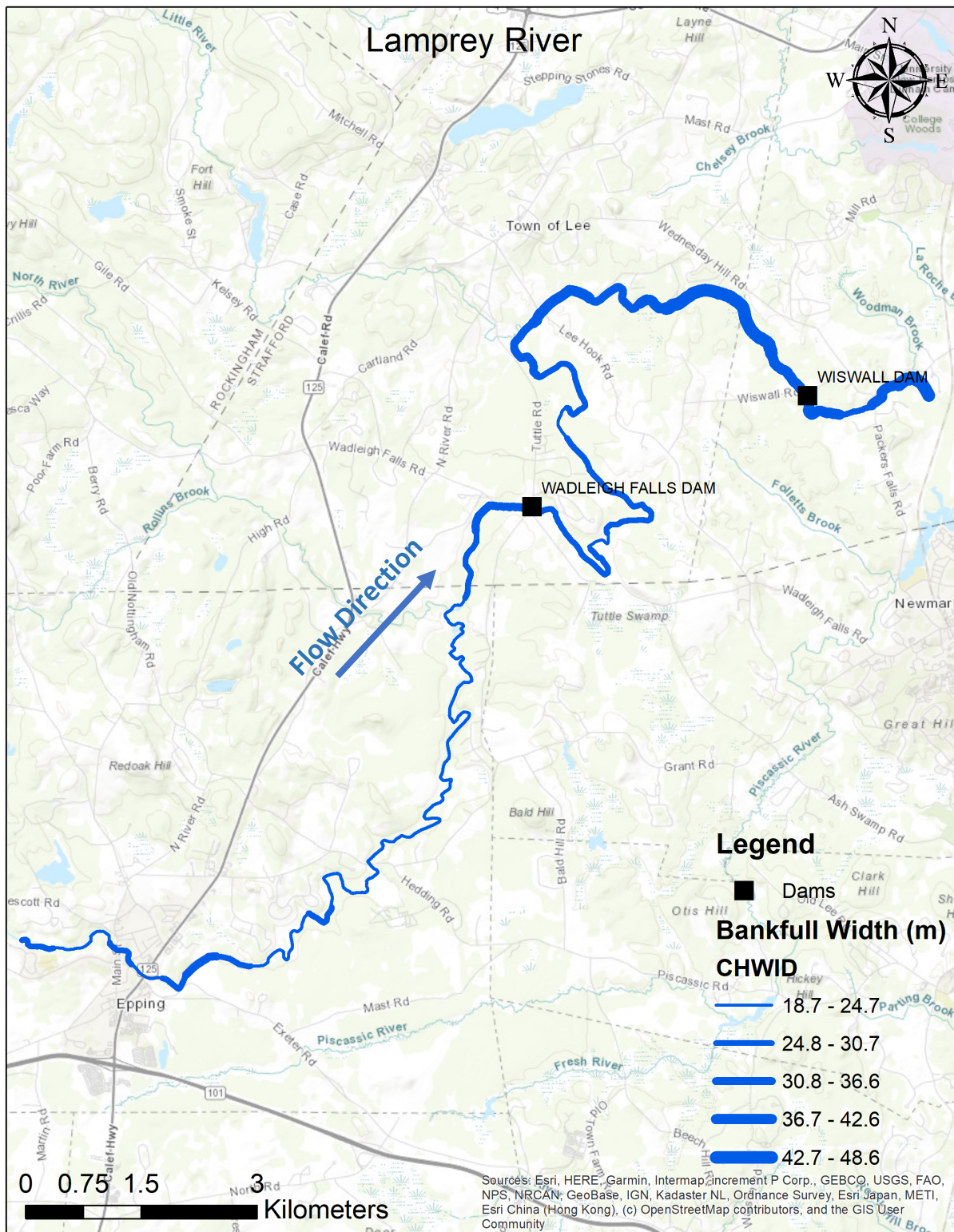


Figure D-4. Mean remotely sensed bankfull width along Lamprey River.

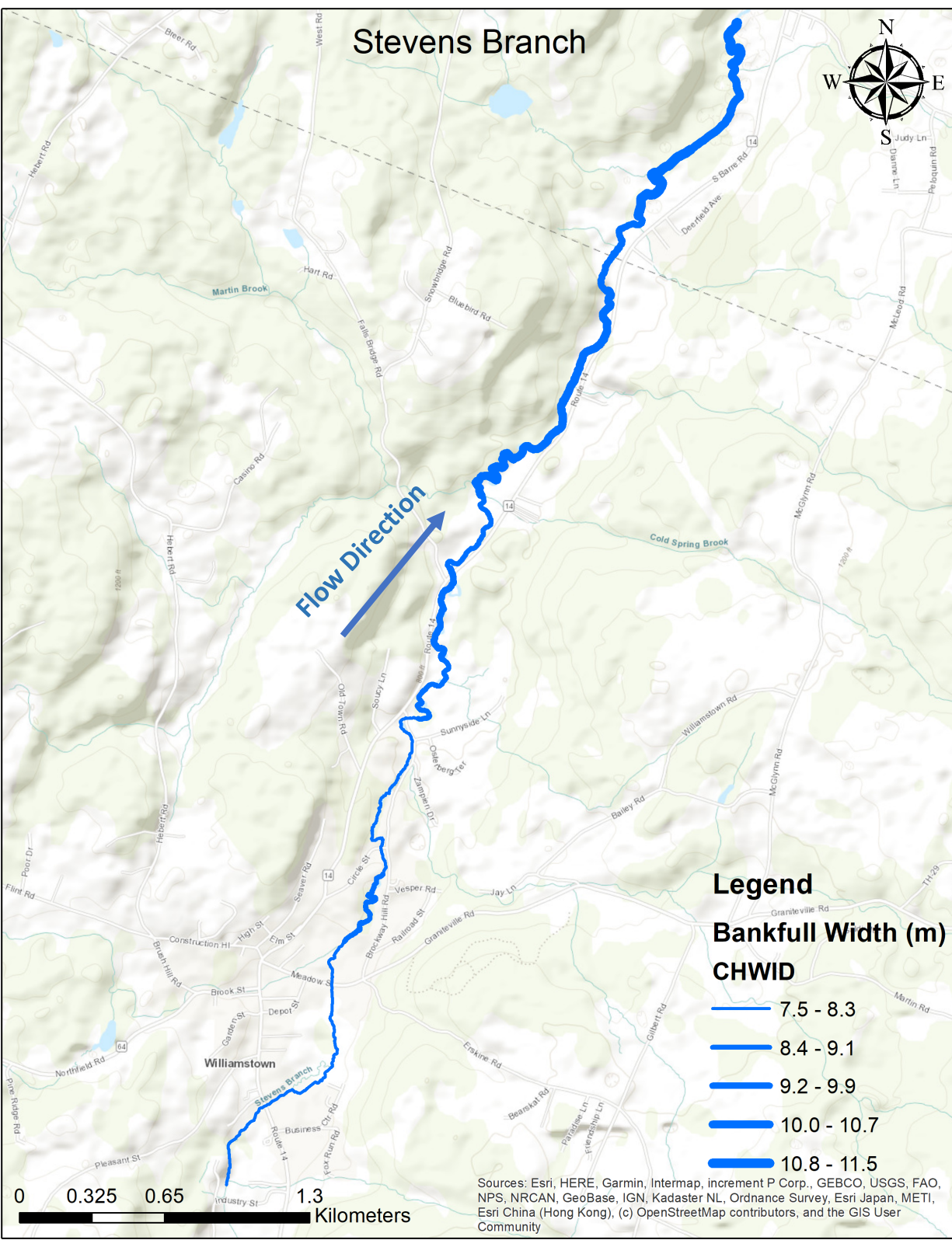


Figure D-5. Mean remotely sensed bankfull width along Stevens Branch.

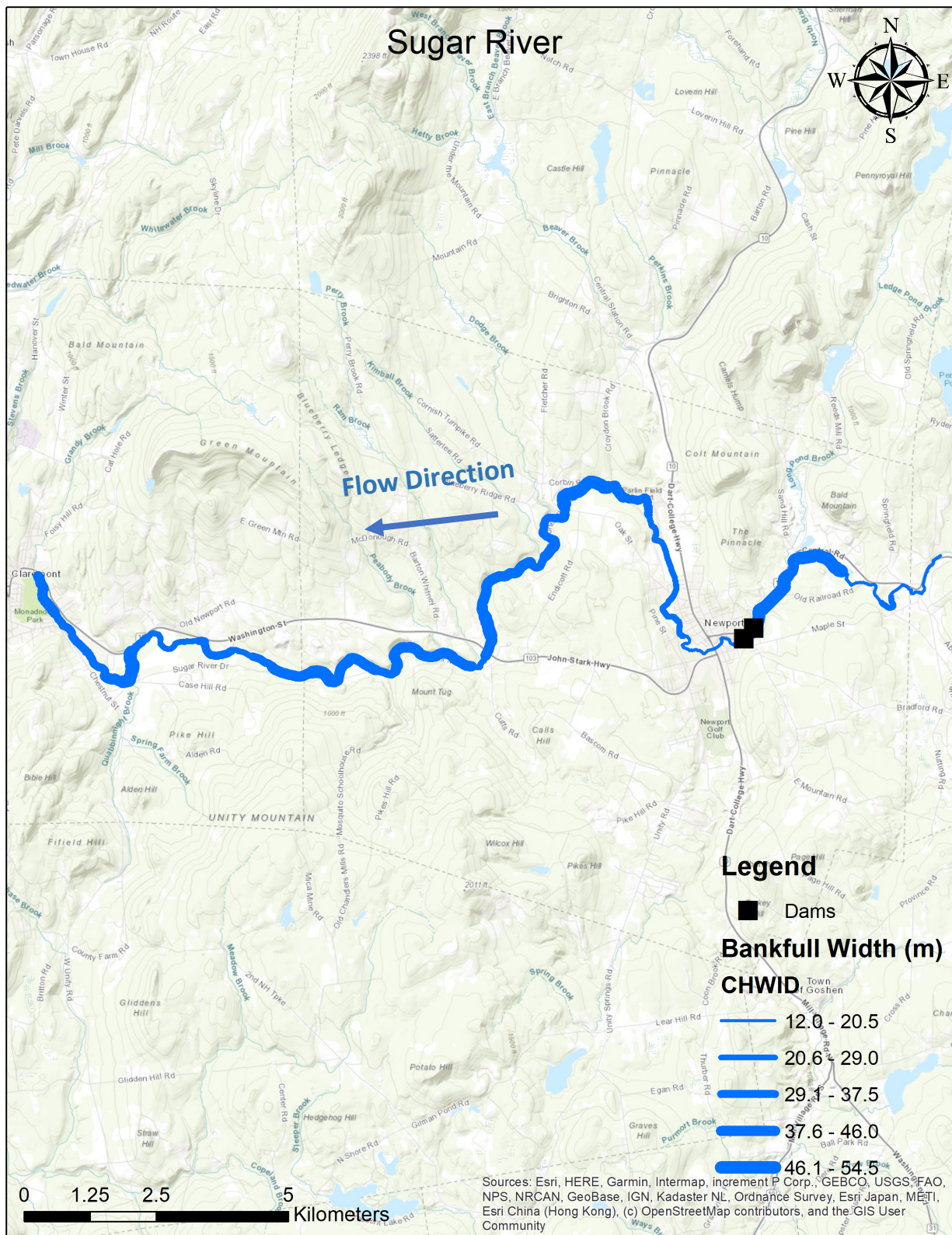


Figure D-6. Mean remotely sensed bankfull width along Sugar River.

## LIST OF REFERENCES

- Abernethy, B., Rutherford, I.D. (1998). Where Along a River's Length Will Vegetation Most Effectively Stabilize Stream Banks? *Geomorphology* 23:55-75.
- Anderson, L. W. (2004). Width of streams and rivers in response to vegetation, bank material, and other factors. *Journal of the American Water Resources Association*, 40(5), 1325-1336.
- Anning, D. W. (2011). Modeled sources, transport, and accumulation of dissolved solids in water resources of the southwestern United States. *Journal of the American Water Resources Association*.
- Bent, G.C., Waite, A.M., (2013). Equations for estimating bankfull channel geometry and discharge for streams in Massachusetts: U.S. Geological Survey Scientific Investigations Report 2013-5155, 62 p., <http://dx.doi.org/10.3133/sir20135155>.
- Bessar, M. A., Matte, P., Anctil, F. (2020). Uncertainty Analysis of a 1D River Hydraulic Model with Adaptive Calibration. *Water*, 12(2), 561. MDPI AG. Retrieved from <http://dx.doi.org/10.3390/w12020561>.
- Bieger, K., Rathjens, H., Allen, P. M., Arnold, J. G. (2015). Development and evaluation of bankfull hydraulic geometry relationships for the physiographic regions of the United States. *Journal of the American Water Resources Association (JAWRA)*, 51(3), 842-858.
- Caruso, M., Cavalli, M., Tarolli, P. (2019). Mapping riverbed grain size distribution with a small unmanned aerial vehicle (UAV). *Water*, 11(10), 2021.
- Casado, A., Peiry, J-L., Campo, A.M. (2016). Geomorphic and vegetation changes in a meandering dryland river regulated by a large dam, Sauce Grande River, Argentina. *Geomorphology*, 268, 21-34.
- Costigan, K.H., Daniels, M.D., Perkin, J.S., Gido, K.B. (2014). Longitudinal variability in hydraulic geometry and substrate characteristics of a Great Plains sandbed river. *Geomorphology*, 210, 48-58.
- Davies-Colley, R.J., (1997). Stream Channels are Narrower in Pasture Than in Forest. *New Zealand J. Marine and Freshwater Research* 31:599-608.
- De Rosa, P., Fredduzzi, A., Cencetti, C. (2019). A GIS-Based Tool for Automatic Bankfull Detection from Airborne High-Resolution Dem. *ISPRS International Journal of Geo-Information*, 8(11), 480. MDPI AG. Retrieved from <http://dx.doi.org/10.3390/ijgi8110480>.

- Dewitz, J., & U.S. Geological Survey. (2021). National Land Cover Database (NLCD) 2019 Products (ver. 2.0, June 2021). US Geological Survey.
- Earth Science Data Systems, NASA. (n.d.). Lidar. NASA. Retrieved April 1, 2023, from [https://www.earthdata.nasa.gov/technology/lidar#:~:text=Lidar%20stands%20for%20Light%20Detection,\(near%20IR%20and%20green\).](https://www.earthdata.nasa.gov/technology/lidar#:~:text=Lidar%20stands%20for%20Light%20Detection,(near%20IR%20and%20green).)
- Eke, E., Czapiga, M., Viparelli, E., Shimizu, Y., Imran, J., Sun, T., Parker, G. (2014). Coevolution of width and sinuosity in meandering rivers. *Journal of Fluid Mechanics*, 760, 127-174. doi:10.1017/jfm.2014.556.
- Faustini, J., Kaufmann, P., Herlihy, A. (2009). Downstream Variation in Bankfull Width of Wadeable Streams Across the Conterminous United States.
- Faux, R. N., Buffington, J. M., Whitley, M. G., Lanigan, S. H., Roper, B. B. (2010). Use of airborne near-infrared LiDAR for determining channel cross-section characteristics and monitoring aquatic habitat in Pacific Northwest rivers: A preliminary analysis. *Journal of the American Water Resources Association*, 46(2), 245-255.
- Ferguson, R.I., (1973). Channel Pattern and Sediment Type. *Area* 5:38-41.
- Gartner, J.D., Magilligan, F.J., Renshaw, C.E. (2015). Predicting the type, location and magnitude of geomorphic responses to dam removal: Role of hydrologic and geomorphic constraints. *Geomorphology*, 251, 20-30.
- Golly, A., Turowski, J.M. (2017). Deriving principal channel metrics from bank and long-profile geometry with the R package cmgo. *Earth Surface Dynamics*, 5, 557-570.
- Hernández, Danilla S., González-Trinidad, J., Júnez-Ferreira, H. E., Bautista-Capetillo, C. F., Morales de Ávila, H., Cázares Escareño, J., Ortiz-Letechipia, J., et al. (2022). Effects of the DEM and Hydrological Processing Algorithms on the Geomorphological Parameterization. *Water*, 14(15), 2363.
- Hladik, C., Alber, M. (2012). Accuracy assessment and correction of a LIDAR-derived salt marsh digital elevation model. *Remote Sensing of Environment*. 121. 224–235. 10.1016/j.rse.2012.01.018.
- Hopkins, K.G., Lamont, S., Claggett, P.R., Noe, G.B., Gellis, A.C., Lawrence, C.B., Metes, M.J., Strager, M.P., Strager, J.M. (2018). Stream Channel and Floodplain Metric Toolbox: U.S. Geological Survey data release. <https://doi.org/10.5066/F7X34WF4>.
- Jarrett, R., Brannaka, L.K., Ballestero, T., Woodard, C. (2010). Elements of stream restoration.
- Johnson, P.A., Heil, T.M. (1996). Uncertainty in estimating bankfull conditions. *Journal of the American Water Resources Association*, 32, 1283-1291.

- Jugie, M., Gob, F., Virmoux, C., Brunstein, D., Tamisier, V., Lecoœur, C., Grancher, D. (2018). Characterizing and Quantifying the Discontinuous Bank Erosion of a Small Low Energy River Using Structure-from-Motion Photogrammetry and Erosion Pins, *Journal of Hydrology*, 563. 10.1016/j.jhydrol.2018.06.019.
- Leopold, L.B. (1994). River Morphology as an Analog to Darwin's Theory of Natural Selection. *Proceedings of the American Philosophical Society*, 138(1), 31-47.
- Li, D., Wang, G., Qin, C., Wu, B. (2021). River Extraction under Bankfull Discharge Conditions Based on Sentinel-2 Imagery and DEM Data. *Remote Sensing*, 13(14), 2650. MDPI AG. Retrieved from <http://dx.doi.org/10.3390/rs13142650>.
- Lindsay, J.B. (2016). Efficient hybrid breaching-filling sink removal methods for flow path enforcement in digital elevation models. *Hydrological Processes*, 30(6): 846–857. DOI: 10.1002/hyp.10648.
- Ludy, J., Kondolf, G. M. (2012). Flood risk perception in lands “protected” by 100-year levees. *Natural Hazards*, 63(2), 1103-1124.
- McKay, P., Blain, C.A. (2014). An automated approach to extracting riverbank locations from aerial imagery using image texture. *River Research and Applications*, 30, 1048-1055.
- Muthusamy, M., Casado, M. R., Butler, D., Leinster, P. (2021). Understanding the effects of Digital Elevation Model resolution in urban fluvial flood modelling. *Journal of Hydrology*, 596, 126088.
- Montgomery, D. R., Buffington, J. M. (1997). Channel processes, classification, and response. In *Rivers of North America* (pp. 27-42). Academic Press.
- New Hampshire Granit GIS Database. (2019). GRANIT LiDAR Distribution Site. Retrieved from <http://lidar.unh.edu/map/>.
- Palace, M., Herrick, C., DelGreco, J., Finnell, D., Garnello, A., McCalley, C., McArthur, K., Sullivan, F., Varner, R. (2018). Determining Subarctic Peatland Vegetation Using an Unmanned Aerial System (UAS), *Remote Sensing*, 10(9), 1498. <https://doi.org/10.3390/rs10091498>.
- Rosgen, D.L. (1994). A classification of natural rivers. *Catena*, 22(3), 169-199.
- Savitzky, A., Golay, M. J. E. (1964). Smoothing and differentiation of data by simplified least squares procedures. *Analytical Chemistry*, 36(8), 1627-1639.
- Schumm, S. A. (1977). *The Fluvial System*. Blackburn Press.
- Tarboton, D. (2006-2007). *Hydrology Research Group-Terrain Analysis Using Digital Elevation Models (Taudem) Version 5*.

- Tong, B., Li, Z., Wang, J., Yao, C., He, M. (2020). Development of Topography-Based River Width Estimation Model for Medium-Sized Mountainous Watersheds. *Journal of Hydrologic Engineering*. 25. 04020018. 10.1061/(ASCE)HE.1943-5584.0001888.
- Trimble, S.W., (1997). Stream Channel Erosion and Change Resulting from Riparian Forests. *Geology* 25(5):467-469.
- U.S. Geological Survey. (2014, April 29). Digital Elevation Models: Hydro-Flattening and Hydro-Enforcement.
- Vermont Agency of Natural Resources (2004). Identification of Bankfull stage.
- Vermont Agency of Natural Resources (2009). Vermont Stream Geomorphic Assessment Phase 2 Handbook.
- Vermont Center for Geographic Information-VCGI. (2017). LidarFinder. Retrieved from <https://maps.vcgi.vermont.gov/LidarFinder/>.
- Vetter, M., Höfle, B., Pfeifer, N., Rutzinger, M., Stötter, J. (2009). On the use of airborne LiDAR for braided river monitoring and water surface delineation. *Earth Surface Processes and Landforms*.
- Weng, Q. (2012). Remote sensing of impervious surfaces in urban areas: Requirements, methods, and trends. *Remote Sensing of Environment*, 117, 34-49.
- Wing, O. E. (2018). Estimates of present and future flood risk in the conterminous United States. *Environmental Research Letters*, 13(3), 034023.
- Wolman, M.G., Miller, J.P. (1960). Magnitude and frequency of forces in geomorphic processes. *Journal of Geology*, 68, 54-74.
- Yang, X., Pavelsky, T. M., Allen, G. H., Donchyts, G. (2020). RivWidthCloud: An Automated Google Earth Engine Algorithm for River Width Extraction from Remotely Sensed Imagery. *IEEE Geoscience and Remote Sensing Letters*, 17(2), 217-221.
- Zimmerman, F., Maniak, U. (1967). Scour behind stilling basin with end sills of baffle piers. *Proceedings of 12th Congress IAHR, Ft. Collins, September*, 117-124.